AN EXPERIMENTAL INVESTIGATION OF THE PHOTOPRODUCTION OF π^+ MESONS FROM HYDROGEN NEAR THRESHOLD.

BY

ERWIN GABATHULER

PRESENTED TO THE UNIVERSITY OF GLASGOW AS A THESIS FOR THE DEGREE OF DOCTOR OF PHILOSOPHY, SEPTEMBER, 1961.

ProQuest LLC.
789 East Eisenhower Parkway
P.O. Box 1346
Ann Arbor, MI 48106 – 1346

CONTENTS

PREFACE

This thesis describes the experimental work carried out by the author from 1958 to 1961 on the investigation of the photoproduction of π^+ mesons from hydrogen near threshold in candidature for a Ph.D. degree. The research was motivated by the lack of experimental measurements in the low energy region verifying the predicted threshold energy dependence given by Dispersion Relations and the violation in the well known connection between the low energy pion interactions.

Chapter I provides a summary of the theoretical attempts to describe the photoproduction of pions from hydrogen and gives a detailed study of the field of low energy pion photoproduction.

Chapter II is a review of previous experimental methods and results in the field of low energy pion photoproduction, and illustrates the necessity of an accurate set of experimental results in the low energy region.

Chapter III describes the construction of a specially designed, pressure compensated thin-walled liquid hydrogen target, for the detection of low energy pions. The construction and operation of the target and the

compensator design was carried out by the author. The initial design of the target was carried out in collaboration with Dr. W. Hogg. Chapter IV describes two methods of detecting π^+ mesons, one by a time of flight method and the other by a delayed coincidence technique. The construction and testing of the time of flight telescope were carried out by the author and the experiment was performed in collaboration with Drs. G.M. Lewis and R.E. Azuma. Preliminary tests on the delayed coincidence technique, previously developed by Drs. G.M. Lewis and R.E. Azuma were carried out by the author using a thin polythene target.‡ Chapter V contains a description of the threshold meson experiment which provides the most accurate information showing the non-linear threshold energy dependence of the cross-section. The author was responsible for the operation of the liquid hydrogen target during the complete experiment which was of three weeks duration, while the operation, monitoring and collection of the experimental data was shared with Drs. G.M. Lewis, R.E. Azuma and Mr D. Leith. The analysis of the results have been evaluated independently by the author. The thesis concludes with a discussion of the present state of the knowledge in the field of low energy pion physics.

The author is deeply indebted to his supervisor,

‡ The electronic and counting arrangements described in Section III, Chapter IV, and used in the work of Chapter V, were provided in the main by Dr. G.M. Lewis in association with Dr. R.E. Azuma.

Dr. G.M. Lewis, for his stimulating interest and encouragement at all times, and is grateful to Dr. R.E. Azuma for his contribution at different stages in this work. The author wishes to thank Dr. W. Hogg and Mr. D. Leith for helpful discussion. Sincere thanks are also due to Miss E. Muldoon for her valuable help at all stages of this work. The author expresses his gratitude to Professor P.I. Dee, F.R.S., for his interest in this work, and Dr. W. McFarlane and the synchrotron crew for providing an excellent beam during all the machine experiments. Finally the author thanks the Ministry of Education, N. Ireland and the University of Glasgow for grants held during the course of this work.

CHAPTER I

1. Introduction

The investigation of pi-mesons and their interactions is of fundamental importance to the understanding of nuclear phenomena. For example, one thinks of nuclear forces as resulting principally from the interchange of pions between nuclear particles. The pi-meson exists in three basic forms, the neutral π^0, which decays into two photons (2.10^{-16} sec.) and the charged $\pi^{\pm}$ which subsequently decay into a $\mu^{\pm}$ meson (2.5×10^{-8} sec.). Because of the basic nature of nucleons, i.e. protons and neutrons, their interaction with pions is of particular significance.

The improvement of the quantity and quality of the knowledge obtained from pion experiments will aid the theoretical interpretation of the processes involved. Eventually it is hoped that sufficient data will be available, so that an accurate check can be made on any proposed theory describing the pion-nucleon interaction and its associated phenomena.

One important class of pion experiments is the production of pions from nucleons by γ-rays. The first evidence of this process was given by McMillan et al (1949)

at Berkeley, where the first experiments were later carried out by Steinberger and Bishop (1950) on the basic interaction

$$\gamma + p \longrightarrow \pi^+ + n$$

Since that time extensive experimental studies have been performed in the field of photoproduction, and while the main features are now understood, there are still some details to be investigated in the "classical pion" region, which corresponds to pi-mesons produced by photons of energy up to 400 MeV. Without doubt, among the most outstanding problems in this region in recent years is that of the π^+ photoproduction from hydrogen near threshold, in explaining the apparent inconsistency among threshold pion phenomena. An accurate series of experimental measurements of these cross-sections near threshold forms the main material of this thesis.

2. Theoretical Considerations

Low energy pion physics, although only ten years old, has grown into a field of considerable size. During this time, the theoretical approach to this subject has become more and more refined as new techniques became available, analogous in many ways to the improvement

in experimental data. The pertinent experimental information, which is required by the theorist to determine the validity of his theory are the shape and the location of resonances in the excitation function of the reaction, the angular distribution, and the comparison of the production rate of the various competing reactions.

Because of the success of weak coupling theory in explaining electromagnetic radiation processes, a weak coupling approach was used in the early theoretical work based on the Yukawa assumption. This assumption states that except for obvious differences in the mass, charge, spin and coupling strength, the pi-meson plays a role with respect to the nucleon, which is analagous to that played by the photon with respect to the electron. It is then assumed that in the Hamiltonian of the system, the part corresponding to free particles will be much larger than the term describing the interaction. This interaction term can therefore be considered as a small perturbation in the Hamiltonian, and the usual perturbation expansion methods employed. This theory has been treated by Marshak (1952) who showed that the theory gave poor agreement with experiment. It failed to give the observed shape of the angular distribution,

and gave qualitative agreement in the low energy region only.

The strong coupling approach, in which pions and nucleons were treated classically assumed that the nucleon interacted very strongly with the pion field. This treatment was undertaken by Brueckner and Case (1951), Watson (1952) and Brueckner and Watson (1952). The agreement with experiment was poor however, because the coupling between the pions and the nucleons was not strong enough to allow this approach. The very strong coupling and the very weak coupling theoretical treatments were therefore both incompatible with experimental information, but provided a good basis on which to build moderately strong and weak coupling theories, which provided very good agreement with experiment, as will be seen later.

A very fundamental approach to an understanding of experimental data was the phenomenological one, in which an appeal is made to the basic laws of physics, e.g. conservation of angular momentum, parity and isotopic spin (I). In the energy region under consideration, an analysis of the photoproduction data is possible in terms of S and P waves with a small

admixture of D waves by considering the incoming photon as a multipole expansion of the amplitudes for γ-ray absorption. This treatment was considered by Feld (1953) and since it gives valid conclusions, which are based only on the pseudoscalar nature of the pion independent of any meson theory, the results of his predicted angular and momentum dependence are shown in table (1). Feld pointed out that $W(\theta)$, the angular distribution of the pion with respect to the incident direction of the γ-ray, depends only on J and l_γ, where J is the total angular momentum of the system and l_γ is the order of the radiation. The pion momentum dependence is only reliable near threshold, and will be compared with experimental results in Chapter II.

In particular, if only S and P waves contribute to the photoproduction amplitude, then it is possible to analyse the pion angular distributions in the form

$$\frac{d\sigma}{d\omega} = A + B\cos\theta + C\cos^2\theta$$

where θ is the angle between the meson and the photon in the centre-of-mass co-ordinates, and A, B and C are complex quantities expressed in terms of the electric and magnetic multipoles. In general, the cross-section

Table 1.

γ Ray Absorbed	*Intermediate State*	*l of Meson*	l_j	$W(\theta)$	*π-Momentum Dependence*
Mag. dipole	$\frac{1}{2}+$	1	$P_{\frac{1}{2}}$	constant	p^3
Mag. dipole	$\frac{3}{2}+$	1	$P_{\frac{3}{2}}$	$2+3\sin^2\theta$	p^3
Elect. dipole	$\frac{1}{2}-$	0	$S_{\frac{1}{2}}$	constant	p
Elect. dipole	$\frac{3}{2}-$	2	$D_{\frac{3}{2}}$	$2+3\sin^2\theta$	p^5
Elect. quadrupole	$\frac{3}{2}+$	1	$P_{\frac{3}{2}}$	$1+\cos^2\theta$	p^3
Elect. quadrupole	$\frac{5}{2}+$	3	$F_{\frac{5}{2}}$	$1+6\cos^2\theta-5\cos^4\theta$	p^7

is now given in terms of several adjustable parameters, which can in fact be reduced or simplified by considering a simple model, and the results compared with experiment.

Following the success of the application of charge independence to pion-nucleon scattering, Watson (1954) and Gell-Mann and Watson (1954) considered a model for photoproduction based on three fundamental assumptions:-

(1) range of interaction between nucleon and the pion is limited.

(2) charge independence is valid, i.e. Isotopic spin is conserved.

(3) The state $\left(I = \frac{3}{2}, J = \frac{3}{2}, l = 1\right)$ hereafter referred to as the $\left(\frac{3}{2}, \frac{3}{2}\right)$ state of the pion-nucleon system is one of strong interaction.

The authors analysed their results in terms of a set of scattering phase shifts which had been proved by Watson to be related to the complex angular distribution coefficients.

A brief survey of the situation at the end of 1954 shows that the theory is in agreement with the broad general features of the experimental analysis as presented in fig.1 for π^+ production. There was a maximum in the cross-section for π^+ production from hydrogen at $E_\gamma \simeq 320$ MeV due to the strongly interacting $\left(\frac{3}{2}, \frac{3}{2}\right)$ state of the

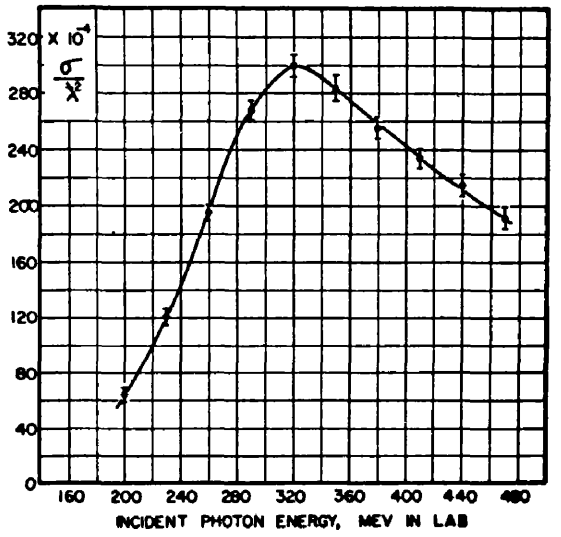

Fig.1a. Total cross-section for π^+ photoproduction from hydrogen showing resonance at 320 MeV.

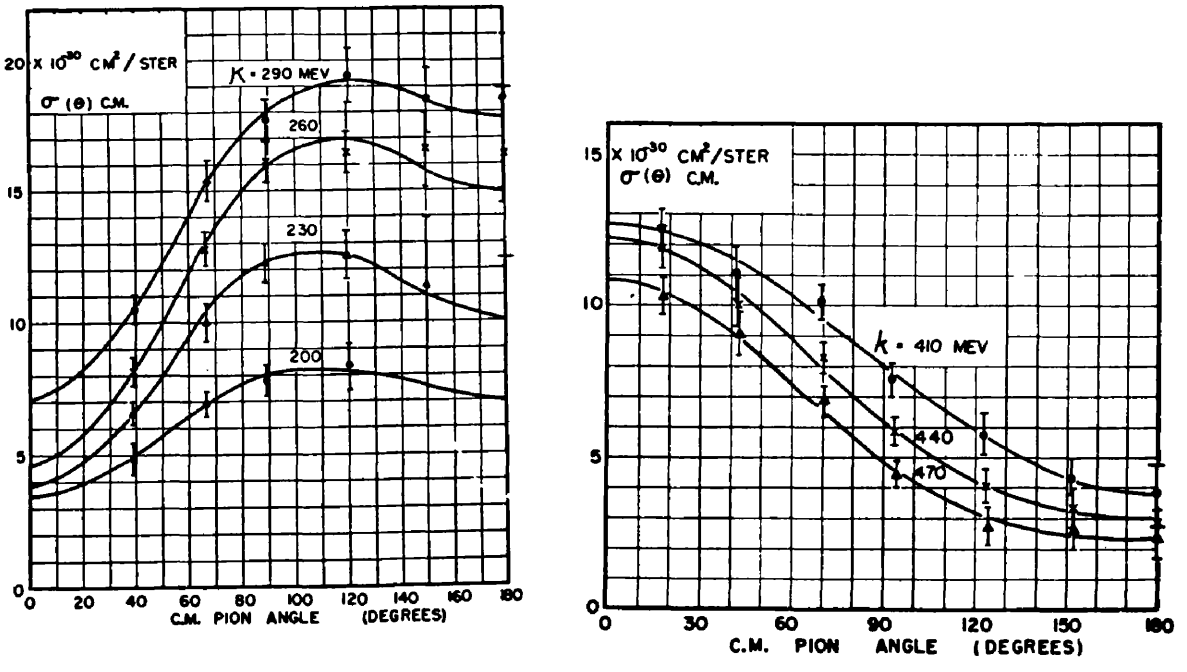

Fig.1b. π^+ photoproduction from hydrogen from 200 to 470 MeV - experimental points due to Walker et al. (1954).

pion-nucleon system. This resonant behaviour was also exhibited by the π^0 cross-section. The angular distributions all showed anisotropy at the higher γ-ray energies, which was reversed at approximately 320 MeV due to the B coefficient changing sign. The angular distribution near threshold was almost isotropic, and the cross-section showed the p dependence indicating that the pion was emitted into an S-state. There was however a lack of information at very forward and very backward angles in the angular distributions, and also in the differential cross-section near threshold, which did not permit any direct comparison with theory.

The biggest step forward in the theoretical understanding of pion photoproduction was provided by Chew and Low (1956) in their static or "cut-off" theory. This non-relativistic model, based on the Yukawa hypothesis was derived from earlier models of Chew (1954) and Low (1954). One of the disadvantages in evaluating the local form of the Yukawa theory was that virtual nucleon-antinucleon pairs were formed in great abundance. In the "cut-off" theory, Chew and Low removed these complications altogether by introducing a non-local form of interaction and smearing out the region of the

pion-nucleon interaction. This introduction of a finite size of source was equivalent to a cut-off in the emergent meson momentum. Essentially Chew and Low removed the unphysical ambiguities, similar to those in the perturbation weak coupling approach by replacing the point source of the pion-nucleon interaction with a source of finite extent. The theory therefore contained only two constants, the pion-nucleon coupling constant and the maximum meson momentum, and was stated to be accurate to approximately 15%.

The final expression for the photoproduction amplitude contained a term due to the direct interaction of the photon with the meson cloud given by

$$\int \underline{\gamma}^{\pi} \cdot \underline{A} \, d\tau \propto \frac{\underline{\varepsilon} \cdot \underline{q} \; \underline{\sigma} \cdot (\underline{k} - \underline{q})}{\omega k - \underline{q} \cdot \underline{k}}$$

where the $\underline{k}$ and $\underline{\varepsilon}$ are the photon momentum and polarisation, $\underline{q}$ and ω are the momentum and energy of the pion, and σ is the nuclear spin. The effect of this retardation or photoelectric term was most easily seen at forward angles, producing an abrupt flattening of the angular distribution for photon energies not too near threshold. This deviation from the previous quadratic in $\cos\theta$ (cf. fig.1)

was experimentally verified by Malmberg and Robinson (1958), Uretsky et al (1958) and Lazarus and Panofsky (1959), and is clearly shown in fig.(2). The cut-off model was therefore the first successful theory in photoproduction, in that it made a definite contribution which had not been previously measured, and gave a semi-quantitative fit to the experimental data up to the $(3/2, 3/2)$ resonance. Chew (1955) has written a very good review of this static theory.

Following the success of the non-relativistic Yukawa interaction, the obvious consequence was to examine the possibilities of deriving a completely relativistic pion theory. An attempt was made to deduce certain functional properties from the Yukawa scattering matrix derived by Low (1955), and modified by Goldberger (1955). This was motivated by the desire to generalise dispersion relations, which had been known in electromagnetic theory for many years, so as to include the forward scattering of particles with mass. It turned out in fact that there was a plausible and unique method to generalise dispersion relations, and their application to the problem of pion photoproduction was presented in the now famous paper of Chew, Goldberger,

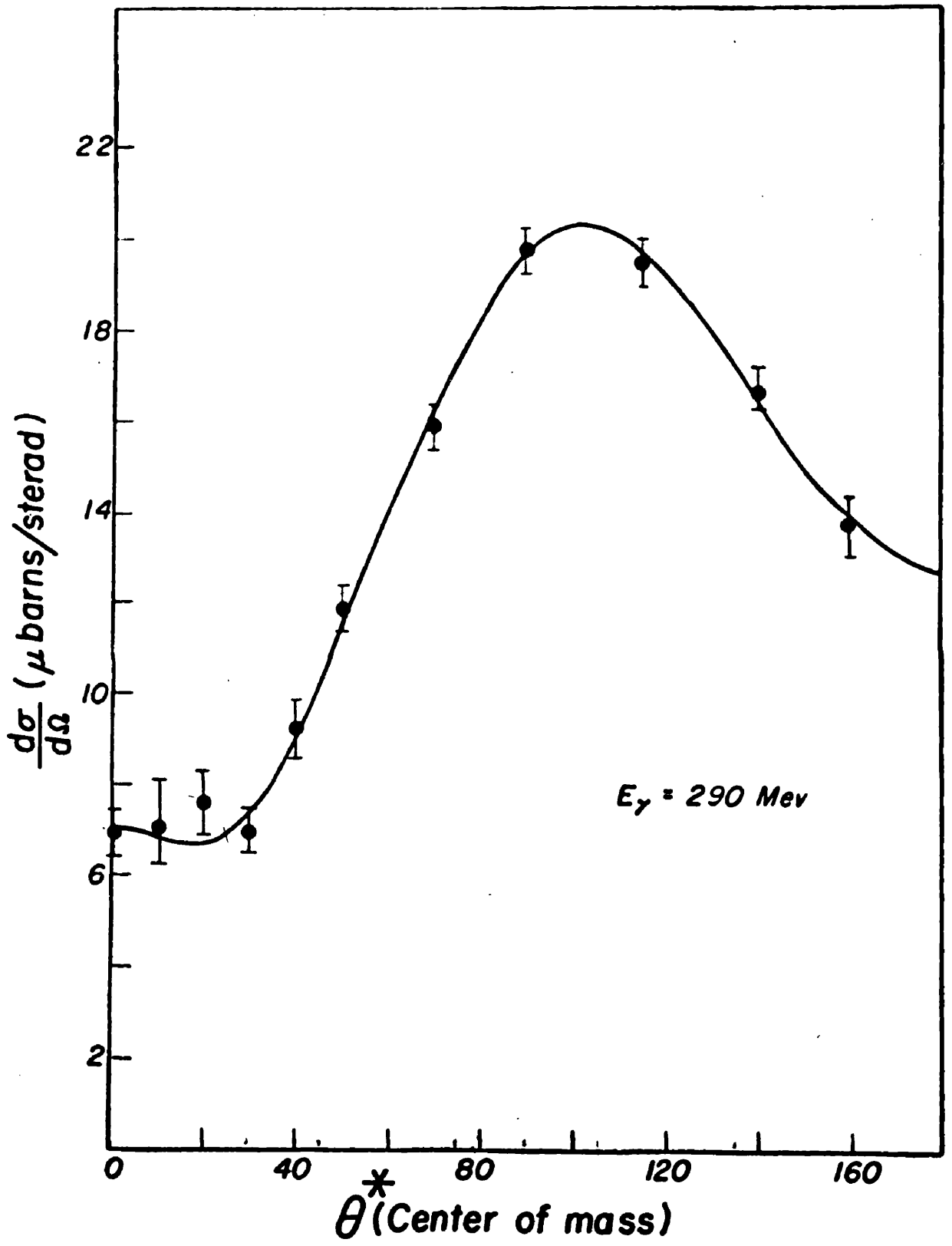

Fig.2. Differential cross-section for π^+ photoproduction from hydrogen showing abrupt flattening at forward angles due to retardation term.

Low and Nambu (1957).

At that time there was no actual proof of the validity of the dispersion relations for photoproduction, but since then a rigorous proof of their exact derivation has been given by Oehme and Taylor (1959) using the general axioms of field theory. It would therefore appear that all the information contained in the Yukawa approach is also contained in the dispersion relations, when these are supplemented by unitarity. The condition for unitarity for photoproduction requires the phase of an amplitude leading to an outgoing pion-nucleon state of definite angular momentum, isotopic spin and parity to be the same as the phase of the pion-nucleon scattering amplitude leading to the same final state, as given by Watson (1954). It was then possible to project out dispersion relations for individual multipole amplitudes, which depended only on the single energy variable W, the total energy in the centre-of-mass system.

The information obtained from the fixed momentum transfer dispersion relation was not very different from the results obtained by the cut-off theory, except that the overall accuracy was improved (10%). The dispersion

relation pion theory stands on a much firmer footing than the intuitive cut-off theory, and all the equations of the latter model can be obtained as approximations of the dispersion theory. Dispersion relations have been applied to pion photoproduction using slightly different techniques by Gartenhaus et al. (1959), in the hope of improving the overall accuracy of Chew's results without success. Hence the overall agreement between experiment and theory is now fairly good in the classical pion region, although some small discrepancies still remain.

The single dispersion relations have however been recently replaced by the so-called double dispersion relations, conjectured by Mandelstam (1958) in connection with pion-nucleon scattering. The Mandelstam representation provides a method for extending scattering amplitudes into the complex plane for both the energy and momentum variables in contrast to just the energy variable in single dispersion relations. This representation has necessitated the introduction of the pion-pion interaction into the pion-nucleon problem, and already experimental evidence of this pion-pion interaction has been reported (Anderson et al., 1961).

The application of the Mandelstam representation

to the photoproduction of π^+ mesons has been carried out in detail by Ball (1960). He found that the results of Chew, Low, Goldberger and Nambu remained practically unchanged. The influence of a possible pion-pion interaction in photoproduction processes has also been examined by Tollis et al (1960), who indicated that the theoretical predictions of the π^-/π^+ ratio could be brought into better agreement with experiment in the region well above threshold by including the pion-pion interaction. The results obtained by Ball have been confirmed by Gourdin, Lurie and Martin (1960).

The Mandelstam representation is now believed by many theorists to have replaced the existing framework of conventional field theory, and can now be used as a starting point to investigate the problem of strong interactions. The theory in itself will not be complete until it is understood how to handle more than two particle systems, which at present limits this method. It is believed however that a further understanding of the pion-pion problem will be required before any further progress can be made in the pion-nucleon theory.

3. Pion Threshold Phenomena

In recent years, much experimental and theoretical attention has been directed to the examination of pion physics at low energies near the threshold of the various processes. This interest has been motivated by the large amount of information which can be derived in the low energy limit. Since this low energy region is very sensitive to any attempted refinements of the theory, accurate experimental information is obviously of the utmost importance.

The first attempt at a coherent interpretation of the energy dependence near threshold of the process

$$\gamma + p \longrightarrow \pi^+ + n$$

was given by Beneventano et al (1956) based largely on their own experimental results. They derived the conventional expression for the differential cross-section

$$\left(\frac{d\sigma}{d\Omega}\right)_{c.m} = \frac{q/w}{\left(1+\frac{\mu}{m}.k\right)^2}\left[a_0^+ + a_1^+\cos\theta + a_2^+\cos^2\theta\right]$$

where q = pion momentum
ω = total pion energy
k = photon energy
μ = pion rest mass
M = nucleon rest mass

} all in the centre-of-mass system.

Terms higher than $\cos^2\theta$ have been neglected, which was in agreement with the parabolic shape of their angular distribution, and was consistent with the assumption that only S and P waves contributed in the final state. If $\cos\theta = 90^\circ$ in the centre-of-mass system, then the above expression can be rewritten

$$a_0^+ = \frac{\left(1 + \frac{\mu}{M} \cdot k\right)^2}{q\omega} \left(\frac{d\sigma}{d\omega}\right)_{c.m.}^{90^\circ}$$

a_0^+ is therefore a direct measurement of the cross-section, if the measurements are made at 90° in the centre-of-mass system.

Figure (3) shows the experimental results obtained by Beneventano et al for a_0^+ versus E_γ, the γ-ray energy in the laboratory. A straight line extrapolation to threshold, substantiated by the measurement of a_0^+ by

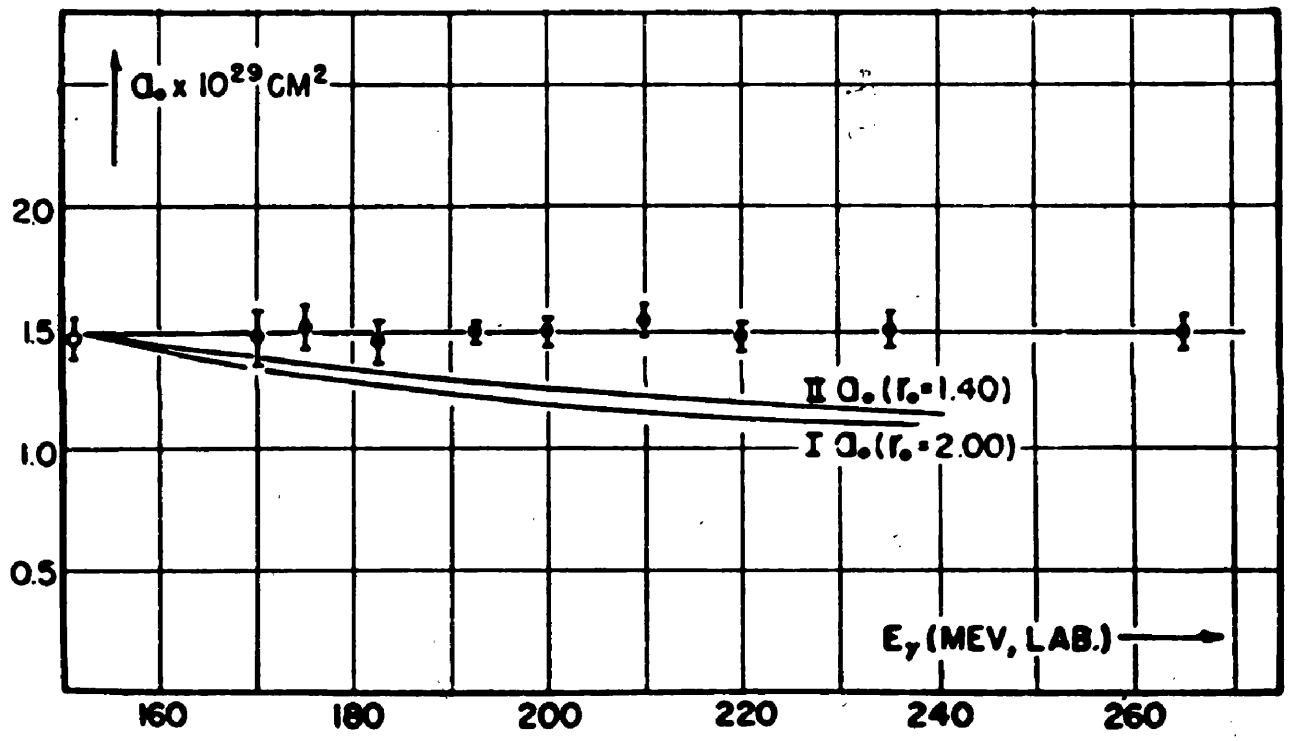

Fig.3. Experimental results of Benevontano et al. showing a_o plotted against the Y-ray energy. The open circle point is that of Leiss et al.

Leiss, Penner and Robinson (1955) gave a value

$$a_o(\text{threshold}) = 14.8 \pm 0.2.10^{-30}\text{cm}^2/\text{ster}.$$

As was first pointed out by Fermi (1952), a basic connection exists between the experimental perameters of low energy pion physics. The pertinent measurements are:-

(1) The Panofsky Ratio $P = \dfrac{\sigma(\pi^- + p \rightarrow \pi^o + n)}{\sigma(\pi^- + p \rightarrow \gamma + n)}$

obtained by allowing negative pions to stop in hydrogen. The reaction takes place from an S state, and the pions are slightly below zero kinetic energy

(2) The charge exchange transition rate

$$\sigma(\pi^- + p \rightarrow \pi^o + n)$$

measured at low π^- energies and extrapolated to zero giving

$$\Delta = \frac{\delta_1 - \delta_3}{q} = \alpha_1 - \alpha_3$$

where δ_1 and δ_3 are the S-wave scattering phase shifts, corresponding to isotopic spin states $T = \frac{1}{2}$ and $T = \frac{3}{2}$

q is the pion momentum in the centre of mass.

(3) The transition rate

$$\sigma (\gamma + p \rightarrow \pi^+ + n)$$

measured at low energies and extrapolated to threshold

(4) The ratio $R = \left. \dfrac{\sigma (\gamma + n \rightarrow \pi^- + p)}{\sigma (\gamma + p \rightarrow \pi^+ + n)} \right|_{Th.}$

which can in principle be obtained from the experimentally observed π^-/π^+ ratio in deuterium.

The connection between these various perameters is clearly illustrated in fig.(4), from which it can be seen that it is possible to arrive at the product $P \times R$ by two independent routes. Unfortunately neither of these two routes are direct, as extrapolations are necessary along the way.

Beneventano et al took the current value of $P = 1.25$, and a value of $R = 1.87 \pm 0.13$ obtained from deuterium to give

$$P \times R (\downarrow) = 2 \cdot 34 \pm 0 \cdot 46$$

This value therefore compared favourably with the value of

$$P \times R (\uparrow) = 2 \cdot 64 \pm 0 \cdot 3$$

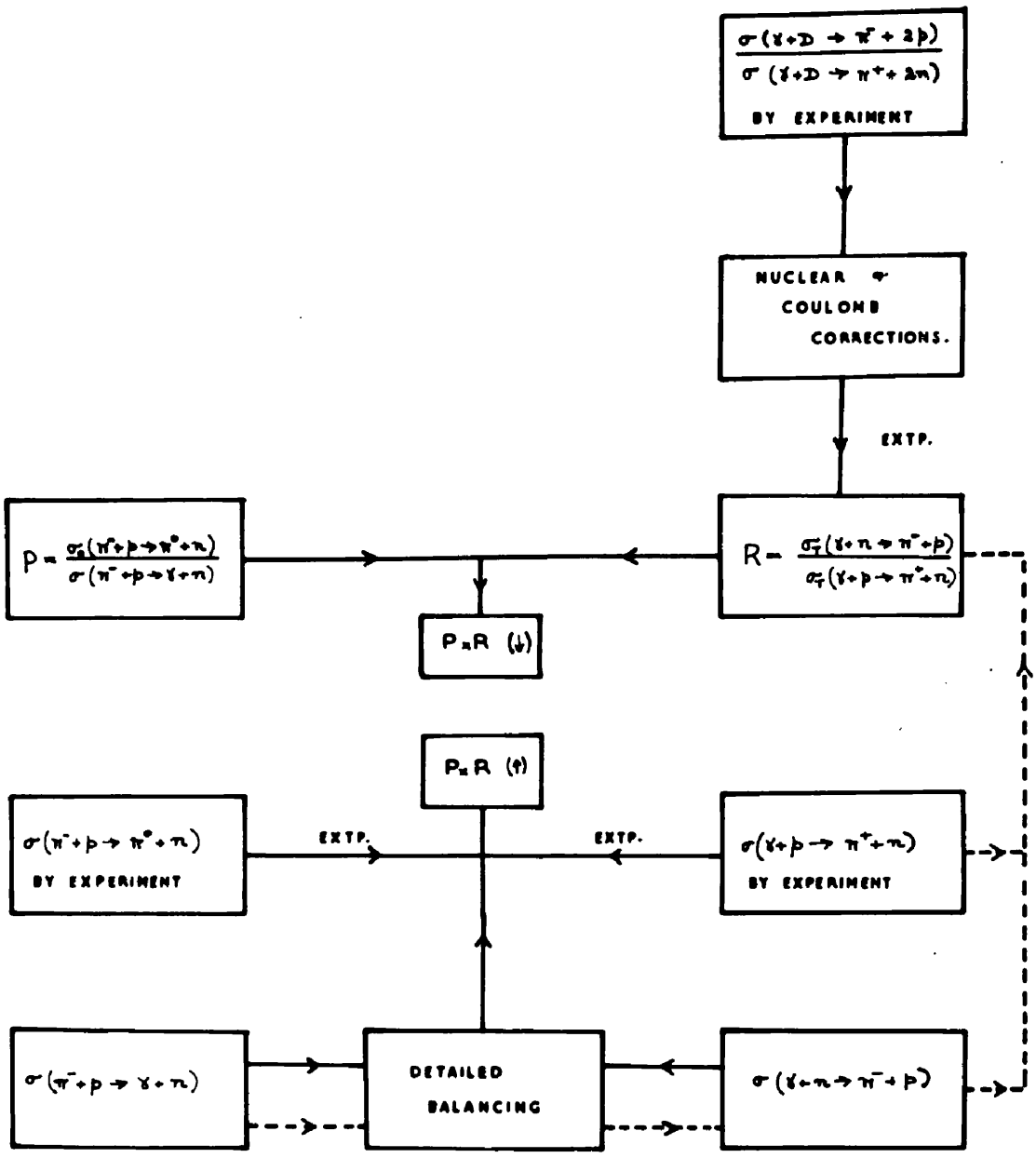

Fig.4. Diagrammatic representation of the connection between the various reactions in low energy pion physics.

when they assumed their value of a_0^+ at threshold, and the current value of $\Delta = 0.27 \pm 0.03$ given by Lederman (1956). It was remarked by the authors that their experimental value of 1.87 was not in agreement with the theoretical value of 1.4 predicted by threshold theorems (Kroll and Ruderman, 1954), but the higher value was in agreement with the other threshold pion perameters.

The derivation of R from the measured π^-/π^+ ratio in deuterium has been calculated by Baldin (1958), who obtained a value of R = 1.4, when the nuclear and coulomb interactions are taken into account. The value of 1.87, extrapolated by Beneventano et al from the deuterium measurements was shown to be consistent with this new calculated value of R. Experimental evidence for the validity of Baldin's calculations has been provided by Adamovich et al (1958) using photographic emulsions loaded with deuterium. By comparing their π^- results with the π^+ results of Beneventano, they obtained a ratio R = 1.3 ± 0.14. More recently however, Adamovich et al (1960) have carried out a complete set of measurements on the photoproduction of positive and negative pions from hydrogen and deuterium respectively, and they derived a value R = 1.3 ± 0.15 in agreement

with the previous ratio. This latter experiment was necessary because of the difficulty of comparing measurements carried out in different laboratories using different beam monitors.

If therefore the value of R was taken as 1.3, then

$$P \times R\,(\downarrow) = 1 \cdot 62$$

which was in definite disagreement with the value

$$P \times R\,(\uparrow) = 2 \cdot 64 \pm 0 \cdot 3$$

In order to remove this discrepancy, the following steps can be taken:

(1) Raise the value of P - obtained directly from experiment.

(2) Adjust R - obtained indirectly from deuterium measurements.

(3) Decrease Δ - extrapolated from experiment.

(4) Raise a_0^+ - extrapolated from experiment.

(5) Introduce a new particle, the π_0^0

The last proposal, the introduction of a new particle was put forward by Baldin (1958), who assumed that the discrepancy was real. He therefore concluded that the π^0 particle measured in the Panofsky ratio determination

was in fact a π_o^o , i.e. a neutral pseudoscalar meson of isotopic spin equal to zero. Cassels et al (1959) have excluded the possibility of the production of two neutral pions by a precise measurement of the angular distribution of the two photons emitted in the Panofsky reaction. The existence of the π_o^o was also refuted by a more direct experiment performed by Akimov (1959), who studied the reaction

$$D + D \rightarrow \pi_o^o + He^4$$

which would be permitted by the charge independence principle.

The value of the Panofsky ratio has increased from the original value quoted by Beneventano et al, but this was not sufficient to remove the discrepancy. The value of Δ at threshold was derived by Orear (1956), who assumed that α_1 and α_3 were constant at low energies, and therefore made a linear extrapolation to threshold. Cini et al (1958) pointed out however, that the value of Δ is energy dependent and hence must vanish at zero pion energy. A value of $\Delta = 0.24$, which was 10% lower than the previous value was obtained, using an S wave effective range approximation based on dispersion relations.

The discrepancy in the pion threshold inter-dependent system was removed by Cini et al in the same publication by raising the value of a_0^+ . They pointed out that the previous analysis by Beneventano et al did not take into account the direct photo-meson interaction term $\frac{\underline{\sigma}\cdot(\underline{k}-\underline{q})\,\underline{\varepsilon}\cdot\underline{q}}{\omega k - \underline{q}\cdot\underline{k}}$ mentioned earlier in the cut-off and dispersion relation theories. This term contains the factor $(1-\beta\cos\theta)^2$ in the denominator, and therefore makes a contribution to all partial waves. This has the property that at E_γ = 170 MeV it provides a fairly large contribution to the S-wave amplitude, but goes to zero at threshold. The experimental evidence for this term was given in fig.(2) by the abrupt flattening of the angular distribution at forward angles.

The importance of the direct interaction term was also pointed out by Moravcsik (1956), who concluded that the angular distribution should be written in the form

$$(1-\beta\cos\theta)^2\frac{d\sigma}{d\omega} = K\left[A + B\cos\theta + C\cos^2\theta + D\cos^3\theta + E\cos^4\theta\right]$$

where K is a kinematical factor. The energy dependence of a_0^+ determined by Cini et al using single dispersion relations is reproduced in fig.(5) showing the rising

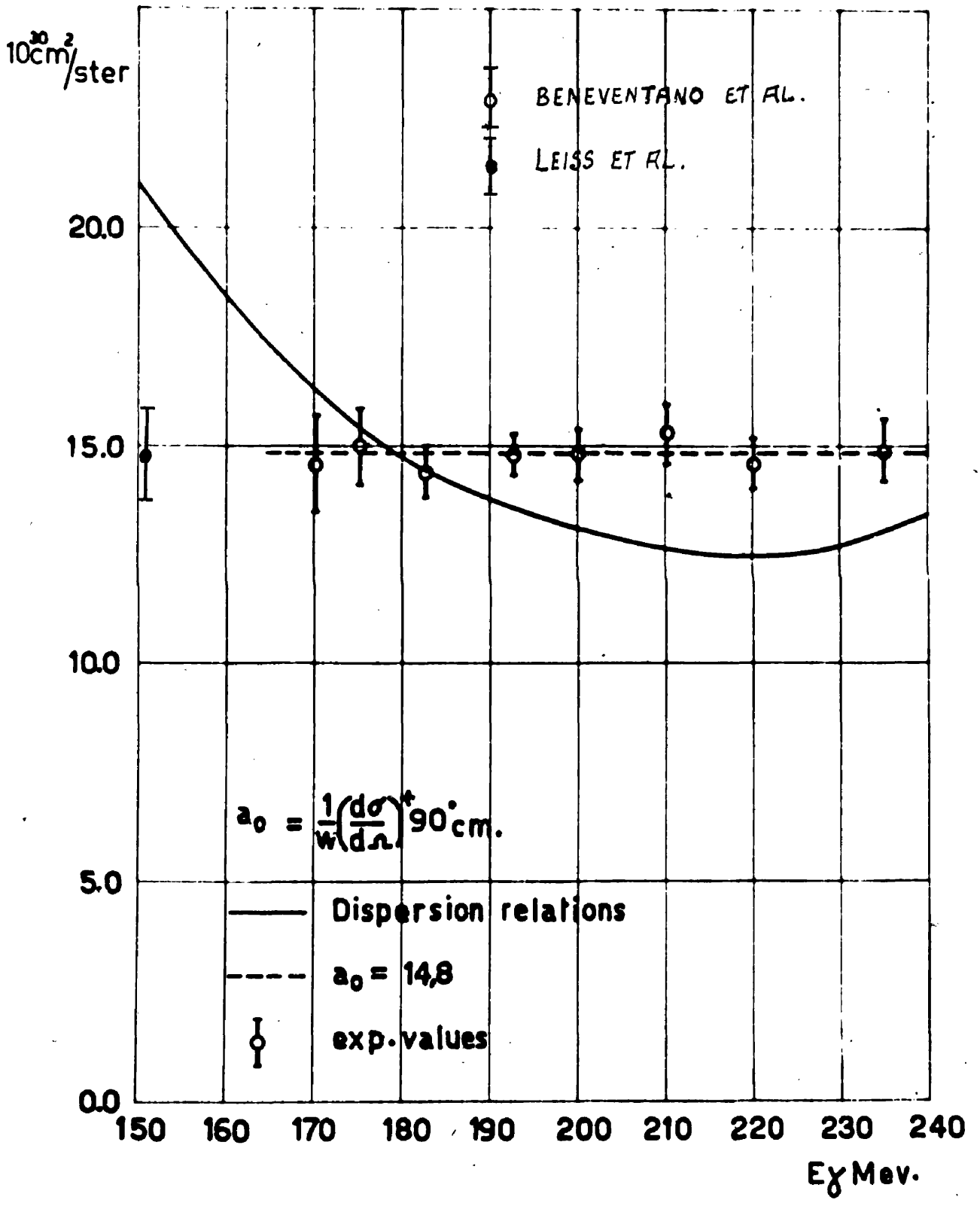

Fig.5. The large discrepancy between experiment and the single dispersion relation theory (solid curve) in the threshold value of a_0

trend towards threshold, when the retardation term is included. It is worth pointing out here that the original weak and strong coupling theories both included this retardation term (cf. Marshak, 1952), and therefore would have given the correct energy dependence near threshold.

The value of α_o^+ at threshold obtained from dispersion relations of 20 μb /ster. can be combined with the value of $\Delta = 0.24$ to give

$$P \times R(\uparrow) = 1.85 \pm 0.2$$

in good agreement with

$$P \times R(\downarrow) = 1.95$$

It must be pointed out that the argument is still very dependent on the various perameters employed. In particular, the derivation of R was based on a somewhat precarious analysis of the photoproduction from deuterium. An experiment which would in fact measure the energy dependence of the π^+ cross-section from hydrogen in the threshold region was therefore of vital interest for the following reasons:-

(1) There did not then exist an overall set of measurements in the threshold region.

(2) Any published measurements which did exist (1958) were in complete disagreement with the energy dependence predicted by single dispersion relations.

(3) A direct determination of f^2 - the pion-nucleon coupling constant.

(4) Further evidence for the introduction of the photo-pion interaction term.

(5) A concrete contribution to the relationship between the low energy pion perameters.

An examination of the experimental measurements and results obtained in the threshold region are given in the next chapter.

CHAPTER II

Previous Experimental Results

1. General Behaviour

A study of the behaviour of pions produced in the process

$$\gamma + p \rightarrow \pi^+ + n$$

requires a measurement of the angle and energy of the emitted pion, because of the continuous energy distribution of the bremsstrahlung beam. As the Compton electron and pair production cross-sections are of the order of 10^{-25} cm^2/ster compared with the π^+ cross-section of $\sim 10^{-29}$ cm^2/ster, it is necessary to select the pions from a large electron and γ-ray background, especially at forward angles. Unfortunately however, the kinematics of the above reaction necessitate forward angle measurements to study the low energy region near threshold. Further, since the π^+ cross-section falls off rapidly towards threshold, and the pions have very little kinetic energy, very few measurements have been made in this region, as can be seen from table 2 where all the relevant previous experimental work has been tabulated.

From this table, it can be seen that the determination of the pion involves the measurement of at least two

TABLE 2.

Author	Method	Photon Energy MeV	Lab.	Year
Steinberger et al.	Fast Coinc.	190 - 320	Berkeley	(1950)
White et al.	Emulsions & Coinc.	200 - 300	Berkeley	(1952)
Walker et al.	Magnetic Spectrometer & Fast Coinc.	200 - 470	Cal.Tech.	(1955)
Jenkins et al.	Proportional Counter	200 - 265	Cornell	(1954)
Feld et al.	Nucl. Emulsions	210 - 305	M.I.T.	(1952)
Janes et al.	Counters	165 - 280	M.I.T.	(1954)
Bernardini et al.	Nucl. Plates	175 - 195	Illinois	(1954)
Leiss et al.	Counters	TH - 170	Illinois	(1955)
Beneventano et al.	Nucl. Plates	170 - 230	Illinois	(1956)
Lewis et al.	Counters	170 - 185	Glasgow	(1959)
Barbaro et al.	Nucl. Plates	160 - 220	Illinois	(1959)
Adamovich et al.	Nucl. Plates	156 - 174	Lebedev	(1960)

characteristic properties of the charged particle. In general, the magnetic spectrometer utilises the momentum and the range properties of the particle, while the scintillation counter and photographic emulsion employ the energy or range of the particle and the characteristic $\pi^+ \rightarrow \mu^+ \rightarrow e^+$ decay.

The early experimental results in the higher region were not very accurate, mainly due to the poor counting rate. They were all consistent however, in that there was general agreement on the shape of the total cross-section showing the pronounced $(3/2, 3/2)$ resonance at approximately 300 MeV in accord with a strong P-wave pion-nucleon interaction. The angular distributions all showed the anisotropy with more pions emitted in the backward hemisphere than in the forward hemisphere (cf. Bethe and De Hoffman, 1955 and fig.1) which was reversed beyond 320 MeV, as stated previously.

There was disagreement among the results of the various laboratories in the measured values of the total cross-sections, which was mainly due to the uncertainty in the absolute calibration of the γ-ray beam monitoring systems. However the experiments performed at the California Institute of Technology

using two different detection techniques were in disagreement by as much as 15% in the energy region where they overlap. The scintillation telescope data was subject to large corrections for nuclear absorption in the absorbers at high energies (50% for 100 MeV pions) and the magnet data required large corrections for decay in flight at lower energies (60% for 20 MeV pions in a 1.5 metre flight path). The disagreement between the experiments was therefore not surprising, when all the uncertainties in the range and scattering corrections etc. were taken into account.

From the above considerations, it is obvious that magnetic spectrometer techniques in their present form are inadequate for accurate detection of low energy pions. The photographic emulsion and the scintillation counter therefore provided the most promising method of detecting low energy pions. Both of these methods have been extensively used in previous threshold measurements, which are considered in some detail in the next section of this chapter.

2. Experiments Near Threshold

Despite the impact on low energy pion physics

introduced by Beneventano et al, it must be remembered that their experiment in itself was not the main cause of the inconsistency, but rather the extrapolation, which was in fact directly substantiated by the experiment of Leiss, Penner and Robinson (1955). The experiment introduced a new degree of refinement into the measurements of the field of photoproduction of charged pions, and provided a statistical accuracy of approximately 4%.

Beneventano et al detected the positive pions by means of nuclear pellicles immersed in blocks of emulsion. The pions were produced in a 1.25 m. diameter thin brass-walled target, around which the emulsions were placed at angles of 45°, 75°, 105° and 150°. It was therefore possible to obtain a complete angular distribution in the one exposure. Fig.(6) shows the angular distributions for different γ-ray energies and the plot of α_0^+ versus E_γ. The scanning efficiency was reported to be around 99% and never less than 97%. The authors considered all possible corrections including decay in flight, nuclear interaction of the pions before coming to rest, background from target walls and edge effects of the pellicles. It is therefore very difficult to offer any reasons why

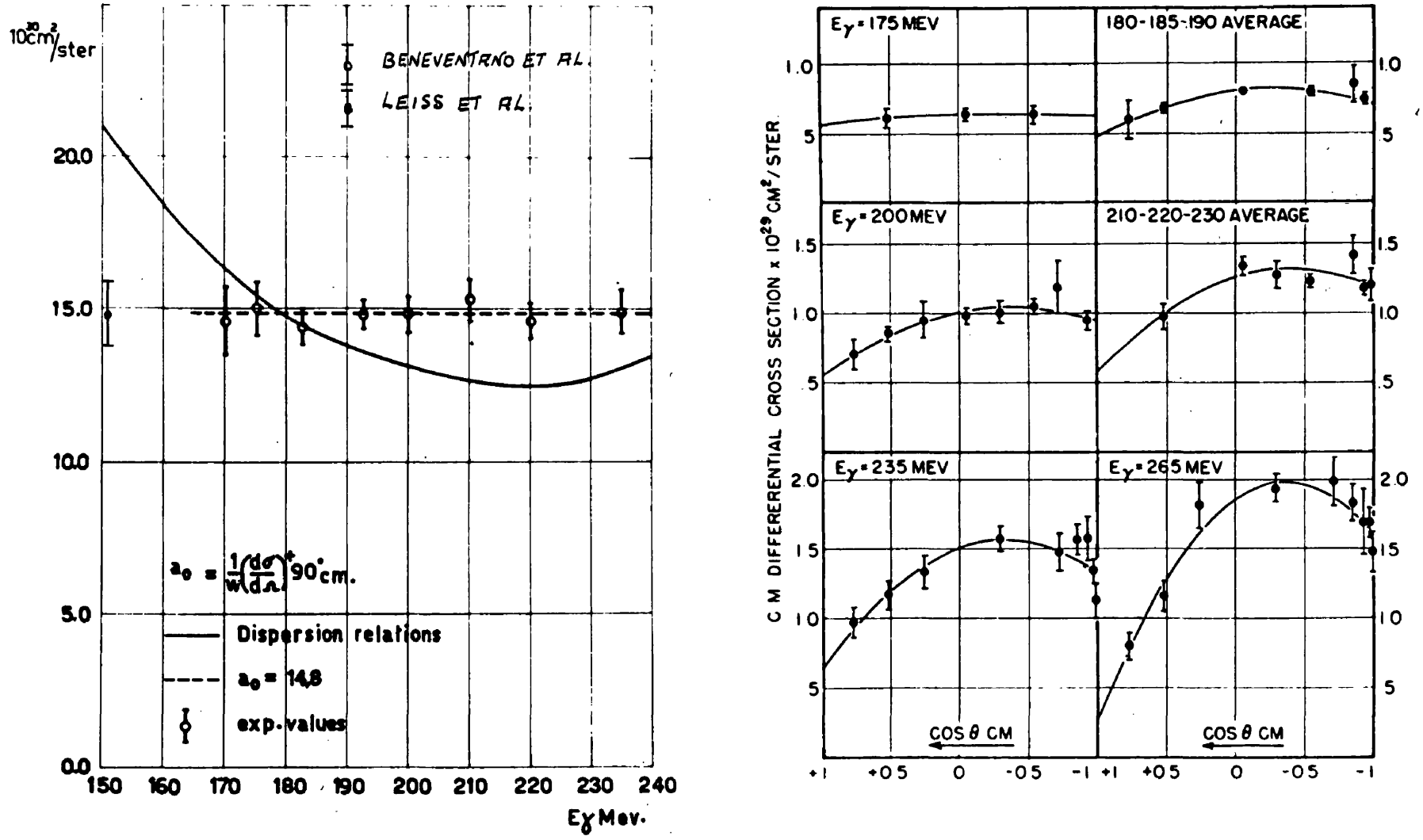

Fig.6. The experimental results of Beneventano et al. obtained by exposing nuclear emulsions to a liquid hydrogen target.

their results are not in agreement with theory, and the only valid criticism which can be made was their attempt to extrapolate from 170 MeV to threshold.

The experiment carried out by Leiss, Penner and Robinson provided a determination of the differential cross-section at a γ-ray energy of 155 MeV which was and still remains the value of a_0^+ nearest to threshold. The experiment itself was a novel one and the technique employed for detecting the lowest energy pions was quite ingenious.

A liquid hydrogen target was surrounded by a hollow carbon cylinder 6 in. in diameter with 0.5 gm walls to stop most mesons produced by γ-rays of less than 185 MeV, as shown in fig.7. The duration of the γ-ray beam was very short, ~ 2 μsec, permitting the detection of the positrons from the $\pi^+ \rightarrow \mu^+ \rightarrow e^+$ in a triple coincidence scintillation telescope. By varying the betatron energy in 2 MeV steps from 140-200 MeV, the activation cross-section at 155 MeV was evaluated. The background counting rate from positrons produced by pair formation was obtained from the counting rate measured below threshold.

The derivation of the cross-section involved an exact knowledge of the shape of the energy spectrum in

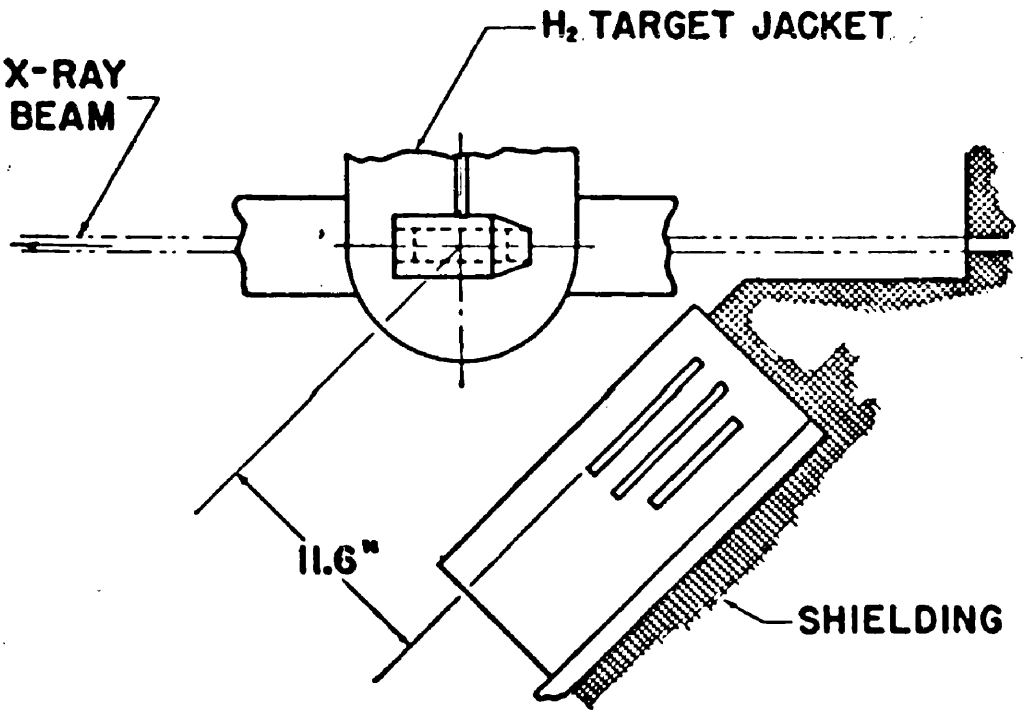

Fig.7. Experimental detection system of Leiss et al. showing liquid target surrounded by carbon block, in which the pions were stopped.

the region of the bremsstrahlung end-point, which they computed from the theoretical Bethe-Heitler formula. The cross-section was then corrected for the counting efficiency, which was calculated from the fraction of mesons which stop in the hydrogen target or in the carbon, the solid angle of the counters, and the fraction of positrons emitted in the direction of the telescope, which are in fact counted. The authors claimed that the calculated efficiency was accurate to less than 10%, and their results were also in agreement with those of Beneventano et al giving the linear extrapolation of α_o^+ to zero.

The result of Leiss et al was retracted and the same experimental data was re-analysed by Leiss and Penner (1959), who obtained a value of 20.10^{-30} cm^2/ster. in contrast with their previous value of 15.10^{-30} cm^2/ster, a change of ~30%. This result was obtained by applying corrections for a more accurate μ^+ spectrum, corrected betatron energy scale, better beam calibration and a correction for positron annihilation in flight in the counter telescope. This statement obviously refutes their previous claims of a calculated efficiency accurate to less than 10% and throws suspicion on their new

determination of α_o^+ , even though it is in agreement with dispersion relations.

Barbaro, Goldwasser and Carlson-Lee have obtained values of α_o^+ at 160 and 219 MeV Y-ray energy. The values were

$$a_o^+ \text{ (160 MeV)} = 18.9 \pm 1.2 \times 10^{-30} \text{ cm}^2/\text{ster}.$$

$$a_o^+ \text{ (219 MeV)} = 16.0 \pm 0.62 \times 10^{-30} \text{cm}^2/\text{ster}.$$

No details of this experiment have been published, but as the experiment was done at Illinois using nuclear emulsions, it can be assumed to closely resemble the experiment of Beneventano et al. The value of α_o^+ was in agreement with the rising trend predicted by dispersion relations, but one point is not enough to show the energy dependence, nor does it provide the necessary information for a threshold extrapolation. However, it did indicate that the Beneventano linear extrapolation was not valid.

The most complete experiment in the threshold region from 153 to 175 MeV was performed by Adamovich et al (1960) using the nuclear emulsion technique. The experimental procedure involved three separate methods corresponding to three Y-ray energy intervals. The cross-section was measured in the interval 153-161 MeV

by simultaneous irradiation of thin polythene and carbon targets, and the pions were detected at angles of 60° and 120° with nuclear emulsions. The experiment was feasible in this energy region, because the Coulomb field inside the carbon nucleus inhibits the production of low energy π^{+} mesons. The cross-section was then derived by a CH_2-C subtraction.

The pions produced in a liquid hydrogen target by γ-rays of energy 160-165 MeV were detected by inserting the emulsions into the target vacuum chamber, at an angle of 78° to the γ-ray beam. The cross-section for the maximum energy γ-ray interval was measured by placing the nuclear emulsions right in the liquid hydrogen, at a distance of 2 cm from the axis of the photon beam, thus increasing the pion counting rate. The thin solid target method was necessary because the low energy mesons could not escape from the liquid target.

The results of the experiment are illustrated in fig.(8), where the units differ from those given previously by a factor of π. The statistical accuracy of the experiment however was not sufficient to indicate the rising trend of α_0^{+} towards threshold. The authors claimed that the comparison of their results with those

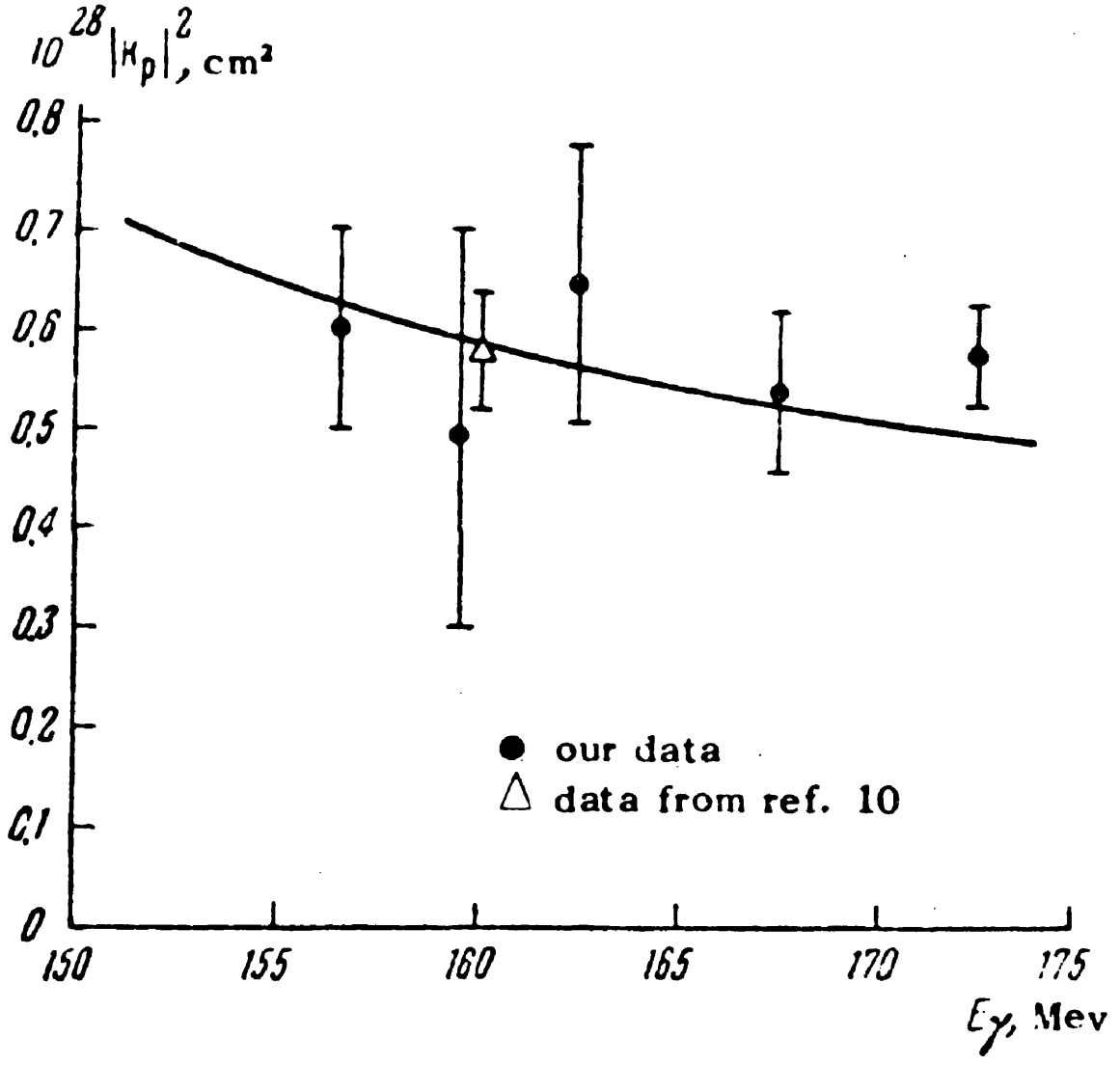

Fig.8. Experimental results of Adamovich et al.
$|K_p|^2 = \pi a_0^+$ - Ref.10 refers to the results of Barbaro and Goldwasser.

of Beneventano et al at higher energies showed that the experimental values of a_o^+ was increasing towards threshold. This is however not a very reliable procedure because of the variation in absolute beam monitoring calibrations among the various laboratories. Indeed it was stated recently by Goldwasser (1960) that the results of Beneventano et al should be raised by 10% because of errors in the beam monitoring which therefore nullifies the previous claim.

The first experiment using the scintillation counter technique for the direct detection of low energy positive pions from photoproduction was that of Janes and Kraushaar (1954). Using a CH_2-C subtraction, they were able to detect 10 MeV pions at a laboratory angle of 90^o to the direction of the γ-ray beam, corresponding to a γ-ray energy of 168 MeV. The method utilised the fast $\pi^+ \rightarrow \mu^+$ decay to separate the positive pions, similar to the detection method used in this experiment. The error on the lowest energy experimental cross-section was of the order of 50%, and it was difficult to compare their data with other experimental results as the absolute calibration of their synchrotron beam was uncertain by a factor of two. They did provide the first experimental

evidence of the approximate linear dependence of the cross-section with pion momentum, consistent with the assumption that only S-wave pion emission was important for photon energies up to 200 MeV, as shown by the Feld scheme in table 1.

The direct detection of low energy pions using the scintillation counter technique was developed further by Lewis and Azuma (1959). They measured the π^+ cross-section from protons in the Y-ray interval 165-190 MeV using thin polythene and carbon targets. The statistical accuracy of their results did not provide any conclusive evidence as to the energy dependence of a_0^+ but the method did show that it was feasible to detect positive pions down to 5 MeV. The scintillation counter is therefore comparable with the photographic emulsions as a low energy pion detector.

An overall picture of the available experimental information on the photoproduction of positive pions from hydrogen as presented by Bernardini (1959) is given in fig(9). It can be seen that there was not a complete set of measurements in the photon energy range from threshold up to 200 MeV, which indicated the energy dependence of the π^+ cross-section. The difficulty

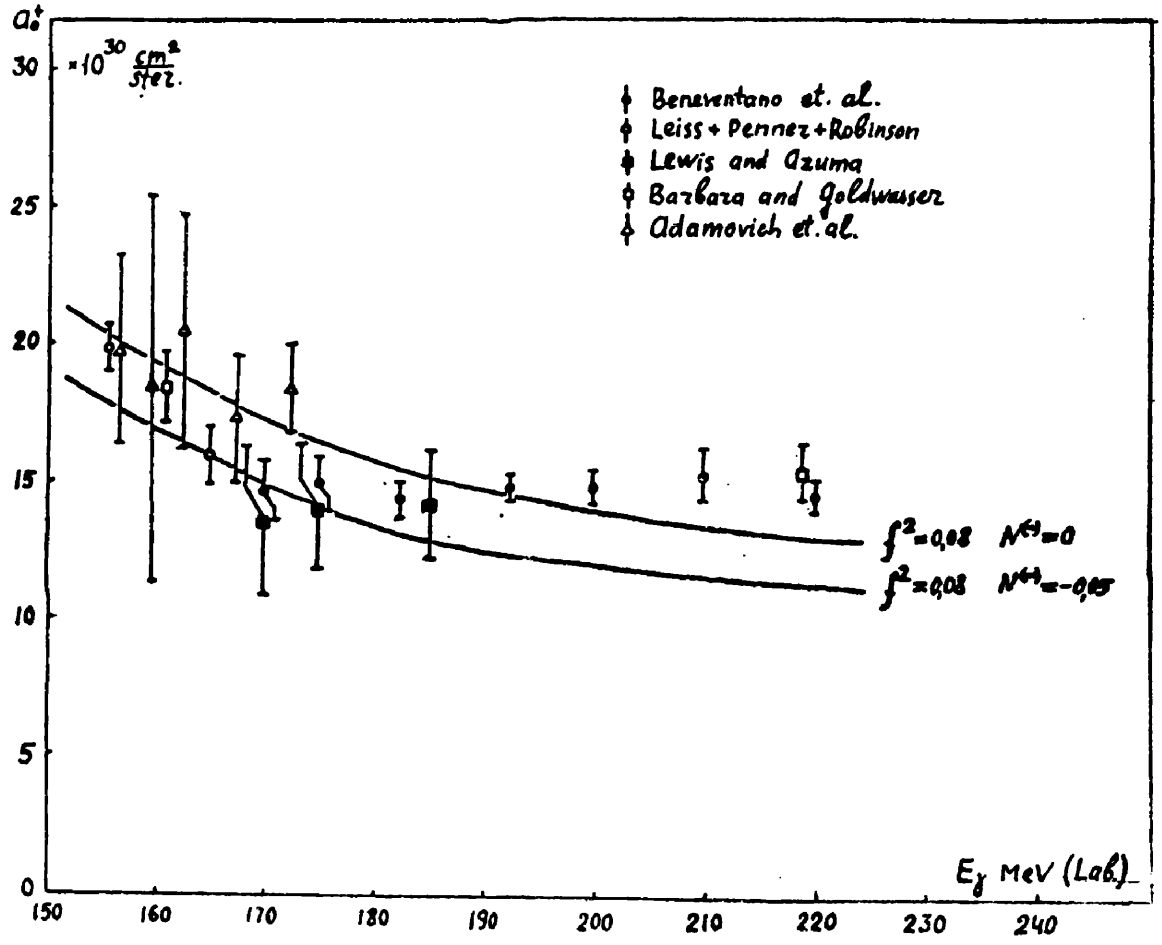

Fig.9. The experimental values of a_0^+ versus E_γ as presented by Bernardini at the Kiev Conference (1959). The solid curves are the predictions of single dispersion relations.

of comparing the results from different laboratories has been amply illustrated, emphasizing the importance of a complete set of measurements of the π^+ cross-section from hydrogen in the energy region from threshold up to 200 MeV.

3. Present Experiment

Consider an ideal experiment in which there is a large number of quanta available for pion production. The proton target could then consist of a thin film of liquid hydrogen which would not disturb the pion once it was created. The particle detector would only be sensitive to positive pions and would be located close to the hydrogen target at a very small angle to the γ-ray beam direction. By this method it would then be possible to measure the energy dependence directly down to threshold. Obviously such an experiment is out of the question at the present time, but it does provide a fundamental approach on which to design a threshold experiment.

In the present experiment, a thin-walled flat target was exposed to the 250 MeV bremsstrahlung beam of the Glasgow electron synchrotron. Pions in the energy

range from 6 to 40 MeV were detected by a counter telescope placed at an angle of 58° to the γ-ray beam. The counter telescope consisted of two counters, a thin front counter and a second main counter in which the pions were brought to rest and detected by their characteristic $\pi^{+} \rightarrow \mu^{+}$ decay. Further separation of the pions from the electron and γ-ray background was provided by $\frac{dE}{dx}$ and E pulse height selection measurements in the thin and main counters. Pions in the higher energy region were studied by placing a copper absorber between the two counters. This enabled the energy dependence of the cross-section to be studied in the γ-ray interval from 160 to 195 MeV, which according to the dispersion theory should show a variation in the value of a_0^+ by $\sim$ 20%. A description of the liquid hydrogen target and the pion detection system are given in the next two chapters.

CHAPTER III

Liquid Hydrogen Target

1. Introduction

In all branches of high energy nuclear physics, involving a study of the free proton, solid CH_2 targets provide the simplest source of protons. The cross-section from hydrogen is obtained by performing a second experiment with a carbon target and carrying out a straight forward subtraction. This type of target has advantages over a liquid hydrogen target in that it is well defined geometrically and the experimental effort is greatly reduced.

In a threshold experiment however, when the pions have very little penetrating power, the target must be very thin to avoid absorption and scattering of the emerging π^+ mesons. Long experimental runs are therefore required to provide a statistical accuracy of 5%, and unless the polythene and carbon runs are performed simultaneously e.g. Adamovich (1960), the targets should be interchanged repeatedly to avoid any error in instabilities of the synchrotron or the detection system. Further, the background of electrons and γ-rays from this solid target is a source of embarrassment at

forward angles for any detector of low energy pions. Figures (10a) and (10b) illustrate the angular distribution of the electrons and γ-rays from pair production and Compton effect respectively. Since the Compton process has a Z dependence, and the pair production has a Z^2 dependence, the carbon provides a very large proportion of the total background. The solid target has the further disadvantage that it produces a large flux of protons from the photo-disintegration of carbon ($\sim$ 10 μb/ster).

High pressure hydrogen gas targets have been used extensively in the photoproduction of pions from hydrogen (White et al 1952, Walker et al 1955). They readily satisfy the condition of small energy degradation and scattering of the reaction products, but a substantial background is produced in the thick pressure windows. The targets are generally of large dimensions, and therefore cannot be used with scintillation counters because of the lack of angular resolution. This difficulty has been overcome by placing photographic emulsions inside the pressure vessel (Kirk 1961). Nuclear emulsions have been irradiated with γ-rays, the emulsion providing both the target and the detector

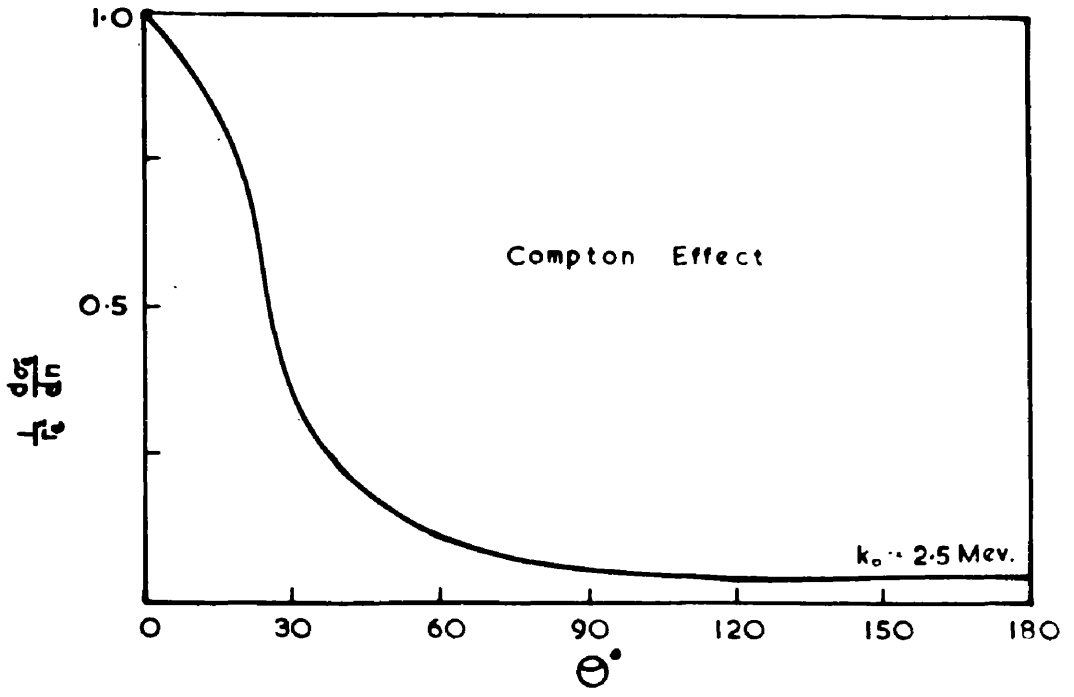

Fig.10a. Angular distribution of Compton scattering for incident photon K_0 for carbon.

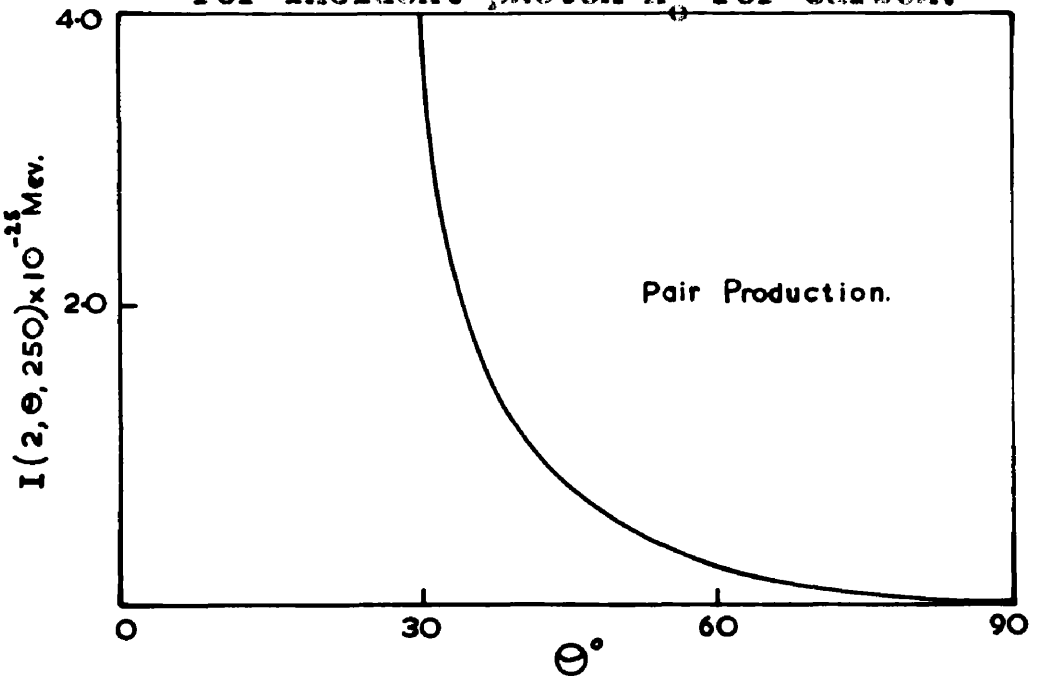

Fig.10b. Angular distribution of electrons produced by pair production. $I(2,\theta,250)$ is the number of electrons of energy greater than 2 MeV per proton per erg./cm^2 beam energy per steradian for a 250 MeV beam.

(Adamovich, 1958), but the method has been mainly confined to π^- star measurements in emulsions loaded with deuterium.

The liquid hydrogen target has the advantage over the solid target that long background runs are not generally required and the background from the liquid hydrogen is very much reduced. For the liquid hydrogen target to retain this advantage and exhibit a better overall performance, it must satisfy the following specification:-

(1) The walls of the target chamber must be thin to let the pions escape, and of low Z material to reduce the background as much as possible.

(2) The target must be parallel-sided and remain uniform in thickness throughout the experiment.

(3) Small angle pion scattering from the walls of the target chamber must be avoided.

(4) The distance from the target to the pion detector must be as short as possible.

(5) The target should accept the total γ-ray flux to avoid any uncertainty in the beam profile.

A liquid hydrogen target was designed to meet these requirements.

2. Description of Hydrogen Target

The design of the liquid hydrogen target from the practical point of view is to keep the loss rates of the liquified gases in the system as low as possible, and to facilitate ease in assembling. The target was therefore constructed in two separate sections, as shown in fig.11, which is a scale drawing of the complete target assembly.

The liquid hydrogen target A was enclosed in a liquid hydrogen cryostat similar in design to that of Whalin and Ritz (1955) and Bellamy et al (1960). The liquid hydrogen refrigerant at atmospheric pressure was contained in the hydrogen reservoir, which comprised a copper cylinder 19 in in length, 3.5 in in diameter and three litres in volume. This reservoir was supported from a brass plate (fig.12) by four copper-nickel (low conductivity) tubes, three of 3 mm diameter and one of 12 mm diameter; the latter provided the inlet tube to the liquid hydrogen reservoir. These four tubes were thermally anchored to the liquid nitrogen reservoir by an intermediate bridge, which increased substantially the temperature gradient between this bridge and the top plate at room temperature. By this method, the heat input by conduction to the liquid hydrogen was

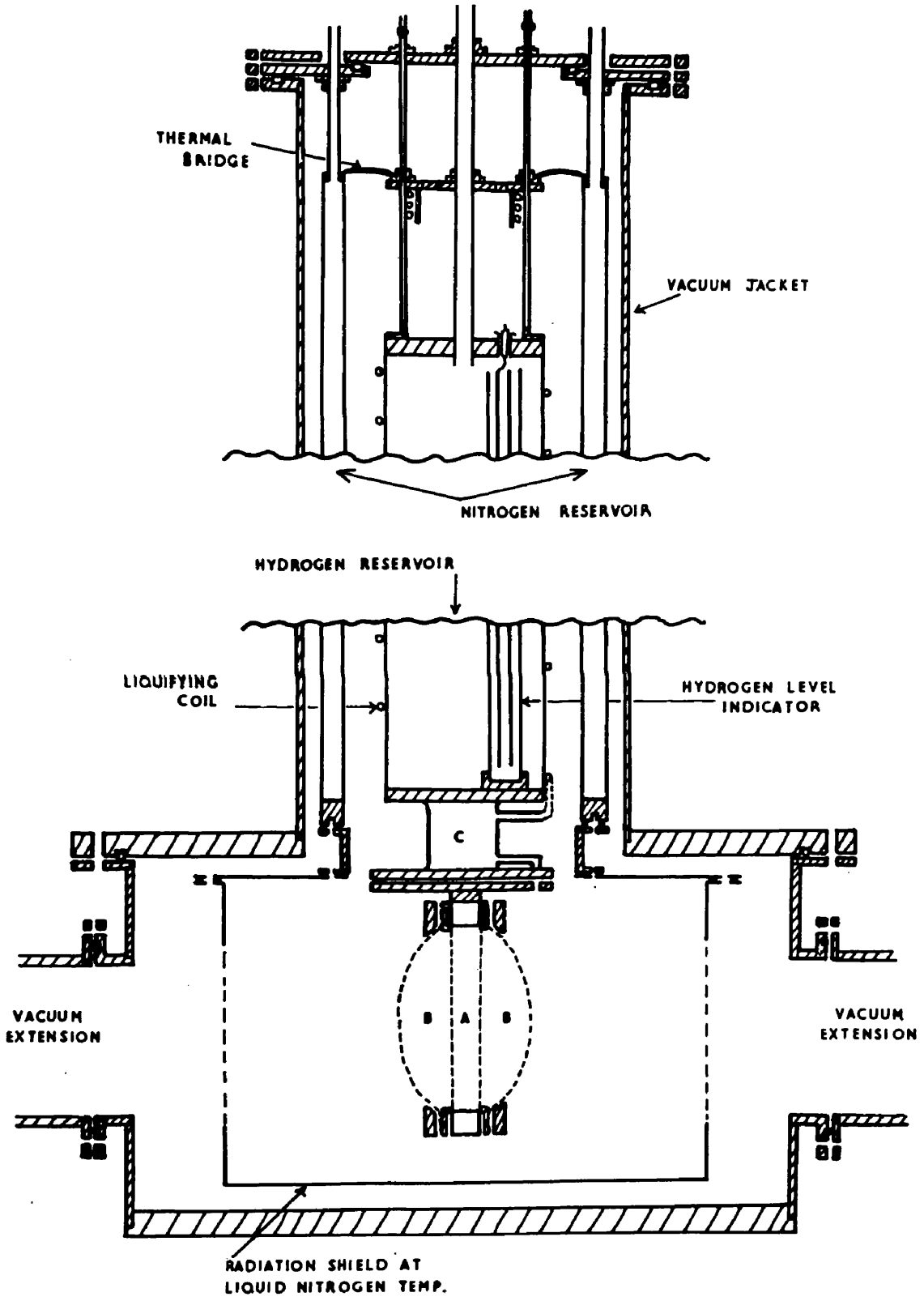

Fig.11. Vertical section of complete liquid hydrogen target.

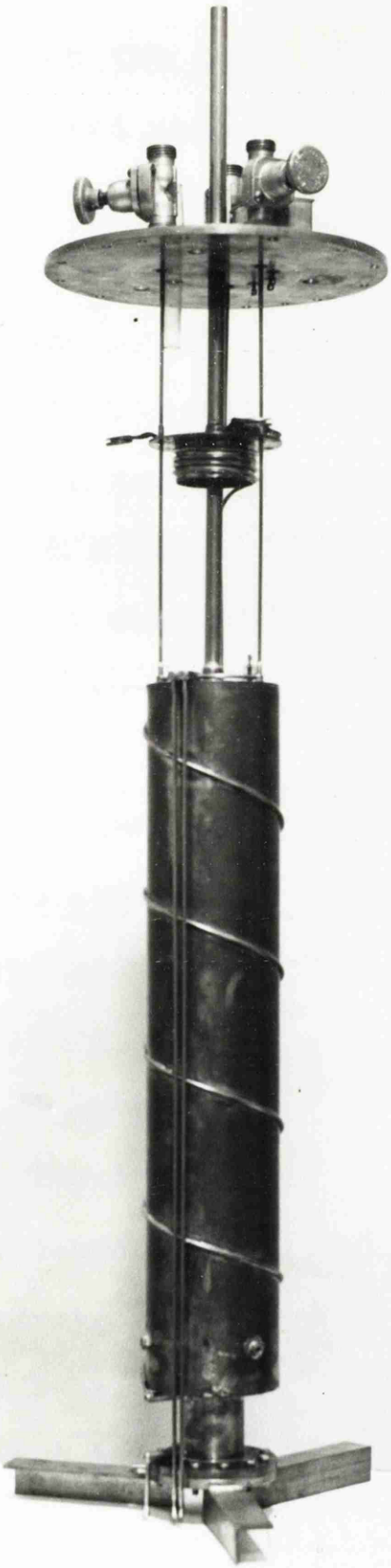

Fig.12.
Liquid hydrogen cryostat showing liquefying coils and the liquid nitrogen thermal bridge below the brass plate.

reduced at the expense of the liquid nitrogen. The level of the liquid hydrogen refrigerant was monitored by a level indicator device which relied on the small change in capacitance ($\sim$12%) of two concentric tubes when the intervening space was filled with liquid hydrogen or liquid hydrogen vapour. This capacitance ($\sim$50pF) formed part of a tuned circuit fed from a standard oscillator, and the resonant current was measured through a cathode follower output.

The small target reservoir C, silver-soldered to the bottom of the main hydrogen reservoir was connected directly to the liquefying coils as shown in figure (11). Of the two thin copper-nickel tubes running the entire length of the reservoir, one was coupled directly to the target slice A and the other was coupled to B. The target reservoir and the target chamber A formed a closed system separate from the main hydrogen refrigerant.

The heat input to the hydrogen cryostat was reduced by a liquid nitrogen radiation shield. The nitrogen reservoir consisted of two concentric brass cylinders of 5 in and 6 in external diameter, suspended from an annular brass disc by three equally spaced 10 mm diameter copper-nickel tubes. The annular volume of the liquid

nitrogen reservoir was 4 litres. The target radiation shield was maintained in thermal contact with the nitrogen reservoir by a demountable copper ring. Good thermal conduction was ensured by inserting indium wire between the reservoir, the copper ring and the target radiation shield. The latter, a rectangular aluminium box of 0.125 in wall thickness was attached to a 0.125 in copper plate, which permitted the heat input to the target radiation shield to be easily transferred to the liquid nitrogen reservoir. The walls of the radiation shield, through which the γ-ray beam and the emerging mesons passed, were covered with 0.0006 in aluminium. Very thin target viewing slots were cut in this aluminium and were covered with Melinex.

The complete low temperature cryostat was enclosed in a brass-walled vacuum jacket, connected directly by a 2 in diameter port to an oil diffusion pump, which maintained a vacuum of less than 10^{-6} mm Hg. The heat input by convection was therefore eliminated, while the heat input through the residual gas was negligible. The outer vacuum jacket consisted of two parts which were joined together by a rubber "O" ring vacuum seal. The beam exit and entrance ports of 3.25 in diameter

were located in the bottom section of the vacuum jacket, to which beam extension pipes, one metre in length were attached. The counter telescope was therefore easily shielded from the considerable background produced by the Y-rays in the air and also in the 0.001 in Melinex beam windows.

A 0.003 in thick Melinex sheet, through which the pions emerged, covered a port, which was of large diameter (5.5 in), to avoid small angle pion scattering into the counter system. An additional sheet of 0.001 in Melinex was attached to each window of the vacuum jacket forming a double wall. Dry nitrogen gas was passed through the space formed by the double wall to prevent condensation of water vapour on the aluminium walls of the radiation shield, at liquid nitrogen temperature. If this frost was deposited on the heat shield, it introduced a slowly increasing background and gave a higher liquid nitrogen loss rate due to increased emissivity.

Fig.(13a) shows the completely detachable target chamber, consisting of a copper annulus 5.5 in o.d., 4.25 in i.d. and $\frac{15}{32}$ in thick, on both sides of which thin Melinex sheets were cemented with Araldite to form

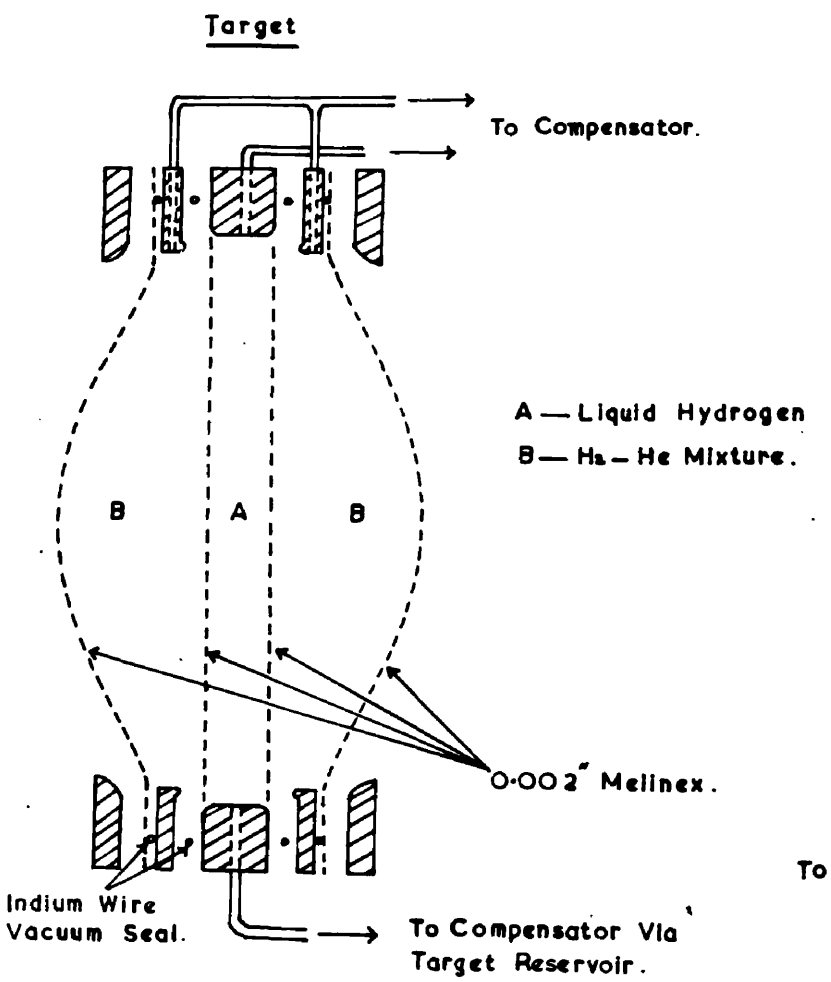

Fig.13a. Target Chamber - the inner compression ring is stopped to keep the walls of the target taut.

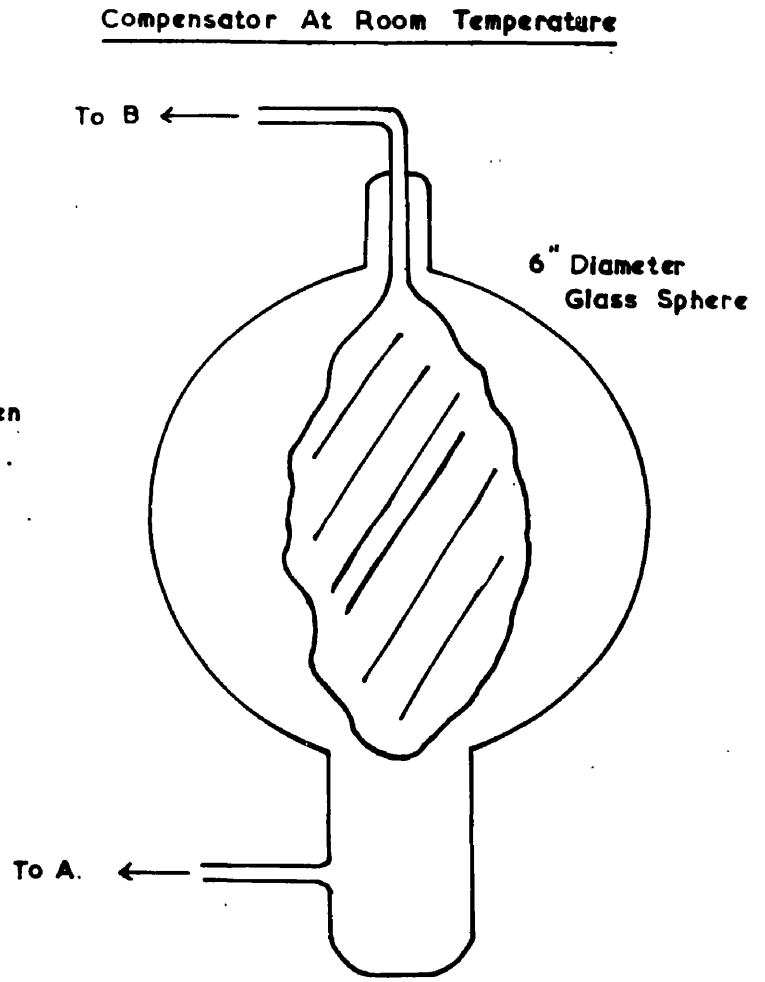

Fig.13b. Compensator consisting of rubber bladder inside glass sphere.

the walls. Compression rings, as shown in fig.(13a), were provided to keep the walls taut. Thin target walls satisfy one of the requirements previously stated, but these walls would bulge into the vacuum space, and therefore would not remain parallel and uniform in thickness throughout the experiment. For example, with this present target geometry the walls would bulge outwards by 1.5 cm at the centre for a pressure difference of 1 atmosphere. In order to ensure that the target walls remained flat under all experimental conditions, a special technique of pressure compensation was developed.

A Melinex sheet was clamped to the outer surface of each compression ring and the enclosed space B was filled with a non-condensable gas at liquid hydrogen temperature, e.g. a helium-hydrogen mixture. The liquid hydrogen part of the target is indicated by A in the diagram. The pressure of the gas mixture in B was always maintained exactly equal to the vapour pressure of the liquid hydrogen in A by a compensator, thus ensuring that the walls remained accurately flat. The target bulge has therefore been taken up by the outer walls of the helium jacket. The description of the compensator is given in section 3.

The complete structure was clamped together by twelve 4 B.A. brass screws, and the vacuum seals were achieved with indium wire, which has been found to make an excellent vacuum seal between metal and Melinex at liquid hydrogen temperature, provided that a high uniform pressure distribution can be permanently maintained. Araldite was preferred for the vacuum seal of the liquid hydrogen target chamber A, since the hot setting process helped to keep the Melinex walls taut.

The actual target chamber which was in operation in the threshold experiment is illustrated in fig.(14). Two 68 ohm carbon resistors, situated at the top and bottom of the vertical brass tube constituted the target liquid level indicator. This device depended on the principle of the more rapid dissipation of heat from a carbon resistor when in the liquid than in the vapour, and the high temperature coefficient of a carbon resistance at very low temperatures. In operation the resistors were independently connected into an external Wheatstone bridge, the resistor in the vapour causing a rapid shift in balance point, in contrast to the negligible shift when in the liquid. The three thin copper tubes, which emerge from the target, were soldered directly to

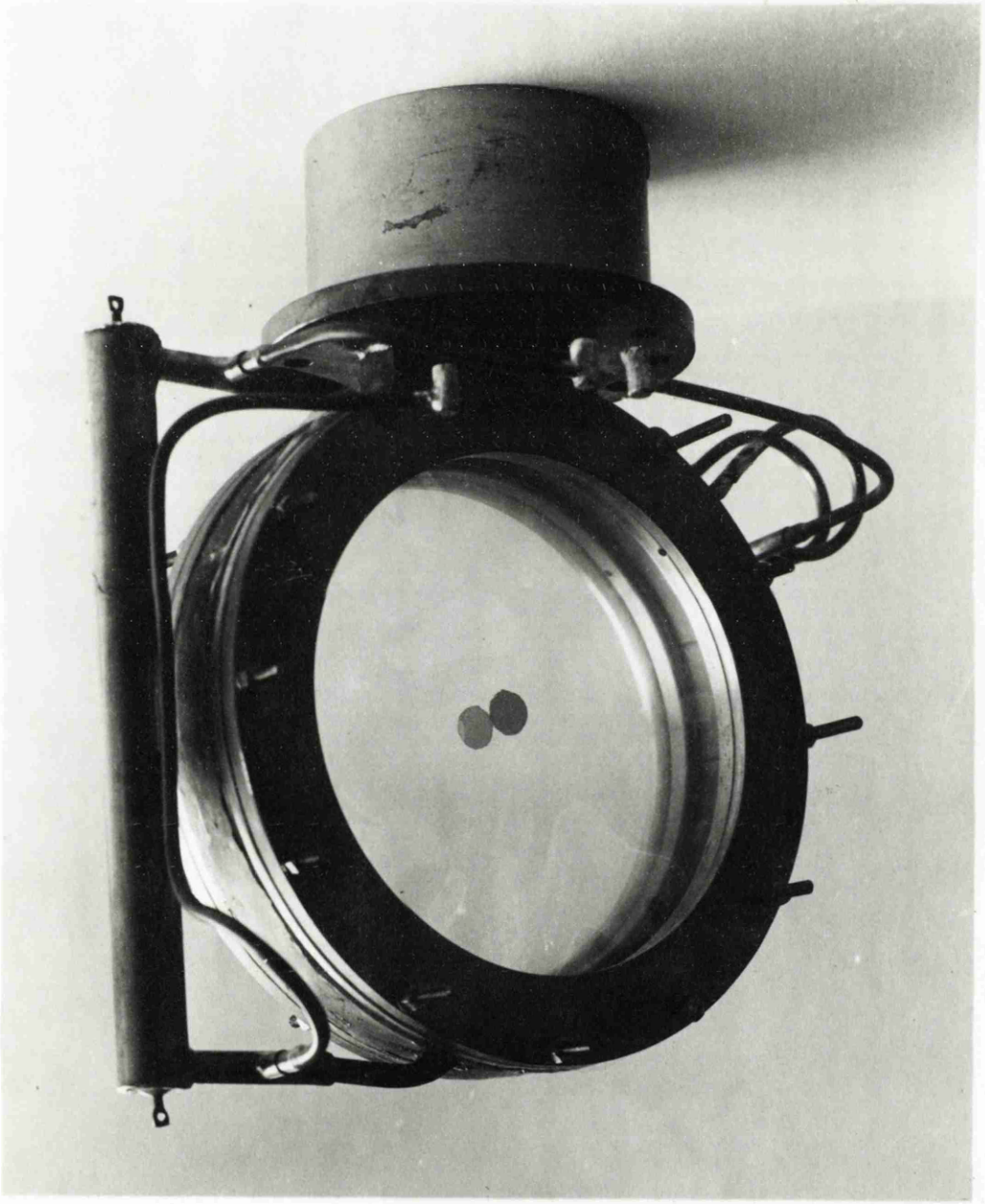

Fig.14. Liquid Hydrogen Target used for the a_o^+ measurements. The target centre is defined by the aluminised spot.

the three thin copper-nickel tubes, which were connected to the main hydrogen reservoir. One of these tubes was connected to the helium jacket B, and the other two, connected in parallel with the level indicator, formed the inlet and exhaust of the liquid hydrogen chamber.

The target was in good thermal contact with the target reservoir by the insertion of indium wire pressed between two 0.25 in copper plates clamped together by 6 B.A. screws.

3. The Compensator

The compensator was designed to keep the target walls flat, i.e. to ensure that there was never any pressure difference between A and B. The changes which could have occurred in the vapour pressure of the liquid hydrogen in the target were due to the changes in the atmospheric pressure, or due to ortho-para conversion in the liquid hydrogen of the target, or the refrigerant. For example, a normal day-to-day variation in atmospheric pressure could change the temperature of the refrigerant by as much as 0.05°K, corresponding to a change of approximately one cm Hg in the vapour pressure of the target liquid. The change in vapour pressure due to

ortho-para conversion was a slow process in comparison, and depended on the age of the liquid hydrogen.

The compensator is illustrated in fig.(13b). It consisted of a thin flexible rubber bladder, contained within a 5 in diameter glass sphere at room temperature. The bladder was connected directly to the hydrogen-helium gas mixture in B, and the sphere to the vapour of the liquid hydrogen in A. Any pressure difference in A and B was immediately referred to the flexible walls of the rubber bladder, which automatically deflated or inflated to counteract this effect. The target chamber A, the target reservoir C + liquefying coils and the glass sphere, formed a closed system, as did the helium jacket B and the bladder. The two closed systems could be joined together by a tap T (not shown).

The overall performance of the compensator was determined by measuring, with a microscope, the variation in target thickness at room temperature against an applied pressure difference across the target window separating A and B. The results given in fig.(15) show that the compensator operated successfully over a range of approximately 45 cm Hg pressure difference. This was equivalent to a range of $\sim$ 3 cm Hg when the

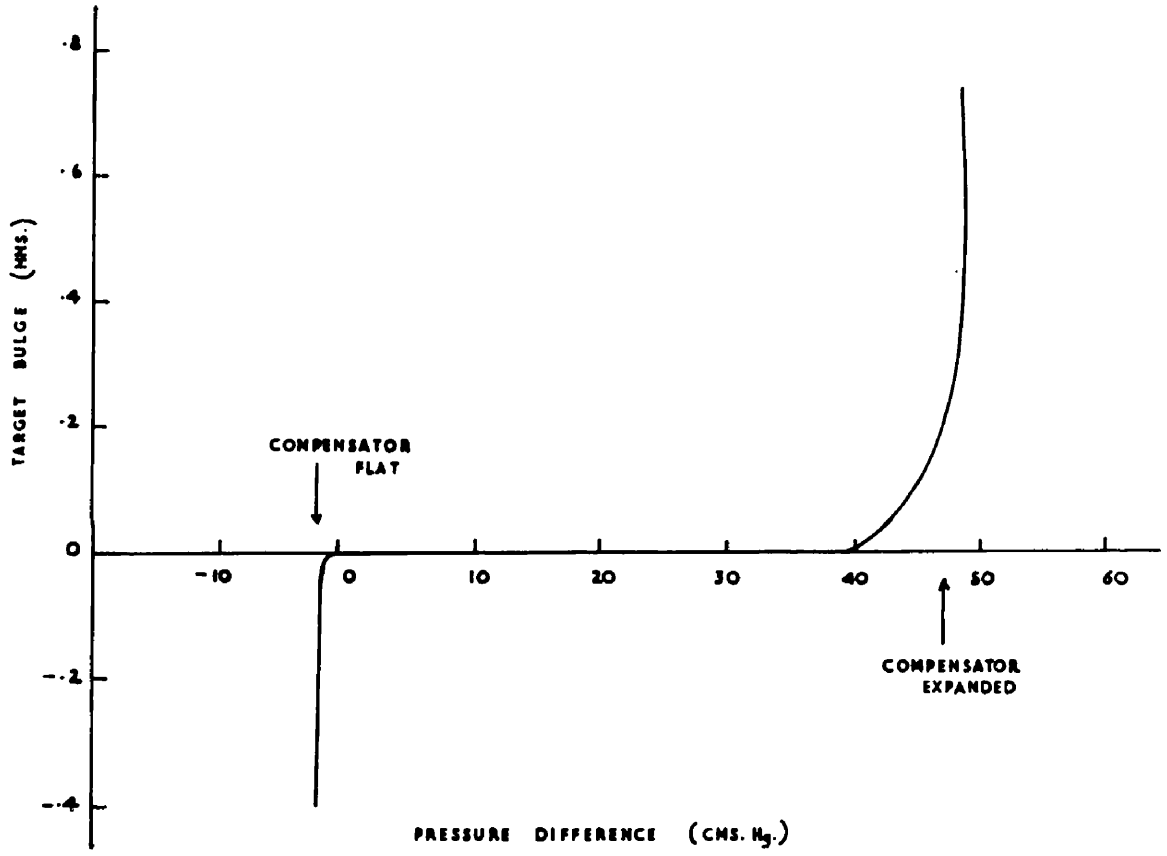

Fig.15. The variation in target thickness with pressure difference across the walls of the target slice.

target chamber was at liquid hydrogen temperatures, because the volume of the compensating gas was reduced by a factor of ~ 15 in going from room temperature ($\sim 300^{\circ}K$) to liquid hydrogen temperature ($20.4^{\circ}K$).

4. The Filling Procedure

As the filling procedure for this type of target was fairly complex, the operation will be presented for clarity in chronological steps. The target was initially evacuated to diffusion pump pressures ($\sim 10^{-3}$ mm Hg) at room temperature, and the hydrogen and nitrogen reservoirs were filled with dry hydrogen gas to one atmosphere. The tap T was opened, and the target chamber A, helium jacket, and compensator were evacuated to approximately 10^{-2} mm Hg by a backing pump. The nitrogen reservoir was then filled with liquid, and approximately 24 hours were allowed for the whole assembly to reach an equilibrium temperature. The hydrogen reservoir was then connected to a liquid hydrogen Dewar by a vacuum jacketed transfer tube, and the reservoir was filled with liquid hydrogen by judicious use of a football bladder to provide the overpressure required to fill the target.

To fill the target, hydrogen gas was passed through a cold trap to remove any moisture and through activated charcoal at liquid nitrogen temperatures to remove any impurities. The dry gas was filled in to both A and B simultaneously to a pressure of 4 cm Hg below the pressure at which liquefaction occurred. The tap T was then closed, and hydrogen and helium gas were slowly fed into A and B separately until the liquefying pressure was reached ($\sim$ 75 cm Hg). This process was carried out manually using two separate needle valves, any small pressure difference being counteracted by the compensator. The compensator was then closed off from the target system and the hydrogen gas was fed into A, only, at a few cm Hg overpressure. This was possible as the design of the target allowed the walls of A to bulge slightly outwards. The purified gas was cooled to 77°K initially by the thermal bridge and was subsequently liquefied in the coils and in the target reservoir. The target was then filled by the flow of liquid from the target reservoir into the target chamber under gravity. The pressure in B was adjusted by adding or subtracting gas until the bladder was in a semi-inflated position, the pressure in A equal to that in B. If the compensator

was approaching the extremes of its operational range i.e. fully inflated or fully deflated, it was returned to its central position by addition or subtraction of helium gas.

The background counting rate from the target was measured by removing the liquid hydrogen, and filling in the hydrogen-helium mixture into A and B with the connecting tap T open. The error in this method compared to the true background measurement with A evacuated was very small (0.4%). Rapid background measurements were possible with a previous smaller target chamber of similar design, by closing off the exhaust tube from the liquid target and supplying heat to the target liquid via the lower level indicator resistor. This forced the liquid up into the target reservoir C (fig.11) where it remained as long as heat was supplied.

5. Performance of the Liquid Hydrogen Target

The performance of the liquid hydrogen target was judged by comparison with the thin solid target which had the advantage of a well defined geometry.

The target thickness of 1.47 cm, which was measured to an accuracy of 0.3% by means of a microscope, remained

constant as long as the pressure in A, the target chamber, was equal to that in B, the helium jacket. The target thickness was chosen as a compromise between a sufficently high counting rate in the detector and the smallest possible energy loss of the pions in the liquid hydrogen. The performance of the target was improved by placing the target slice at an angle of 60^{o} to the γ-ray beam. This increased the effective target thickness presented to the beam by a factor of 1.16 and also lessened the energy degradation of the pions in reaching the detector. The π^{+} counting rate in the energy range 5 to 25 MeV for a solid angle of 3.10^{-2} ster. was approximately three per minute from the target, bombarded by a 250 MeV bremsstrahlung beam of 10^{9} equivalent quanta per minute. As the detection efficiency of the apparatus for π^{+} mesons was of the order of 30%, the counting rate in the detector would therefore be roughly one pion per minute in the low energy range. The actual average counting rate during the experiment was 0.5 meson/min, as the figure assumed above for the γ-ray flux was high.

It was of the utmost importance in the determination of the number of target protons that the angle of the

target to the γ-ray beam was accurately 60°, since an error of 2 degrees would have changed the target thickness by as much as 3%. The design of the target allowed this measurement to be easily and accurately determined. Similarly, it was essential to ensure that the exact central position of the target coincided with the centre of the γ-ray beam. The verification of this was obtained by defining the path of the γ-ray beam with a parallel beam of light passing through the target and the beam ports. The centre of the beam was defined by cross-wires attached to the beam ports and the procedure was carried out with the nitrogen radiation shield removed. The light beam, reflected through the large 60° port from the central aluminised disc (cf. fig.14) on the target wall, provided additional verification of the inclination of the target to the beam direction.

The number of pions in the absorber-out runs detected in the counter telescope was approximately one in five of the total number of events which were photographically recorded, when the liquid hydrogen target was employed. The ratio of the number of pions to the total number of recorded events with the same detection system was roughly one in twenty for a thin polythene

target. The subsequent analysis of the data was therefore much easier and less time consuming with the large reduction in the random counting rate. Corrections for dead time losses in the electronics were therefore also reduced using the hydrogen target. These corrections are more fully discussed in chapter V.

The background pion counting rate from the empty target was approximately $\frac{1}{8}$th of the full target counting rate. This background was produced mainly from the carbon and oxygen in the Melinex walls, and necessitated a background run of approximately $\frac{1}{5}$th of the total time to obtain the optimum statistical accuracy.

From the above considerations, it can be seen that the geometry of the liquid hydrogen target was as accurately determined as that of the solid target. In addition, the lower background counting rates and the considerable improvement in the efficiency of the true pion counting rate from the target protons, emphasise the importance of the liquid hydrogen target.

In designing the liquid target, an estimate of the approximate rate of transfer of heat into the target assembly was necessary in order to determine the liquid hydrogen and nitrogen loss rates. In general, heat

may be transferred by conduction, convection and radiation. Thermal gas conduction and convection can be neglected as a source of heat transfer by maintaining a vacuum of less than 10^{-6} mm Hg. The heat input to the low temperature cryostat by conduction was reduced as much as possible by use of low conductivity copper-nickel tubing. The inside of the vacuum chamber, the nitrogen and hydrogen reservoirs were lined with highly polished aluminium foil of low emissivity to reduce the heat input by radiation.

The effective heat transfer can be listed as follows:-

(1) Radiant heat inflow from the vacuum jacket to the nitrogen reservoir and radiation shield ~ 7·0 watt.

(2) Heat conducted along three copper-nickel tubes supporting the nitrogen reservoir + 4 tubes to the thermal bridge ~1·8 watt.

(3) Radiant heat inflow from nitrogen reservoir to liquid hydrogen reservoir and target assembly 0·4 watt.

(4) Heat conducted along 4 Cu-Ni tubes from thermal bridge to the hydrogen reservoir and

hydrogen target ~ 0·1 watt.

The total heat input to the nitrogen reservoir was ~ 8·8 watt, which corresponded to a rate of evaporation of liquid nitrogen of ~ 5 litres/day. The corresponding loss rates for liquid hydrogen was ~ 1·3 litres/day. These calculated values, based on cryogenic data from White (1959) were upper limits. The actual loss rates of liquid hydrogen and liquid nitrogen during the experiment were ~ 4·5 and ~ 1 litres per day.

CHAPTER IV

Detection of Low Energy π^+ Mesons

The detection of fast charged particles produced by a γ-ray beam is one of the most difficult problems in nuclear physics because of the presence of a large background radiation. The separation of particles of different mass, which do not have a characteristic decay, necessitates the measurement of two dynamic properties of the particle, which have a separate mass dependence. The detection of π^+ mesons is simplified by its characteristic $\pi^+ \rightarrow \mu^+ \rightarrow e^+$ decay, i.e. the decays at rest into a μ^+ of discrete energy 4.15 MeV with a mean lifetime of $\sim 2.5\ 10^{-8}$ sec. The μ^+ then decays at rest into a positron of variable energy with a mean lifetime of $\sim$ 2.2 microsecond.

In general, the detection of charged particles can be divided into two separate classes, visible and electronic methods of detection. The photographic emulsion and the bubble chamber are most commonly used in particle physics as visible detectors. They give very precise definition in the measurement of the energy and angle of the reaction products and provide a permanently recorded library of information. The photographic emulsion is a continuously sensitive particle detector, and the same is now true of the bubble chamber.

with the advent of fast cycling chambers, which can record every beam pulse. Pions are in general distinguished by their decay characteristic, and the range of the pion in the detector before coming to rest determines the energy. The disadvantage of this technique was the long time spent in collecting and analysing the data to achieve the required statistical accuracy. This disadvantage is however being overcome, with the availability of computers and automatic scanning devices.

The electronic detector is generally designed to count only one particular particle by means of suitable electronic discrimination. This method therefore quickly provides the required information in a given energy region, but of course, involves much careful preparation and precision. The most versatile electronic detector in high energy particle physics is the plastic scintillation counter, where the scintillation response produced by a charged particle is converted into a pulse height at the anode of a photomultiplier. The fast decay time of the plastic phosphor ($\sim 3.10^{-9}$ sec) ensures that the detector has a very fast recovery time, a most important consideration whenever large particle backgrounds are

present. For example, a background counting rate of 10^4 particles per beam pulse of one millisecond duration is equivalent to a counting rate of 10^7 particles per second. The fast response of the plastic scintillation counter enables the incorporation of the $\pi^+ \rightarrow \mu^+$ decay property as a method of separating π^+ mesons.

The most common method employed for the separation of particles of different mass is the determination of $\frac{dE}{dx}$ and E, where $\frac{dE}{dx}$ is the rate of energy loss of a particle and E is the energy. It can be shown (Keck et al, 1952, Wolfe et al, 1955) that to a good approximation

$$\frac{dE}{dx} \propto \frac{M^{0.45} Z^{1.1}}{R^{0.45}}$$

where R is the range of the particle of mass M and charge Z. It is therefore possible to distinguish single-charged particles of different mass M having the same range by a measurement of $\frac{dE}{dx}$

The detection of low energy positive pions near threshold presents an even more difficult problem because of the low production rate and the small penetrating power of the pions. It is therefore essential that a low energy pion detector can separate the π^+ mesons from

the large background of electrons, protons and Y-rays and possess a high detection efficiency. Two methods have been developed combining the electronic and visible techniques for the detection of low energy π^+ mesons. The first method to be described, distinguished the mesons by a time of flight technique (Lewis, Gabathuler and Azuma, 1960), and the second method was an improved version of a fast delayed coincidence technique, initially developed by Lewis and Azuma (1959). The description and performance of these two detection methods are presented in this chapter.

2. Detection of π^+ Mesons by Time of Flight

The separation of low energy π^+ mesons was possible, theoretically, by correlating graphically the energy E of the particle and the inverse of the velocity, i.e. the time interval for a given path length as shown in fig.(16). An increase in the particle separation was easily obtainable by increasing the flight path (ℓ), but this had the adverse effect of decreasing the solid angle of detection ($\propto 1/\ell^2$). Conversely the possibility of a very short flight path could only be entertained by increasing the resolving power of the timing machine.

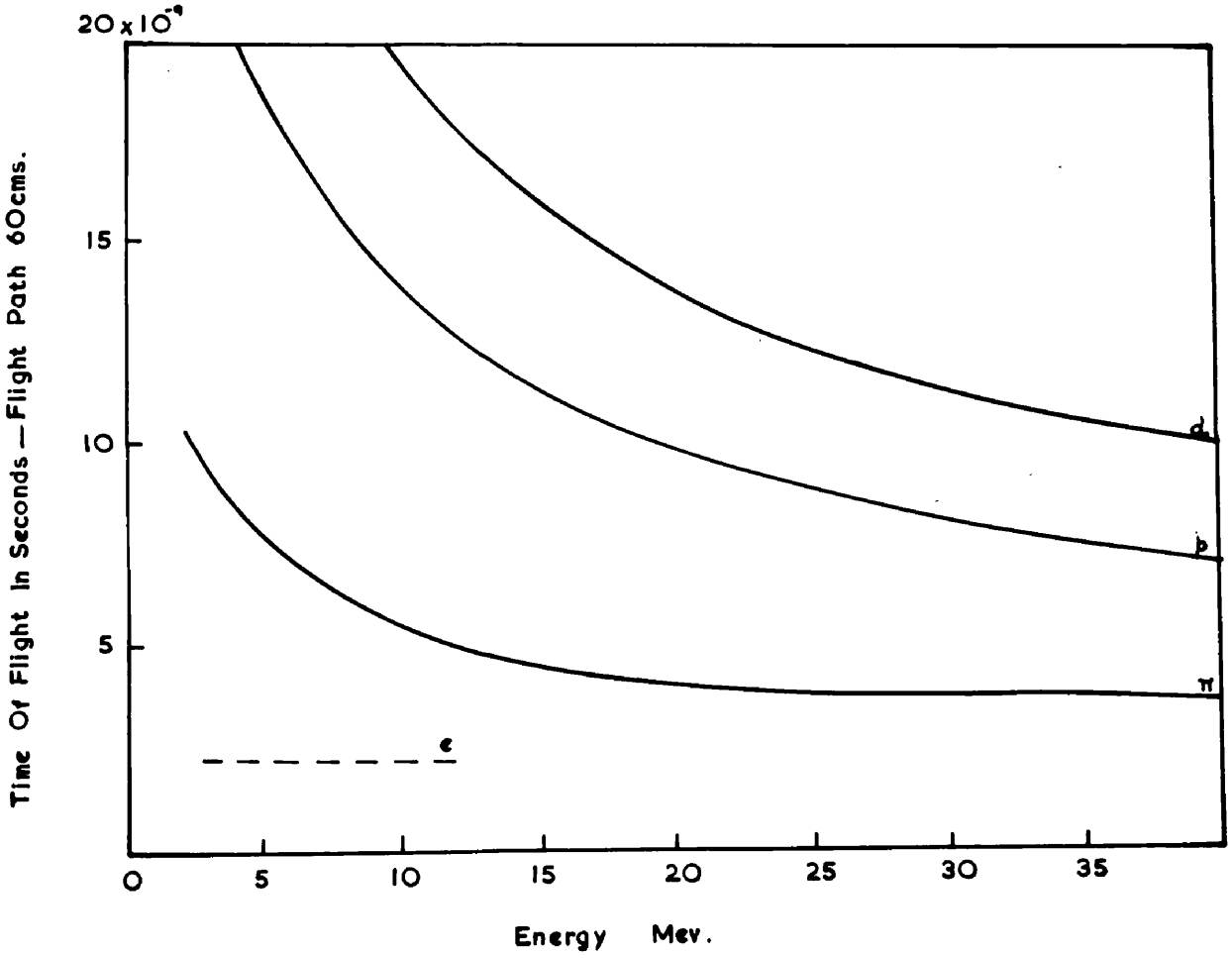

Fig.16. Graph of time of flight versus energy showing the separation between electrons, pions, protons and deuterons for a 60 cm. flight path.

In order to obtain the shortest possible resolving times, high speed electronics were therefore essential for the optimum detection of low energy π^+ mesons.

The π^+ meson detector is shown schematically in fig.(17a). The flight path was defined by two N.E.102 plastic scintillation counters, counter 1 (1.5 x 1.5 x 0.03 in) and counter 2 (3 x 2 x 1 in) placed 60 cmapart. The convention employed in giving the dimensions is height x width x thickness of scintillator. Pulses from the collectors of the two counters turned off E 180 F limiter valves, which generated rectangular pulses of 3.10^{-8} sec duration. These two pulses overlapped and operated the time analysing coincidence unit illustrated in fig.(17b). This latter unit consisted of a 6BN6 gated beam valve, which has the property of producing a current pulse at the anode, whenever two uniform pulses applied to the separate grids of the 6BN6 overlap in time (Janes and Kraushaar, 1954, Azuma and Lewis, 1957). The conversion of time to pulse height was accomplished by integration of the current output of the 6BN6. The integrated pulse was then amplified and fed through a cathode follower output.

This pulse, whose height was proportional to the

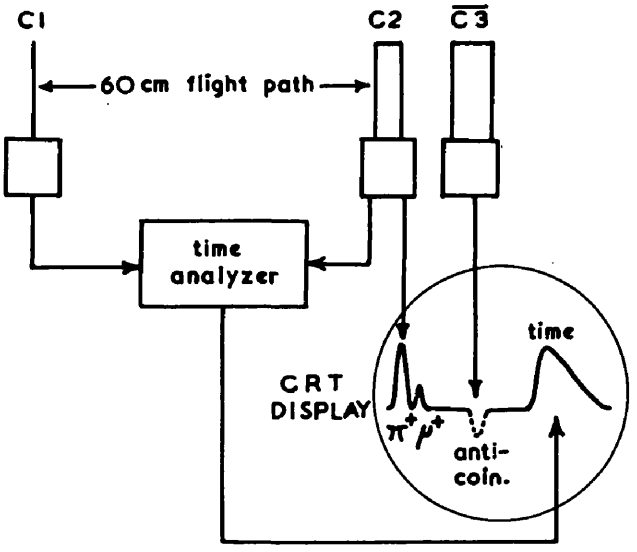

Fig.17a. Detection system and mode of display.

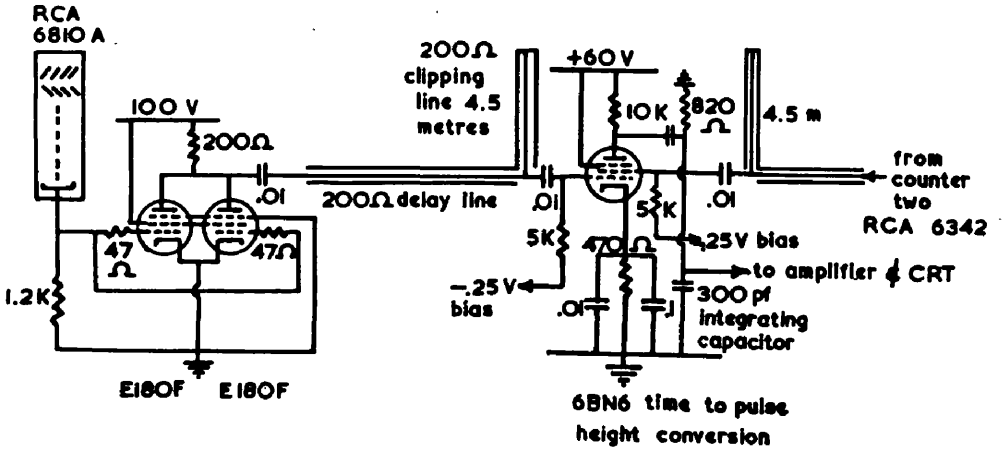

Fig.17b. Time analysing circuit.

time of flight, was used to trigger a Tetronix 517A oscilloscope and was also simultaneously displayed on the fast time sweep as a delayed pulse (fig.17a). The individual oscilloscope traces were photographed on Ilford H.P.3 film. On this same trace was also displayed the energy pulse from the 7th dynode of counter 2. To increase the power of the device, and to help the assessment of the method, the dynode pulses from counter 2 were led into 100 ohm cable to give pulses approximately 10^{-8} sec wide. This output pulse from the 7th dynode of the R.C.A. 6342 had been examined for linearity against the scintillation response of the counter over the complete energy range under investigation, by a calibrated hydrogen discharge tube (Leith, 1959). The π^+ particle was then identified and properly recorded, as both the π^+ and μ^+ decay pulse were displayed as separate entities on the trace of the oscilloscope (5.10^{-8} sec/cm), provided that the pion lived longer than $\sim 10^{-8}$ sec. The time distribution could therefore be plotted and checked with the $2.5\ 10^{-8}$ sec pion lifetime.

Counter 3 served as an anticoincidence counter for particles which passed through counter 2. The

pulses from counter 3 were appropriately delayed and displayed on the trace with inverse polarity (fig.17a), so that traces exhibiting such pulses were rejected in the analysis. Unless the anticoincidence pulse was provided, particles passing through counter 2 only gave up a fraction of their energy and therefore produced uncorrelated events in the time of flight versus energy graph.

The perameters which were in fact measured during the experiment, were the pulse height corresponding to the time of flight of the particle and the scintillation response S,defining the energy E of the particle. The apparatus had, therefore to be calibrated for pulse height against time of flight, which also verified the linearity of the device. The resolving power of the timing system was also of interest in assessing the shortest flight path which could be chosen, without losing particle separation. An approximate time calibration was effected with the aid of the more energetic electrons from an In^{114} β-ray source passed into the system. Various lengths of 200 ohm delay cabling were then inserted between the counters and the time analysing unit. A plot of pulse height versus metres

delay is illustrated in fig.(18b) verifying the linearity of the apparatus. This time calibration, however, when applied to mesons and protons, could be uncertain by $\sim 10^{-9}$ sec because of the variation in pulse rise time as a function of the pulse height.

A resolving time of 7.10^{-10} sec (fig.18a) was obtained with the system using an indium source, when pulse height selection methods were employed. The latter consisted of taking slow dynode pulses from each counter, which were amplified and fed through discriminators into a Rossi coincidence unit of $\sim$1 microsecond resolving time. The output from this unit was supplied as a gate pulse to a Hutchinson-Scarrot type multi-channel kicksorter in coincidence with the amplified pulses from the fast coincidence box. By adjusting the discriminator bias, only those pulses produced by the very energetic β-particles were selected. The advantage of this method was that the resolving power of the fast coincidence unit was measured under conditions similar to those in an actual experiment.

The most difficult technical problem associated with the counter system, was the light collection efficiency required by counter 1 to produce a strongly

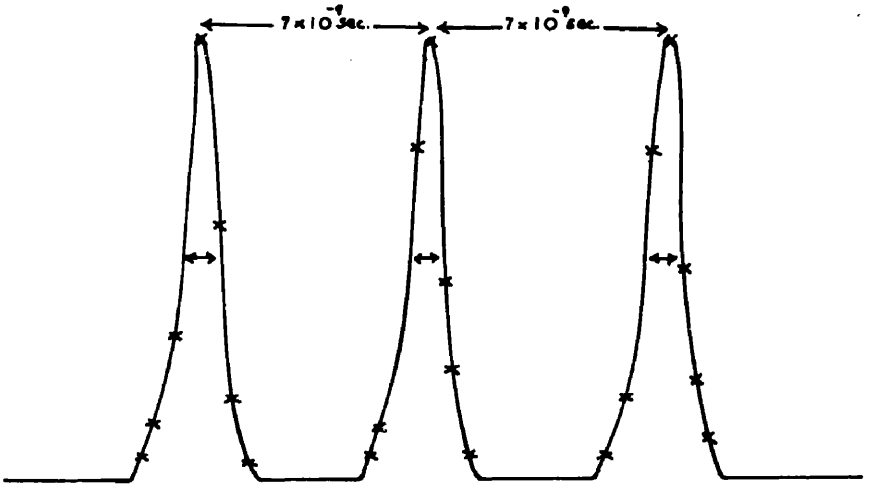

Fig.(18a). Resolving time of apparatus as displayed on kicksorter using pulse height selection methods.

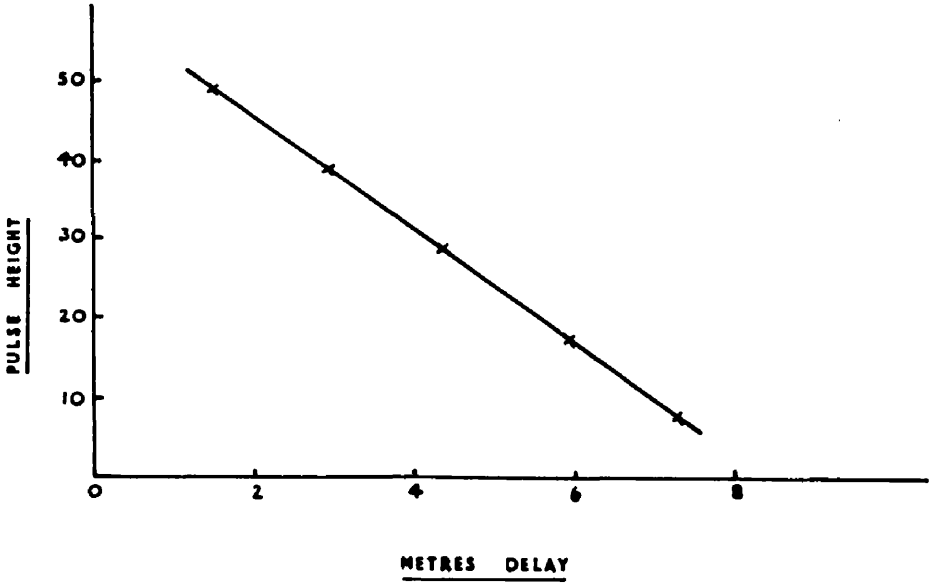

Fig.(18b). Linearity of apparatus obtained by inserting delay cable between C_1 and C_2

limiting pulse at the collector for a fast charged particle. An obvious way of avoiding this difficulty was to increase the thickness of the thin scintillator, but this was prevented by multiple scattering in the plastic material. For example, a 10 MeV pion suffers a deviation of $\sim 15^{\circ}$ in traversing 0.25 in of plastic scintillator, and therefore would not have entered counter 2, separated by 60 cm from counter 1. A specially designed crystal holder coupled to an R.C.A. 6810A photomultiplier, which had superior gain to the R.C.A. 6342, was therefore constructed to overcome this difficulty.

The crystal mounting comprised a cylindrical can, 2.5 in diameter and 4 in in length, containing 2 in. ports for the particle windows. The inside of the container was lined with Plaster of Paris, and the innermost particle windows were of highly reflecting aluminised Melinex, which was found to improve the light collection efficiency by as much as 20%. The energy resolution capabilities of the thin front counter were 50% full-width at half-height using 280 keV Hg^{203} γ-rays. The energy resolution of counter 2 was measured as 14% using the 2.6 MeV γ-ray from Th C^{II}.

The time of flight telescope was set up at

approximately 120° to the Y-ray beam of the Glasgow synchrotron, with the front crystal 8 in from a $\frac{1}{8}$ in. thick polythene target, viewed approximately end-on. The 60 m flight path was evacuated by means of a large 5 in diameter aluminium tube, with 0.001 in Melinex windows, to minimise scattering and absorption in the air. All the photomultipliers were magnetically shielded from the stray synchrotron magnetic field by mu-metal shields. The synchrotron was operated at 320 MeV and the duration of the beam was ~ 600 μ sec.

The film records of the individual traces were analysed and the results plotted. The results of one of a series of experimental runs is illustrated in fig.(19). From this figure, it is seen that the mesons (o), identified positively by the presence of the decay pulses, all lie on the lower band, which is distinct and apart from the upper band of particles, which were predominately protons. The lower band also contained π^+ mesons, which had decayed in such a short time that the μ^+ decay pulse was not distinct from the π^+ pulse, and also μ^+ mesons from π^+ decays in flight. The combined number of these was expected to be of the same order as that of the identified π^+ mesons.

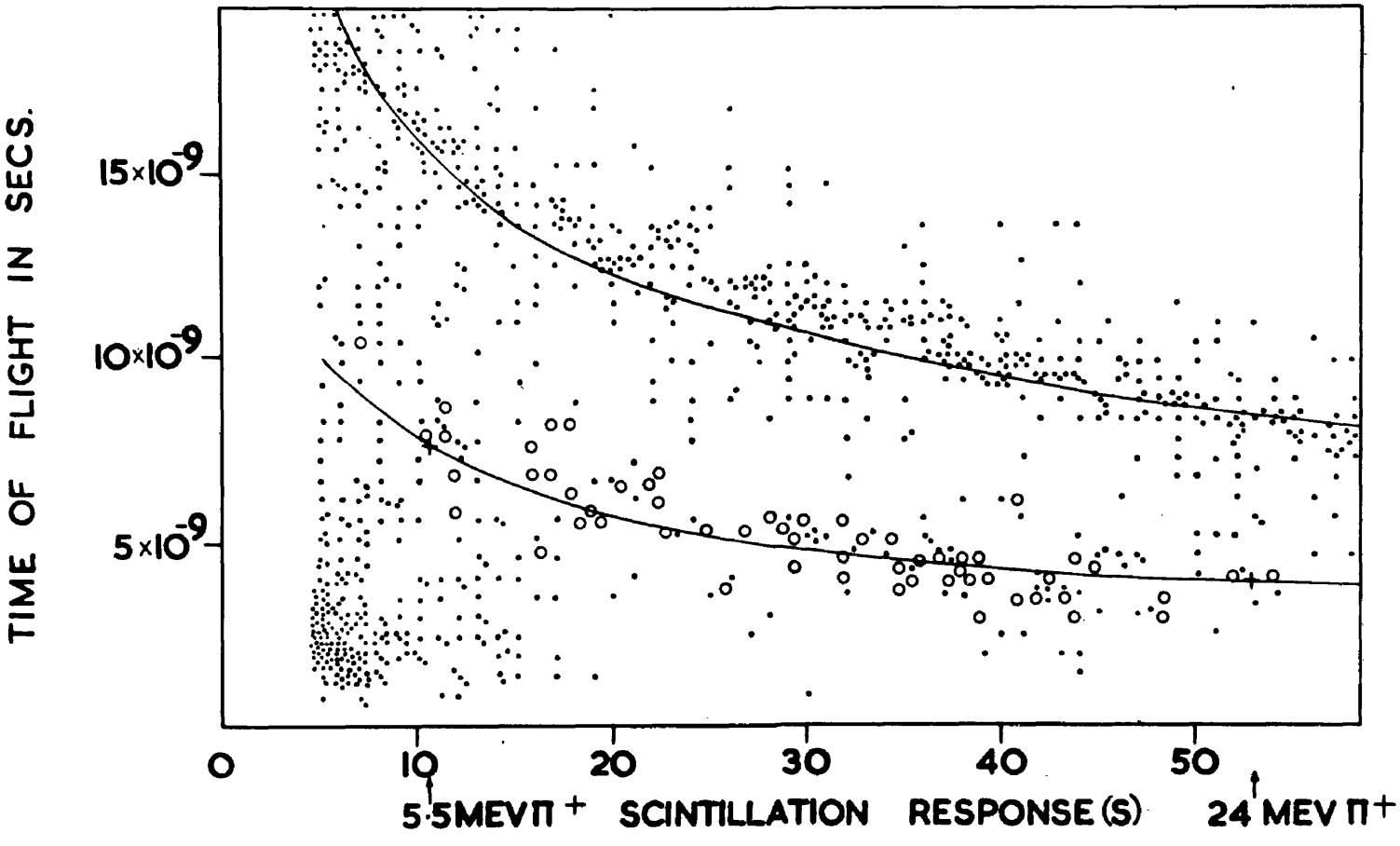

Fig.19. Experimental results showing time of flight plotted against the scintillation response S , defining the energy E of the particle. For details, see text.

Some π^- mesons also contributed to the space between the bands, since the energy released in the main counter from the π^- stars displaced these points from the π^+ band.

The meson curve was to some extent self-calibrating. The π^+ mesons have a maximum energy of 24 MeV, corresponding to their range in the 1 in scintillator. Since the π^+ decay at rest in isotropic in direction, only 50% of the pions which decayed at the rear surface of the counter recorded a μ^+ in the counter. This cut-off provided a high energy calibration point. A low energy calibration point was then obtained from the constant μ^+ pulse height by the Seitz relation (Taylor et al 1951), since the ratio of the π^+ mass to μ^+ mass is close to unity. This relation states that the pulse height from a π^+ particle of energy 4.15 x 1.33 equal to 5.5 MeV is given by 1.33 times that of the μ^+ particle. Two energy calibration points were therefore obtained and the time of flight associated with these meson energies calculated. These two check points are indicated in the meson band (+) and were consistent with the previous time calibration.

The fluorescent response S of organic scintillators

to heavy ionising particles is known to be non-linear. Birks (1951, 1953) has derived the expression

$$\frac{dS}{dX} = \frac{A \frac{dE}{dX}}{1 + kB \frac{dE}{dX}}$$

where $\frac{dE}{dX}$ is the specific energy loss, and A and kβ are constants for a given scintillator. The scintillation response of N.E.102 for protons has been examined by Evans and Bellamy (1959) and by Gooding and Pugh (1960). They found that above relationship was closely followed for kβ = 0.01. Assuming that the same relationship also holds for π^+ mesons, the upper curve was drawn for protons and the lower one for pions. The curves were consistent with the experimental points. It was hoped that the experiment might have given a quantitative measurement of the degree of non-linearity between S and E, since this could be a source of error in any accurate π^+ experiment involving pulse height measurements. However, the uncertainty in the time calibration and the lack of π^+ statistics did not make any quantitative measurements of the non-linearity possible. The experimental results were consistent with the prediction that the effect is small for π^+ mesons.

The results of the experiment provided the first evidence that it was possible to separate pions from protons and electrons in the low energy region. For pion detection from γ-rays, the difficulties appear increasingly at the lowest energies, where the random counts are evident below 4 MeV (fig.19). For reliable pion detection, it is therefore essential to overdetermine the pion by the additional inclusion of $\pi^+ \rightarrow \mu^+$ identification.

The main disadvantages of this method for accurate experimental determinations of low energy π^+ cross-sections are the small solid angle of the detector to the target, and the uncertainty in the time calibration. The corrections for π^+ decay in flight and multiple scattering in the front scintillator would also introduce uncertainties in the evaluation of the cross-sections. Any attempt to increase the dimensions of the main counter in order to obtain a larger solid angle decreases the resolving power of the device, because of the time taken by the light signals to reach the photomultiplier from different parts of the phosphor.

The method, however, does indicate the difficulties involved in detecting low energy pions and did in fact provide the starting point for the development of the

second method, which will be described in section 3. Time of flight methods have been successfully incorporated into the separation of K^+ mesons from pions and protons, using magnetic spectrometers at narrow angles to the γ-ray beam by Donoho and Walker (1957), and McDaniel et al (1958).

3. π^+ Detection by Delayed Coincidence

The π^+ electronic detection methods, which have been considered so far in this chapter, have employed variables which have a separate mass dependence to provide the discrimination between the various particle groups. In the time of flight technique, the $\pi^+ \rightarrow \mu^+$ decay was incorporated as an additional labelling of the low energy positive pion. In the delayed coincidence detection method however, the $\pi^+ \rightarrow \mu^+$ decay provided the basic identification of the pions, and the mass discrimination was incorporated for additional π^+ separation.

If the π^+ mesons are brought to rest in a time which is short compared to their lifetime, then the majority of these pions will decay at rest. Hence only one single counter in principle is required for the

separation of π^+ mesons for energies up to a maximum determined by the thickness of the counter. The advantage of this system over the previous method is immediately obvious, since a single counter can be placed close to the target, subtending a much larger solid angle of detection, i.e. a greater counting rate.

When the detector was operated in the presence of electrons and γ-rays, it was possible to simulate the $\pi^+ \rightarrow \mu^+$ decay, and therefore a thin plastic scintillation counter was inserted immediately in front of the main counter for unambiguous detection of low energy pions. An additional method of identification was included by examining the rate of energy loss in the thin front scintillator, which greatly simplified the subsequent analysis.

The counter telescope and mode of display are illustrated schematically in fig.(20). The thin counter consisted of a N.E.102 plastic scintillator 3.25 x 2.06 x 0.025 in, coupled to an R.C.A. 7265 photomultiplier, and a 3 x 2 x 1 in scintillator coupled to an R.C.A. 6342 photomultiplier constituted the main counter. The arrival of a π^+ meson in the main counter produced a pulse at the collector of the photomultiplier, turning

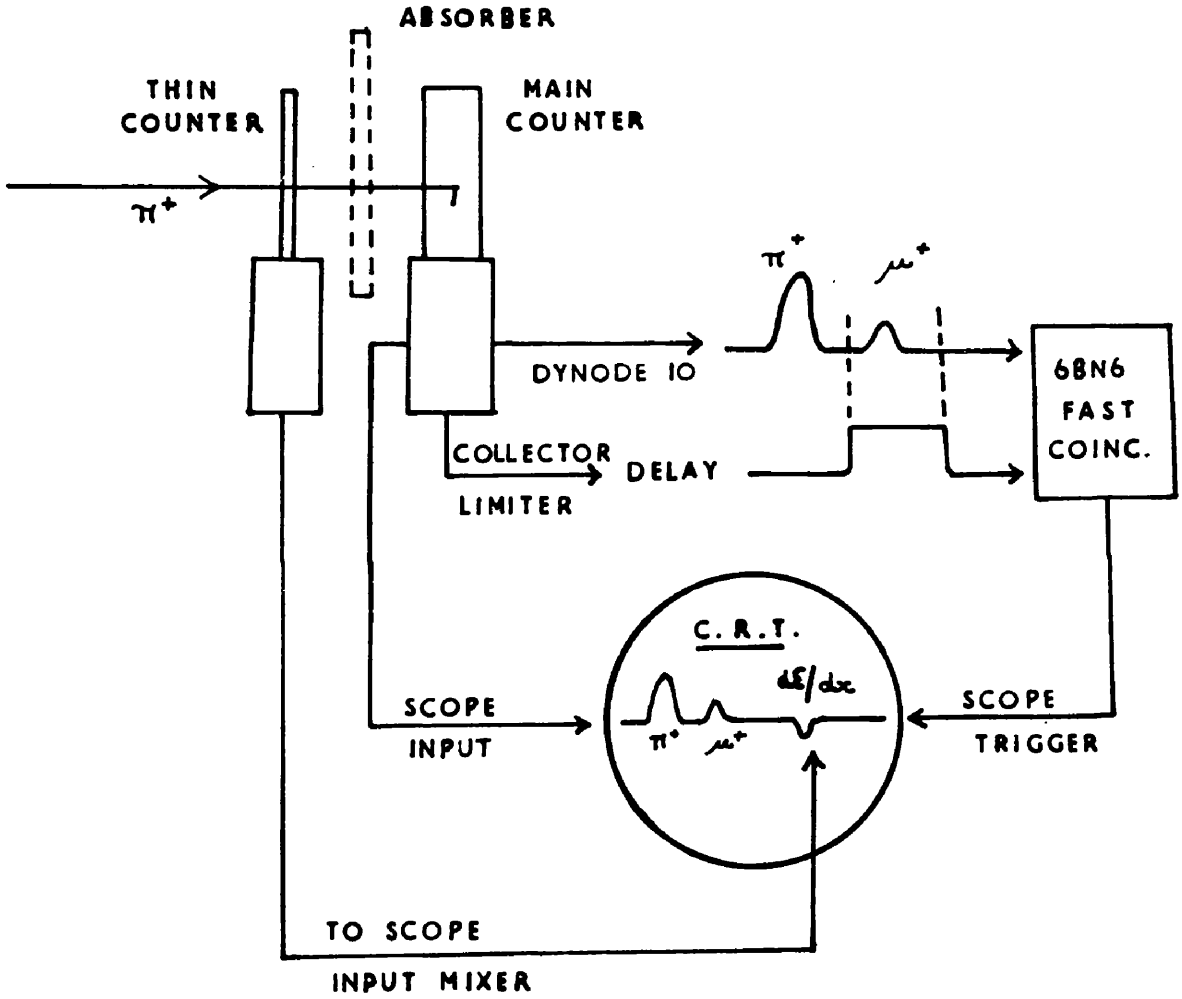

Fig.20. Detection system and mode of display. The pion passes through the thin counter and comes to rest in the main counter. A coincidence between the μ^+ pulse from dynode 10 and a delayed rectangular π^+ gate pulse from the collector operates the 6 BN 6 coincidence unit.

off two E 180 F limiter valves, which generated a rectangular pulse of 3.5 10^{-8} sec duration, similar to the previous method. This gate pulse was then delayed before being applied to one of the grids of the 6BN6 fast coincidence unit. The output pulses from dynode 10 of the main counter led directly into 200 ohm cable in order to keep them as short as possible, so that the π^+ and μ^+ pulses were distinct. The length of the tails of these dynode pulses were further reduced to provide additional $\pi^+ - \mu^+$ distinction by the insertion of a 0.5 metre 200 ohm clipping line terminated by an 80 ohm resistance. These pulses were then amplified by a Hewlett-Packard A type distributed amplifier and fed directly to the other grid of the 6BN6 fast coincidence unit. This unit was then activated if the pulse produced by the μ^+ decay particle appeared in coincidence with the rectangular gate pulse as shown in fig.(20). The coincidence unit therefore operated over a known interval of the $\pi^+ \rightarrow \mu^+$ decay curve, determined by the duration of the rectangular gate pulse. The output of the fast coincidence unit was used to trigger the time-base of a Tetronix 517A oscilloscope operated at a sweep speed of 2.10^{-8} sec/cm.

The output from dynode 8 of the main counter led into a 100 ohm cable to give pulses of approximately 10^{-8} sec duration, which were delayed and subsequently displayed, via a mixer unit, on the trace of the oscilloscope. Any event was therefore identified since both the π^+ pulse and its 4.15 MeV μ^+ pulse were displayed on the trace. Any π^+ meson produced in the target and stopped in the main counter must have passed through the thin counter. The μ^+ meson however produced from a pion of energy greater than 4 MeV in the main crystal would not pass through the thin counter and this provided a powerful method of π^+ detection, if the thin counter pulse was also displayed on the oscilloscope. The output from the thin counter was delayed, mixed opposite in phase with respect to the output display from the main counter in the mixer unit, and displayed on the oscilloscope as shown in fig.(20). The individual traces were then photographed on Ilford H.P.S. film.

A complete chart of all the delayed coincidence events which could trigger the oscilloscope are presented in fig.(21), as they would appear on the trace. Event 2 was produced by the passage of two charged particles into

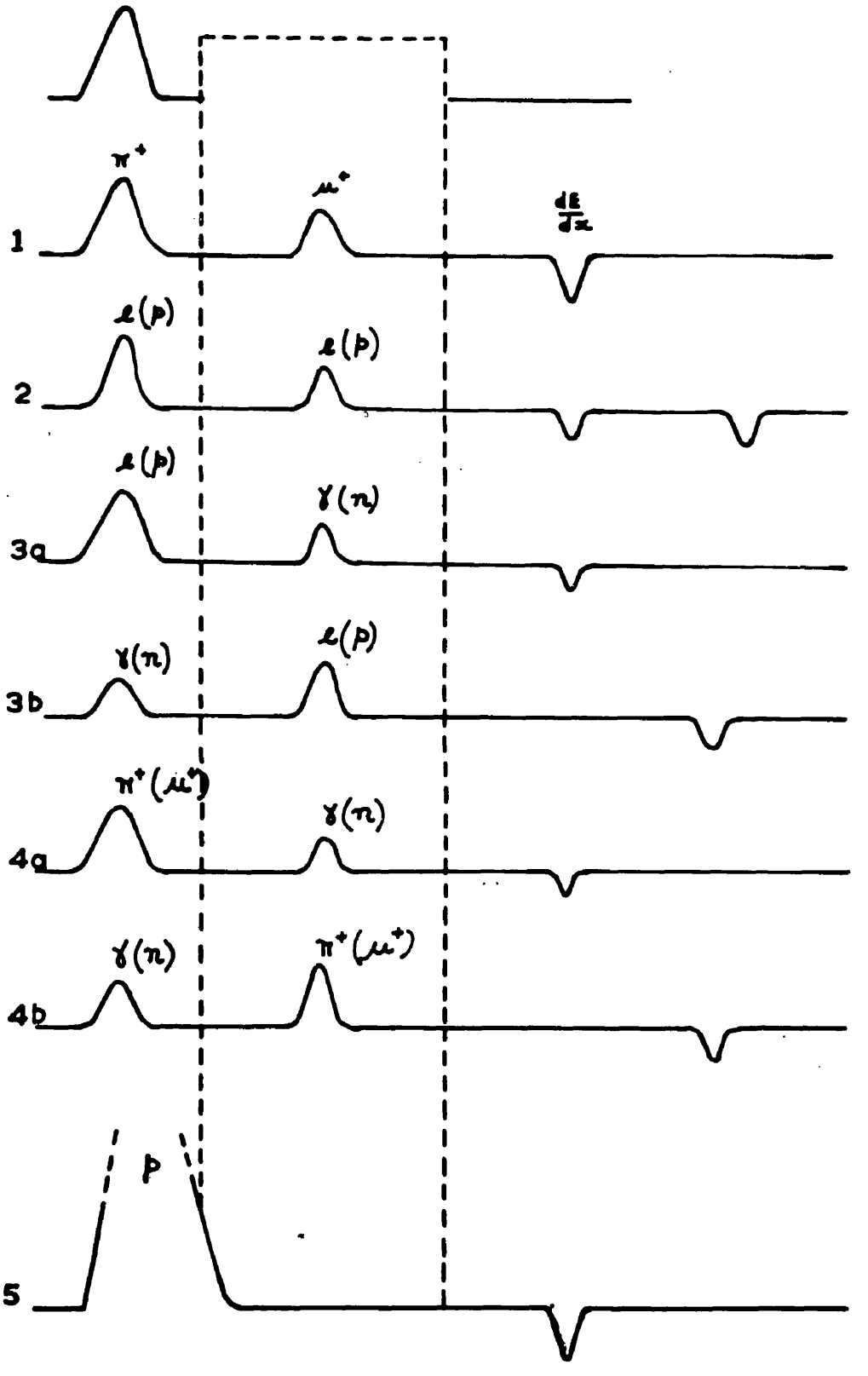

Fig.21. A complete chart of all displayed events which activated the detection system.

the main counter, with the correct time sequence, the later particle giving the same pulse height as the μ^+ meson. This event was easily discarded by the double thin counter pulse. The most common random event which simulated a real pion was due to a charged particle followed by a γ-ray (3a,4a). Since these events were random in time, their inverse must have occurred with equal probability, i.e. a γ-ray of the required energy followed by a charged particle (3b,4b). These inverse events were distinguished from the random events by the position of the thin counter pulse on the trace. Event 5 occurred because the tail of a large pulse, produced by an energetic proton or cosmic ray particle, was in coincidence with the rectangular gate pulse and was readily discarded. This "single" event could have been prevented by introducing extra delay into the collector channel, which then would have separated the gate from the large "single" pulse. This step was avoided as far as possible because it caused a rapid reduction in the detection efficiency due to the exponential nature of the $\pi^+ \rightarrow \mu^+$ decay. The reasons for making the dynode 10 pulses as short as possible and removing the tails of these pulses can now be

clearly understood.

The additional criterion of $\frac{dE}{dx}$ measurement of the thin counter pulse made it possible to distinguish the events of type (3a) and (3b). However event (4a) was not directly recognisable as a random event, since it gave the correct $\frac{dE}{dx}$ pulse height. This event was produced by a π^+ which had rapidly decayed into a μ^+ pulse, or had not decayed within the duration of the rectangular gate, followed by a γ-ray of the correct energy. It was however possible to estimate the number of these events indirectly from a measurement of their inverses (4b). A plot of $\frac{dE}{dx}$ versus E, the main counter pulse height for pions of energy up to 25 MeV produced from the liquid hydrogen target, is presented in fig.(22). As expected, the random $\ell - \gamma$ and their inverse $\gamma - \ell$ events appeared in roughly equal numbers in the left hand corner. The number of random events of type (4a) was very small, since their inverses (o) lying in the meson band were few in number ($\sim 1\%$). From fig.(22), it can be seen that the incorporation of $\frac{dE}{dx}$ and E measurements into the decay detection system provided a very powerful tool for the unambiguous detection of π^+ mesons down to

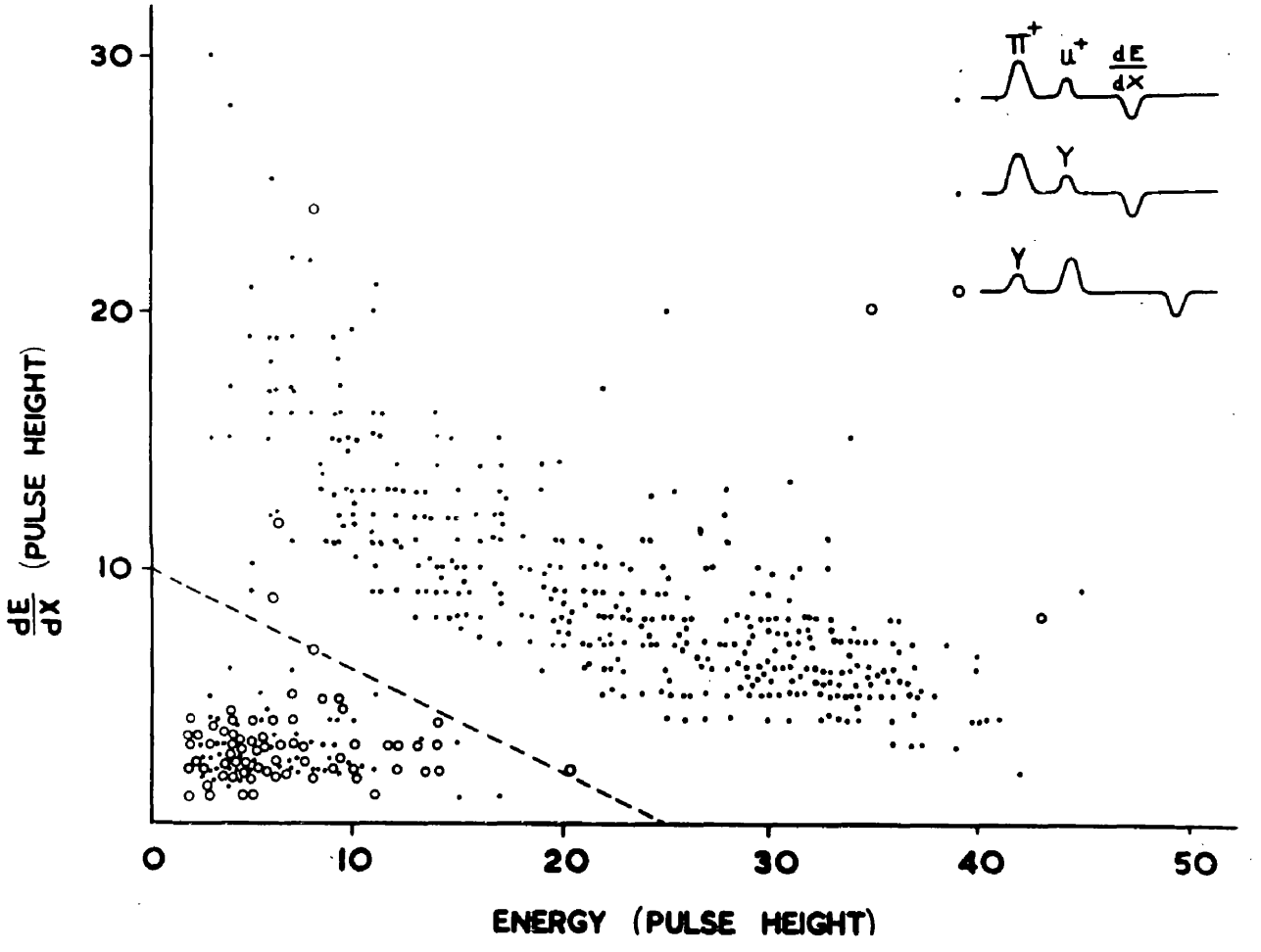

Fig.22. A plot with no absorber of thin counter pulse height against main counter pulse height showing the meson band (·). Note that the random e - γ coincidences and their γ - e inverses (o) are apparent in roughly equal numbers in the left-hand corner.

4 MeV.

As the thin counter provided information on the rate of energy loss $\frac{dE}{dx}$ of the particles entering the main counter, its energy resolution capabilities, i.e. light collection efficiency, was a very important consideration. The crystal holder consisted of an aluminium container coated on the inside with aluminium oxide. The thin scintillator was coupled by a perspex light guide to an R.C.A. 7265 photomultiplier, which was chosen for its high photo-cathode sensitivity. The thickness of the light guide was 0.25 in to prevent Cerenkov effects, and the innermost foils of the particle windows were highly reflecting 0.001 in aluminised Melinex. The pulse height resolution of the thin crystal was then measured, selecting by a coincidence method the very energetic β-rays of In^{114} (~ 2 MeV), which traversed the thin counter. The resolution obtained by this method was 60% full width at half-height.

The maximum energy Compton electrons of the 2.64 MeV γ-rays of Th C^{II} have a scintillation response in plastic, which is equivalent to that of a pion of ~ 4 MeV and just less than that of the μ^+ meson. This source therefore enabled the time gate to be set up and also

the length and resolution of the gate to be approximately determined, by inserting artificial delay between dynode 10 and the collector of the main counter. The main discrimination against unwanted events, e.g. low energy electrons and "single" events, triggering off the oscilloscope trace was provided by the trigger amplitude of the Tetronix 517A, which discriminated on the output from the fast coincidence unit.

In order to ensure that the detection system did not discriminate against the lowest energy π^+ mesons, a method was developed by Dr. G.M. Lewis which provided an accurate knowledge of the trigger amplitude setting. The main counter dynode 8 display pulses from the input mixer unit were amplified, lengthened and fed into the input display channel of a C.D.C. 100 channel kicksorter. A positive gate pulse, obtained from the Tetronix 517A was led into the coincidence channel of the kicksorter as shown in fig.23a. The Compton spectrum of the γ-rays of Th C'' in the main counter was then displayed either independently ("ungated" spectrum), or only in coincidence with the output from the 6BN6 coincidence unit ("gated" spectrum). The latter choice was obtained by adjusting the 200 ohm delay cables to the 6BN6 unit to give prompt coincidences,

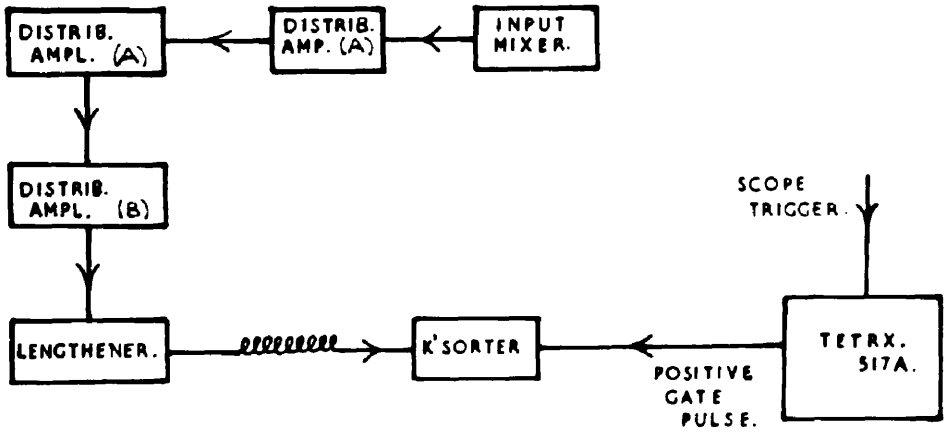

Fig.23a. Schematic diagram of method of kicksorter display.

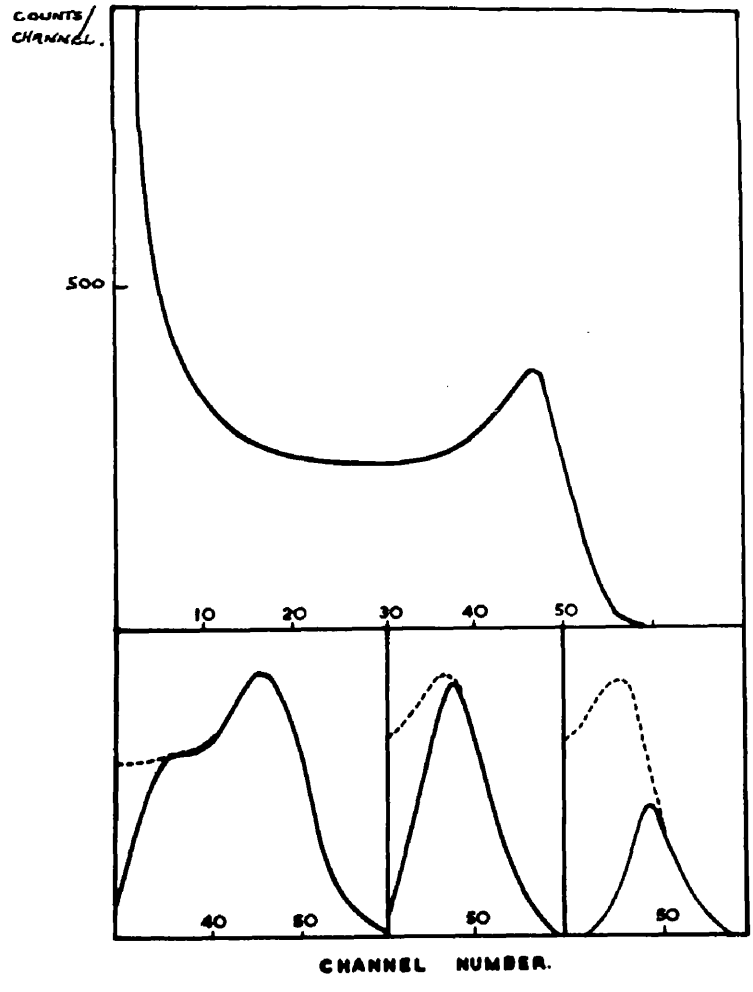

Fig.23b. The complete "gated" ThC" compton spectrum together with partial spectra corresponding to different trigger settings.

i.e. the dynode 10 signal occurred inside the rectangular pulse of the collector. Fig.23b shows the complete "gated" Th C^{11} Compton spectrum, corresponding to zero bias on the trigger amplitude, together with partial spectra, corresponding to various settings of the trigger amplitude of the oscilloscope. This kicksorter display method was therefore capable of providing an accurate visual assessment of the setting of the trigger amplitude discriminator.

The detection system was tested by preliminary machine runs using thin polythene targets. The validity of the detection system was checked by observing the counting rate for different E.H.T. voltages of the main counter and different settings of the trigger amplitude. Measurements of the cross-sections of pions from polythene were also carried out and the results were in accord with those of Lewis and Azuma (1959). Similar tests were also carried out when the apparatus was placed at an angle of 60^{o} to the γ-ray beam direction, proving the validity of the detection system despite the fairly high background.

The detection system was therefore in an operational condition, and the experimental measurement of the

cross-section for π^+ production from the hydrogen target was then carried out as is described in chapter V.

CHAPTER V

The Determination of the π^+ Cross-section from Hydrogen

1. General Experimental Method

The general lay-out of the experiment in the beam of the Glasgow University synchrotron is shown in fig.(24). The bremsstrahlung beam passed through the evacuated target chamber and intersected the liquid hydrogen target, which was inclined at an angle of 60° to the beam direction. The counter telescope was placed at an angle of 58° to the direction of the beam, with the main counter 13 in from the centre of the target. The main counter was separated from the thin counter by approximately one inch. A 0.25 in thick copper screen was inserted in a fixed position between the two counters, allowing a higher range of pion energies to be detected.

The electrons in the synchrotron were accelerated to an energy of 250 MeV before traversing the 0.06 in diameter tungsten wire to produce the bremsstrahlung beam. The duration of this beam was kept as long as possible during the entire experiment ($\sim$2 millisec.) and this was an important factor in the success of the experiment. The bremsstrahlung passed through a 0.25 in defining collimator, through two scrubbing magnets and finally

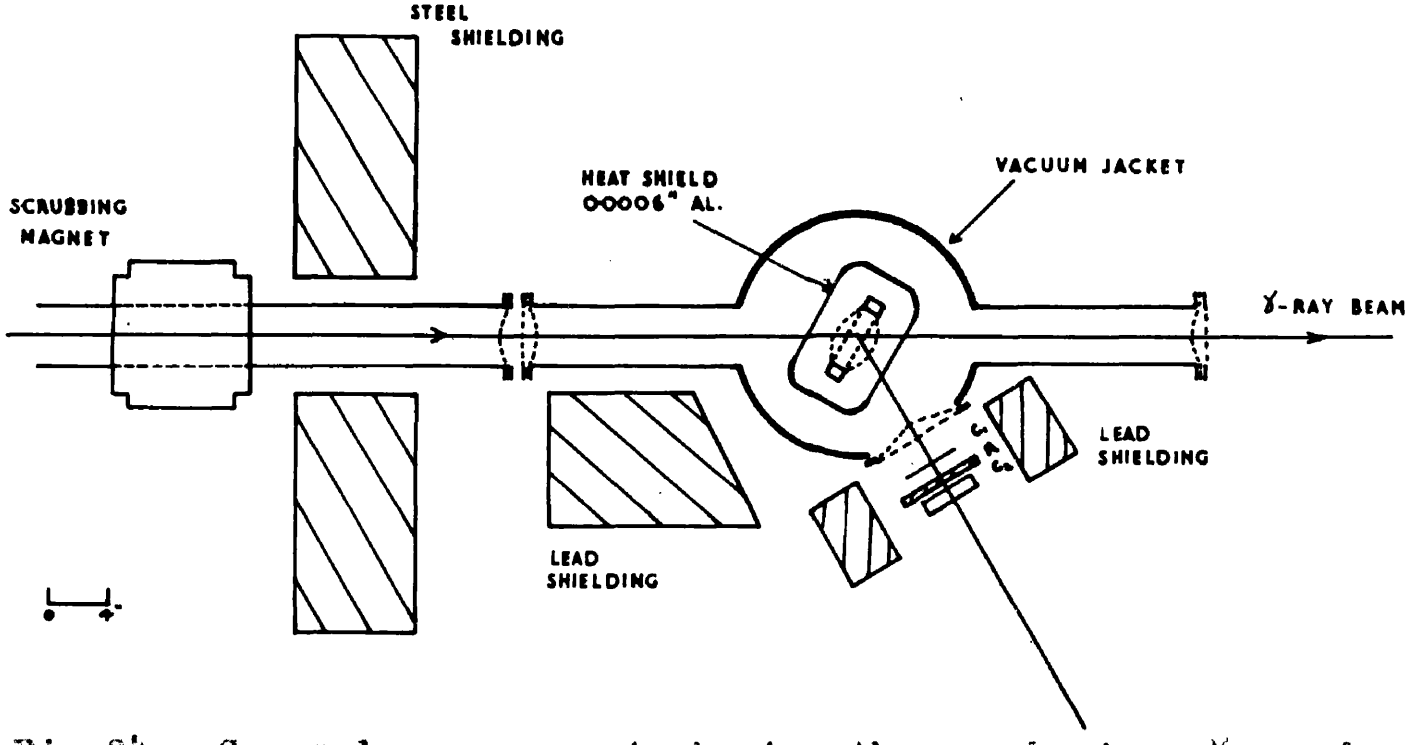

Fig.24. General arrangement showing the synchrotron γ-ray beam, the hydrogen target and the counter system.

into the quantameter of the type developed by Wilson (1957) at Cornell. A vacuum system extended from the beam window of the vacuum jacket through the sweeping magnet to the collimator to minimise the electron background. Lead and iron shielding blocks, which prevented any stray radiation from entering the counters, were positioned so as to avoid possible pion scattering into the telescope. The maximum diameter of the beam at the target was 1.25 in, providing a one inch clearance from any metal parts of the target and vacuum system. The energy of the γ-ray, which produced the maximum energy π^+ meson detected by the telescope was 196 MeV. The maximum beam energy of 250 MeV was therefore chosen to prevent scattering of a high energy pion into the detector from the target walls. Any further reduction of the maximum beam energy would entail a very detailed knowledge of the shape of the upper region of the bremsstrahlung spectrum.

As the experiment was of 3 weeks duration, every effort was made to ensure that the counter system remained stable in operation throughout the entire run. A 1% stabilised voltage regulator provided the A.C. supply for the counter telescope and the oscilloscope, and a

stabilised heater supply was provided for the limiters and the fast coincidence unit. The E.H.T. voltage of the main counter was checked and recorded every morning and evening, and remained constant throughout the experiment. A continuous monitor of the stability of the apparatus was of course provided by direct examination of the pulse height of the μ^+ meson, recorded on the film. Rough subsidiary checks were also obtained by photographing Th C^{11} pulses every evening using prompt coincidences. A direct method of checking the overall stability was performed every morning and evening using the kicksorter display method previously described. The display of the "ungated" Th C^{11} spectrum recorded for a given time interval provided direct evidence of the stability of the main counter and mixer unit. The stability of the oscilloscope and fast coincidence channel were determined by the position of the cut-off in the overlap coincidence spectrum. The trigger setting of the oscilloscope was however not critical, as it was possible to reduce the discrimination level slightly, without any undue rise in the counting rate of the detector. The counter system was able to record mesons down to an energy of 3 MeV in the 1 in counter from the

hydrogen target.

The kicksorter display method was also employed during the experiment to check the efficiency of the gate for all pions which decayed within the time interval of the gate. The number of counts in the gated spectrum (recorded at the experimental trigger amplitude setting) which fully overlapped the ungated spectrum above a given channel were compared for the complete length of the rectangular π^+ gate pulse. The results showed that the pion detection efficiency was 100% in the main operating region of the gate for the energies concerned. Further evidence for the 100% efficiency of the gate was obtained from the analysis of the $\pi^+ \rightarrow \mu^+$ time distribution.

The liquid hydrogen target required very little attention during the experiment, since the liquid nitrogen was automatically supplied every three hours using a time switch, and the liquid hydrogen cryostat only required filling every second day. A photograph of the target assembly and the filling systems is presented in fig.25. The compensator operated successfully and required very little adjustment during the experiment. The background runs were performed

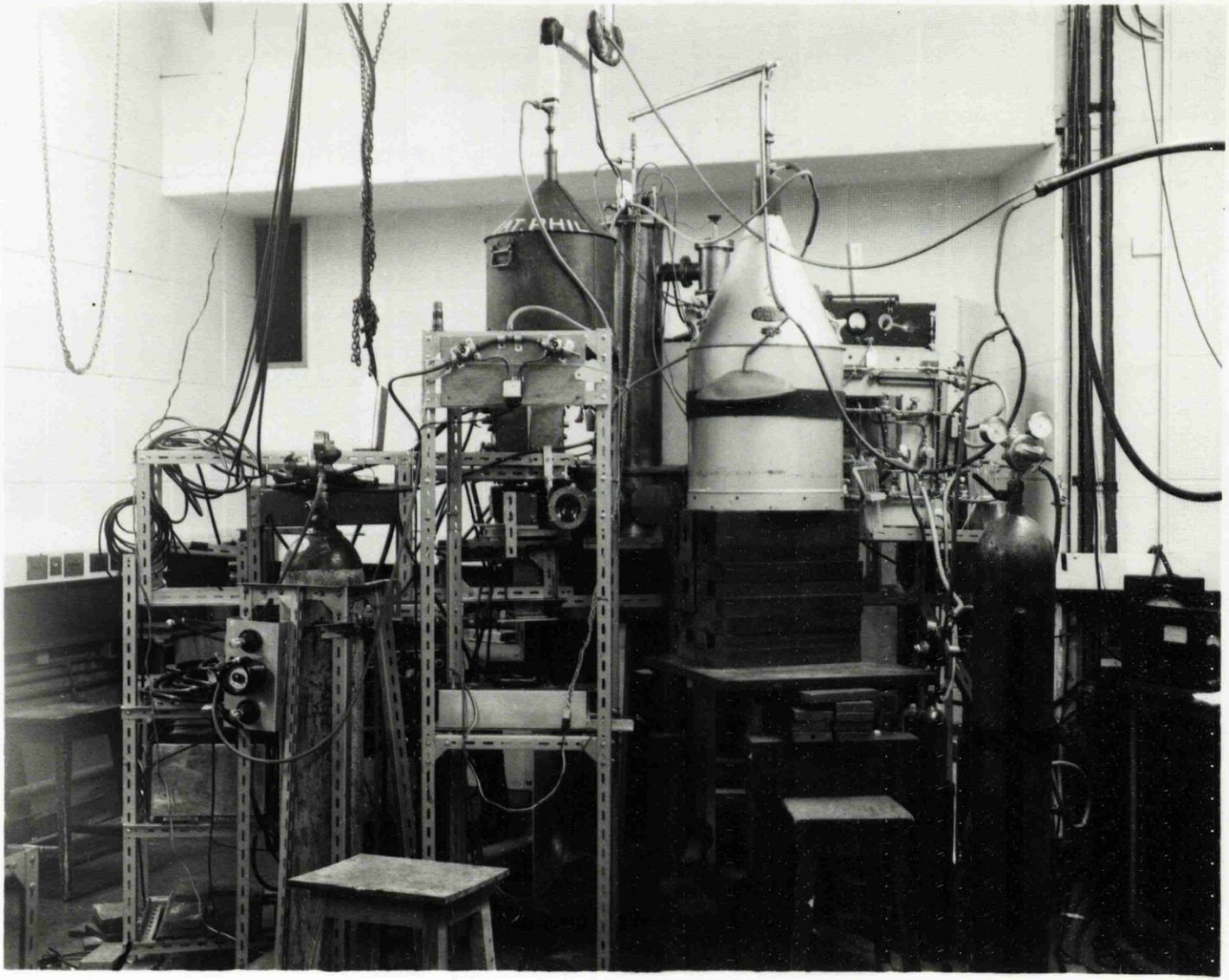

Fig.25. Target assembly in Glasgow University Beam Research Room, showing target assembly and filling systems.

at the beginning and at the end of the experiment to minimise any effects of electronic or accelerator drifts. Similarly, the absorber out and absorber in runs were regularly interspersed throughout the experiment.

The total energy content of the beam was measured by a Wilson type quantameter, since the energy calibration of this device is independent of the γ-ray energy, in contrast to the thick-walled copper ionisation chamber, which is the standard laboratory monitor at 320 MeV γ-ray energy. The quantameter is designed to automatically make a Simpson's rule integration of the shower curve produced in the chamber by the bremsstrahlung beam. The chamber consisted essentially of twelve electrically pure copper plates, accurately machined to a thickness of 1 cm, and spaced alternately 2.0 and 1.0 mm apart, except for the last gap, which was made 6.5 mm to compensate for any leakage of energy out of the chamber. The chamber was filled with a mixture of 95% argon and 5% carbon dioxide to a pressure of 800 mm Hg at room temperature. A small mercury manometer, one end of which was open to the atmosphere, and the other to the chamber, recorded the gas pressure in the chamber. The total energy of the beam was accurately proportional

to the ionisation charge, which was then collected and recorded. The calibration constant relating the energy to the charge has been calculated by Wilson (1957) to an estimated accuracy of 2%, and is given by

$$\frac{U}{q} = 4{\cdot}79 \times 10^{18} \times \frac{0{\cdot}150}{t} \times \frac{273}{P/T} \text{ mev/coulomb}$$

where U is the total beam energy in MeV, t is the average plate separation in cm, P/T is the ratio of gas pressure in mm of Hg to the absolute temperature and q is the charge collected in coulombs. P and T were therefore continuously recorded throughout the experiment.

The charge q from the chamber was collected by an integrating electrometer and recorded as revolutions on a decatron counting tube; one integrator unit corresponding to one revolution. In order to determine the number of coulombs required to give one integrator count, a standard condenser, charged to a known voltage was discharged through the electrometer, and the number of revolutions recorded. The linearity of the integrating system was checked by repeating the process for various known charges. Linearity checks were also carried out continuously during the experiment.

The total energy of the beam U is normally specified in "equivalent quanta" defined as

$$Q = \frac{\text{total energy content of the beam}}{\text{maximum photon energy}} = \frac{\int_0^{k_0} k\, N(k)\, dk}{k_0}$$

where $N(k)\,dk$ is the number of photons between k and $k + dk$. Combining this expression with the constant for the quantameter and the integrator charge calibration, the constant for the monitor was then expressed in units of equivalent quanta/integrator. The total number of equivalent quanta which have been used in any run was then determined from the monitor reading.

2. Calculation of Cross-sections from Measured Counting Rate.

The films collected during the experiment were subsequently analysed and all available information was recorded and plotted. The $\frac{dE}{dx}$ versus E plots, similar to those of fig.(22), provided unambiguous detection of all the π^+ mesons down to an energy of 6 MeV, which was the lowest energy used in determining the differential cross-sections.

Fig(26) shows the $\pi^+ \to \mu^+$ time distribution plotted

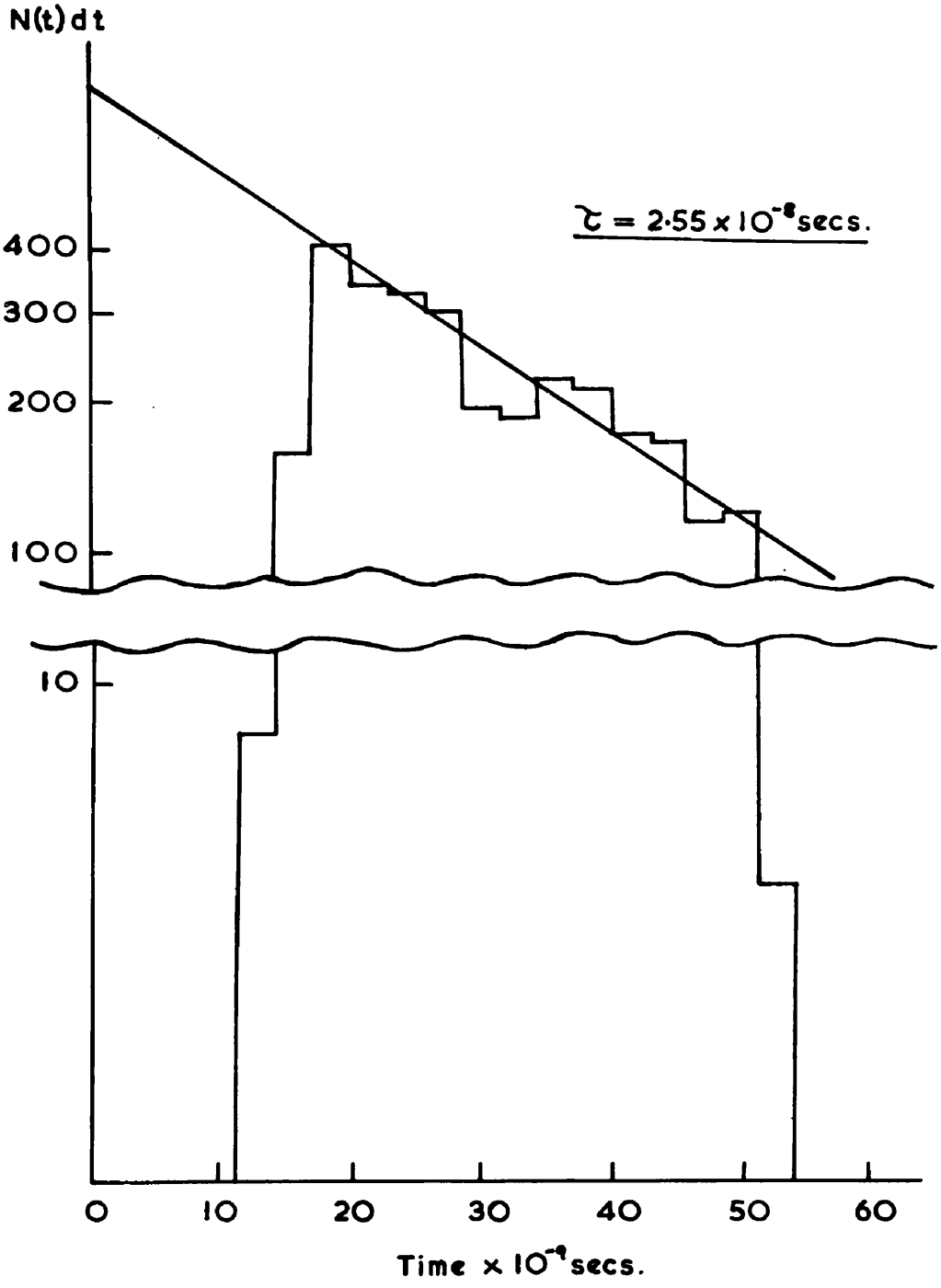

Fig.26. A logarithmic $\pi^+ \rightarrow \mu^+$ time distribution showing that the time gate accepted only pions which existed for times between 1.8 - 5 x 10^{-8} sec., the solid curve is the accepted lifetime ($2.55.10^{-8}$ sec.).

on a logarithmic scale of all mesons of energy greater than 6 MeV. This plot gave a precise measurement of the length of the delayed coincidence gate and showed that the edges of this gate were sharp. The time distribution was in accord with the mean lifetime of $2.55.10^{-8}$ sec. (Ashkin, 1959), indicated by the straight line, and is further evidence of the 100% efficiency of the detection system for all π^+ mesons greater than 6 MeV energy in the main crystal. The sine wave output from a signal generator, calibrated against the 95 Mc. B.B.C. transmission, was displayed and photographed on the Tetronix 517A to check the linearity of the time base.

The histograms of the pion energy distribution obtained with absorber in and absorber out are shown in figs.(27a) and (27b) respectively. The energy scale was graduated in pulse height divisions, accurately determined on the film projector to $\pm$ 0.5 divisions. This scale was calibrated in terms of pion energy in MeV by the sharp cut-off in the energy spectrum, shown in fig.(27), at 24 MeV. The μ^+ pulse height is also shown and provided a low energy calibration point using the Seitz relation, as determined previously. A statistical

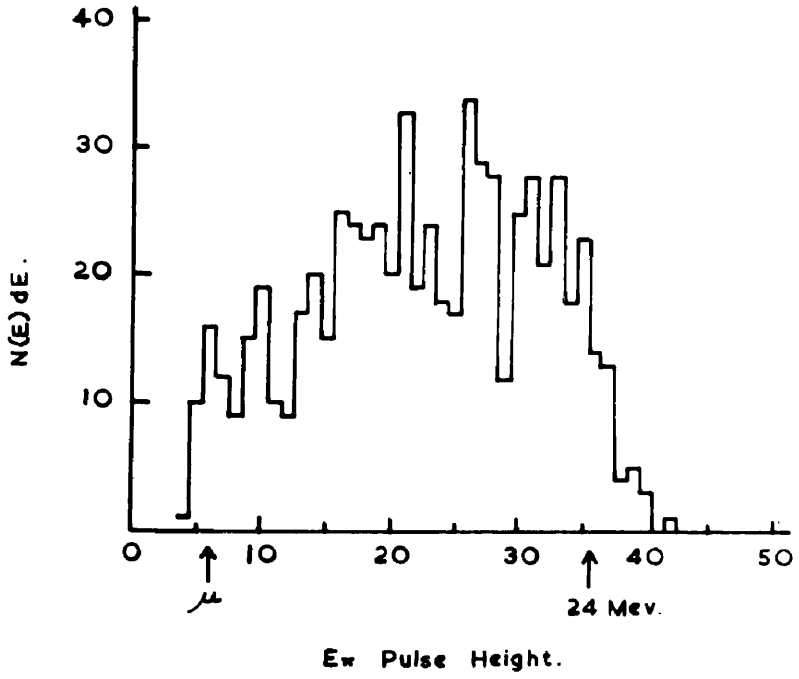

Fig.27a. Energy plot in main counter with absorber in giving a single high energy interval.

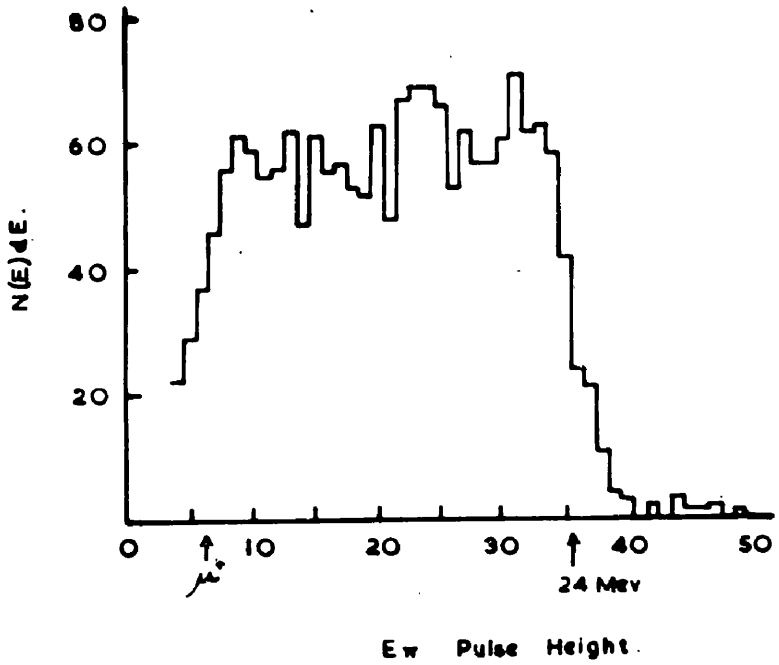

Fig.27b. Energy plot in main counter with absorber out giving 3 energy intervals.

accuracy of 5% was provided by the selection of three energy intervals from the absorber out histogram. The three energy intervals extended from 6 to 23.5 MeV in the crystal, and the meson energy intervals at creation in the target were then determined from the range-energy tables of Rich and Madey (1955). Only one energy interval was selected from the absorber out histogram, in order to minimise the possibility of large angle scattering in the copper absorber. Separate time distributions were also plotted for these energy intervals, which allowed an assessment of the time gate to be made, as can be seen in table 3, where all the experimental data is presented.

Before the π^+ cross-sections were evaluated, the raw experimental data had to be corrected for the various factors, which determined the overall efficiency for the detection of π^+ mesons, produced in the liquid hydrogen target. Corrections were made for the following energy dependent factors.

(a) Decay in Flight

The distance from the centre of the target to the main counter was 33.5 cm, and therefore a proportion of the low energy π^+ mesons decayed in flight before

TABLE 3

5.8 —12.0 MeV	12.0 — 18.2 MeV	18.2 — 23.7 MeV	10.0 — 23.7 MeV	π^+ Energy In Telescope
544	612	568	464	Total number of π^+ (target full)
5	4	3	0	Number of inverses (target full)
5851	5851	5851	3399	No.of Integrators 1 int=4.2x10^8 Eq
66	83	83	56	Total no. of π^+(corrected) target empty
473	525	482	408	Nett no. of π^+
0.33	0.35	0.35	0.31	Fraction of total $\pi^+ \rightarrow \mu^+$ decays detected in counter
0.0808 0.0042	0.0898 0.0045	0.0824 0.0043	0.1200 0.0070	No. of π^+/integrator

reaching the main counter. The calculation was straightforward since only $\pi^+ \rightarrow \mu^+$ decays were counted by the detector. The quantity

$$\frac{N}{N_0} = e^{-\frac{L}{\gamma\tau(\pi^+\rightarrow\mu^+)\beta c}}$$

was computed, where $\beta = v/c$, $\gamma = \frac{1}{\sqrt{1-\beta^2}}$, L was the distance from the centre of the energy interval of the crystal to the centre of the target, $\tau(\pi^+\rightarrow\mu^+)$ was the mean life-time for the decay of a π^+ at rest, and $\frac{N}{N_0}$ was the fraction of those mesons starting which entered the main counter. The effect was quite considerable ranging from 7% to 11.5% in the low energy interval.

(b) Solid Angle Variation.

The solid angle subtended in the laboratory system was defined by the area of the counter and its distance from the target. The solid angle therefore depended on where the mesons were produced in the one inch crystal. The correction was largest in the highest energy interval without absorber ($\sim$12%). The finite thickness of the target introduced an uncertainty into the value of the solid angle, which was less than 1%.

(c) Multiple Scattering and Nuclear Absorption

The geometry of the counter telescope was arranged to minimise the errors due to multiple scattering as much as possible. For the thin counter and the copper absorber, a graphical evaluation of these effects showed that as many pions were scattered out, as were scattered into the main counter. This was further substantiated by calculation, using the extensive results of Sternheimer (1954). The multiple scattering of pions out of the main counter was calculated, and the correction was $\leq$ 2%. The nuclear absorption cross-sections were taken from Martin (1952) and Stork (1954), and were used to calculate the absorption in the plastic scintillator and in the copper. The maximum correction in the plastic was $<$ 2%, and the correction in the copper absorber was also 2%.

(d) Target Corrections

The target corrections due to energy distortion of the pion emission spectrum were complex, because of the continuous creation and degradation of the pions across the target thickness. A detailed analysis of the target corrections has been developed by Lewis and Azuma (1961),

which showed that the target correction was relatively small (~1%), because of the falling cross-section and the thinness of the hydrogen target.

(c) Non-linearity of pion energy/Scintillation Response

The calibration of the pion energy scale was performed assuming $S \equiv E$ dependence. A small correction was applied for the non-linear dependence, which was derived by Birks and was consistent with the previous experimental observations. The correction was zero in the low energy interval and ~ 5% for the higher energies.

Corrections were made for the following factors which were not dependent on the energy of the pion

(1) $\pi^+ \rightarrow e^+$ decay

A π^+ meson which decayed into a μ^+ meson was not counted in the analysis if the e^+ particle from the μ^+ decay occurred within ~ 10^{-8} sec. This correction was small (~ 1%).

(2) Edge effects

A small fraction of the volume of the detector did not provide 100% detection of the pions in the crystal,

since the μ^+ meson could escape. This correction was also ~ 1%.

(3) Dead-time of the detector

If a π^+ meson was preceded by a γ-ray or an electron within ~ 10^{-7} sec, it was possible for the system to miss the π^+, unless it occurred within the delayed coincidence gate, produced by the electron or γ-ray. These dead-time losses were determined from the film records by the inverse effect, i.e. the π^+ meson followed by an electron or a γ-ray, and were of the order of 2%.

The differential laboratory cross-section for the production of π^+ mesons from hydrogen $\frac{d\sigma}{d\omega}$ was derived from the corrected pion counting rate N by the expression

$$N = \frac{d\sigma}{d\omega} \times t \times \Delta\omega \times N(k)\,\Delta k$$

where $N(k)\,\Delta k$ is the number of photons of mean energy k within the interval Δk, $\Delta\omega$ is the solid angle of detection in sterad., and t is the number of protons/cm^2 in the target.

$$\Delta k = \left(\frac{dk}{dE_\pi}\right) \Delta E_\pi$$

where ΔE_π is the energy interval at creation in the target, and $\frac{dk}{dE_\pi}$ is a factor, determined from the kinematics of the reaction, which have been evaluated using the recent value of the pion mass (Crowe, 1957). The expression for the differential cross-section $\left(\frac{d\sigma}{d\omega}\right)_{c.m}$ can then be written

$$N = \left(\frac{d\sigma}{d\omega}\right)_{c.m} \times \frac{d\cos\theta^*}{d\cos\theta} \times t \times N(k)\, \Delta E_\pi \left(\frac{dk}{dE_\pi}\right) \Delta\omega$$

where $\frac{d\cos\theta^*}{d\cos\theta}$ is the solid angle transformation from the laboratory to the centre-of-mass frame of reference.

The value of $N(k)$ has been computed by Penfold and Leiss (1958) as a function of k, for different values of k_0, the maximum photon energy. The calculations were based on the thin target bremsstrahlung cross-sections, as given by Schiff (1951), and the validity of this assumption is now considered. When the synchrotron R.F. power is slowly turned off, the electron beam spirals inwards and begins to traverse the edge of the vertical 0.06 in tungsten wire target. Any electron, which does not radiate on its first traversal, can therefore do so at a later time, since the normal energy loss of the electron in the target should not seriously effect

the electron orbit. The photon angular distribution is therefore uncertain due to multiple scattering of the electrons in the tungsten wire. The collimation of the emerging bremsstrahlung beam by a 0.25 in collimator, placed 125 cm from the target, selects only the bremsstrahlung in an angular interval of 0.002 radian. The characteristic angle of the bremsstrahlung is given by $\frac{m_e c^2}{k_{MAX}}$ = 0.002 radian and hence the bremsstrahlung at the hydrogen target is produced predominently in the first few thousandths of an inch in the tungsten target. Calculations (Powell et al 1951) indicated that this collimation system would produce a change in the thin target spectrum by only 3%. A small allowance (~ 2.5%) was made in the determination of the cross-section for the reduction in the end-point energy of the beam due to its 2 millisec duration.

The centre-of-mass differential cross-sections were calculated at mean Y-ray energies of 162, 168 and 175 MeV with absorber out and 192 MeV with absorber in. The results are presented in column 2 of table 4. The error limits refer to relative values in order to show the observed trend of the differential cross-section with energy. The errors quoted in table (4) are of the

TABLE 4

Lab. γ-ray Energy (MeV)	$\frac{d\sigma}{d\omega}$ (10^{-30} cm^2/ster)	$W = \frac{\gamma w}{\left(1+\frac{\mu}{m}.k\right)^2}$	$a_0^+ = \frac{1}{W}\frac{d\sigma}{d\omega}$ 10^{-30} cm^2/ster	$\theta_{c.m.}$
162	5.42 ± 0.38	0.27	20.0 ± 1.4	82
168	5.77 ± 0.41	0.35	16.4 ± 1.2	79
175	6.74 ± 0.47	0.43	15.6 ± 1.1	76
192	8.22 ± 0.58	0.60	13.6 ± 1.0	73

order of 7%, and were compounded from the statistical deviations, which form the largest contribution, the uncertainties in the correction factors previously determined, together with small uncertainties in the range-energy determinations.

An error in the absolute calibration could have occurred in addition, which would shift the experimental points as a whole, because of uncertainties in the beam calibration. The information pertaining to the bremsstrahlung beam monitors has been discussed by De Wire (1959), and from the evidence presented there, the absolute error in the calibration for the quantameter is $\lesssim 5\%$. A comparison of the quantameter with the Cornell thick-walled copper chamber was obtained at 320 MeV (Aitken and Gabathuler, 1961) and the measured ratio was consistent with the given ratio of the calibration constants of the monitors.

A transformation of the cross-sections at the centre-of-mass angles, shown in table 3, to 90° in the centre-of-mass was necessary in order to compare the results with the theoretical predictions and with the previous experimental data. The expression for the cross-section presented in Chapter 1 was

$$\frac{d\sigma}{d\omega_{cm.}} = W\left[a_0^+ + a_1^+ \cos\theta + a_2^+ \cos^2\theta + \cdots\cdots\right]$$

and therefore the values of a_1^+ and a_2^+ which determined the anisotropy of the angular distribution were required. According to Adamovich (1960), this anisotropy was small for the pion angular distribution for γ-rays of energy 185 MeV. Hence the value of a_0^+ was determined directly from $\frac{d\sigma}{d\omega}$ by the kinematical factor W , which was calculated as a function of the γ-ray energy. The values of a_0^+ are shown in the last column of table 3.

3. Discussion of Results

The graph of the variation of a_0^+ with γ-ray energy is illustrated in fig.(28), and the predicted rise of a_0^+ towards threshold is clearly visible. The solid curve shown for comparison is the single dispersion relation of Chew, Goldberger, Low and Nambu (1957), calculated by Robinson (1959) for a laboratory angle of 58°. The two perameters of this theory are the coupling constant f^2 and the $(\frac{3}{2},\frac{3}{2})$ resonance energy. The theory relies in addition on the choice of experimental values of the S wave phase shifts, but the results are not sensitive to this choice close to threshold. The experimental results are in good absolute agreement with the single dispersion relations and therefore with the value of $f^2 = 0.08$.

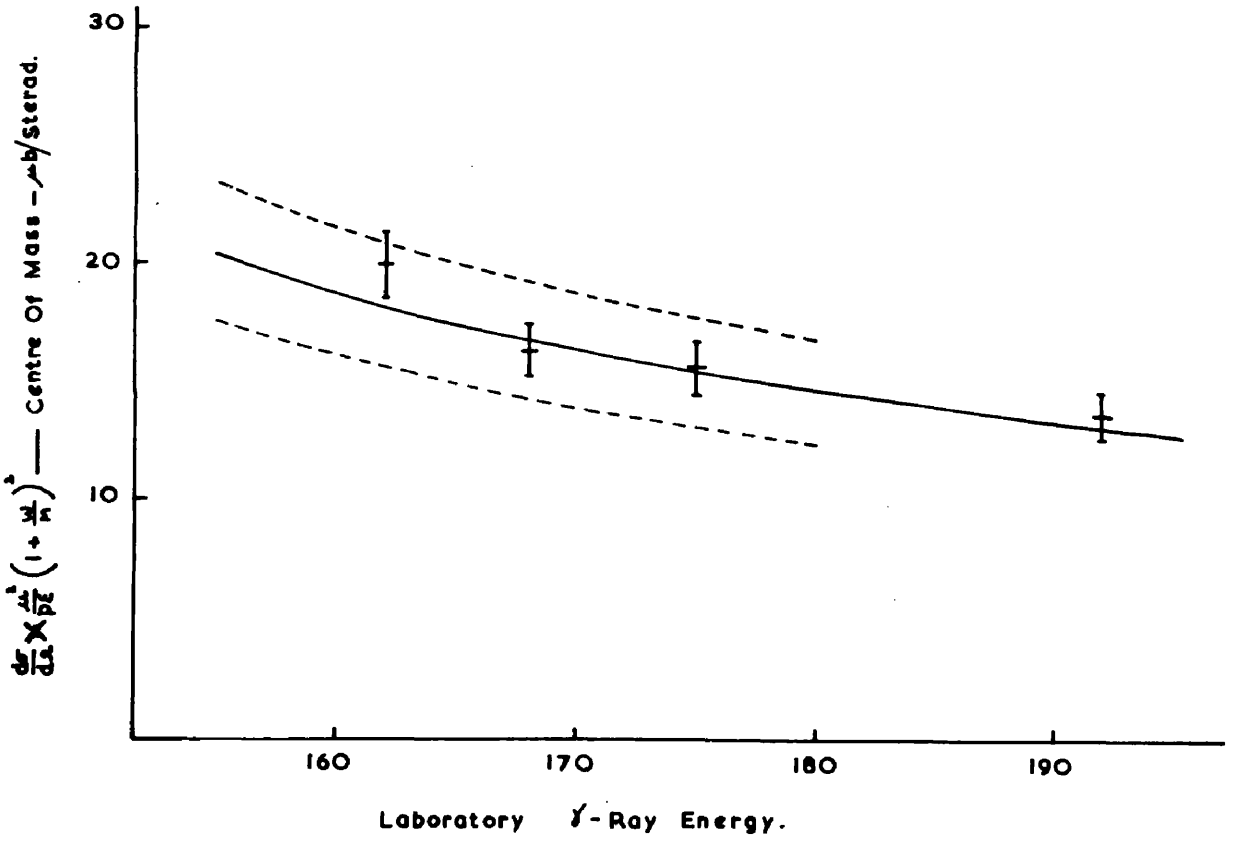

Fig.28. Experimental plot of a_0^+ against γ-ray energy for a laboratory angle of 58°. The solid curve is the single dispersion relation for 58°, the dotted curves are those of Ball for $\Lambda = \infty$ 1.8.

The solid curve also corresponds very closely to the double dispersion relation predictions given by Ball (1960). The inclusion of the π-π interaction is represented by the dotted line in fig.(28), which limits the π-π interaction to the value $\Lambda = \pm 1 \cdot 8\mu$ The experimental results do not lie outside these results, and seem to favour the $\Lambda = 0$ curve.

This experiment was also carried out simultaneously in this laboratory by Rutherglen et al. (1960), by detecting the π^+ mesons with a four-fold coincidence telescope, employing $\frac{dE}{dx}$ and E selection, to provide a separate independent measurement of a_o^+ . The results of this experiment are shown in fig.(29) together with the experiment results presented in fig.(28). The experiments were carried out using different modes of detection and different beam monitoring systems, yet the overall agreement between the results is good. Rutherglen et al. in their transformation to 90^o in the centre-of-mass used the values of a_1^+ and a_2^+ given by Beneventano et al. (1956), which raised the values of a_o^+ at the higher energies by as much as 15%. If the angular distribution given by Adamovich is assumed, then the value of a_o^+ determined by Rutherglen et al. at 191 and 200.6 MeV

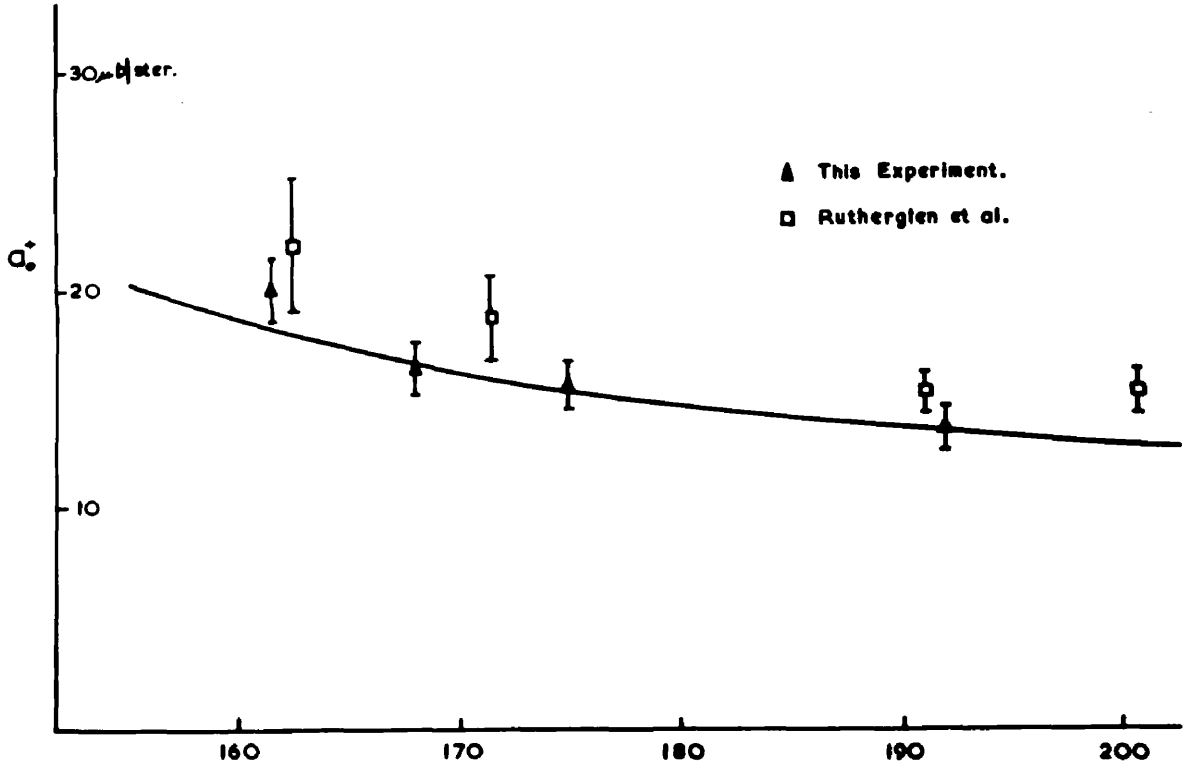

Fig.29. Experimental plot of a_o^+ versus E_γ showing the results of this experiment and those of Rutherglen et al. (1960).

would coincide with the solid curve giving even better agreement botween the experiments.

Conclusions

When this experiment was commenced in 1958, there were discrepancies in the field of low energy pion physics. Since then more accurate information concerning the various other low energy experiments has been put forward. This recent data will now be compared with the values given in Chapter 1, and an assessment of the overall state of the field of low energy pion physics will be made with reference to fig.(4).

The value of Δ, the difference in the S-wave scattering lengths, which was derived by Cini et al in Chapter 1 was

$$\Delta = 0.24 \pm 0.02$$

and gave good agreement with the other low energy perameters. Barnes (1960) derived a value of

$$\Delta = 0.320 \pm 0.06$$

which had the effect of increasing the value of $P \times R(\uparrow)$ by as much as 40%. Hamilton and Woolcock (1960) collected together all the available S-wave scattering experimental data on which they performed a threshold

extrapolation as illustrated in fig.(30). They obtained a value of

$$\Delta = 0.265 \pm 0.007$$

which is still relatively high compared to that given by Cini et al. They pointed out that in order to obtain the correct phase shifts for pion-nucleon scattering, it was necessary to remove a factor due to pure Coulomb scattering, which had been ignored previously. This then gave a value

$$\Delta = 0.245 \pm 0.007$$

consistent with the previous value given by Cini et al.

The results of this thesis are in agreement with the threshold value of a_0^+ , predicted by dispersion relations as given by Hamilton et al.

$$a_0^+ = (20.2 \pm 1.5)10^{-30} \text{ cm}^2/\text{ster}.$$

These results can now be combined as shown in fig.(4) to give

$$P \times R(\uparrow) = 2.0 \pm 0.15$$

The Panofsky ratio (P) has been measured in many different laboratories and the results are presented in table (5). Despite a wide fluctuation in the initial measurements of the ratio, the value

$$P = 1.60 \pm 0.06$$

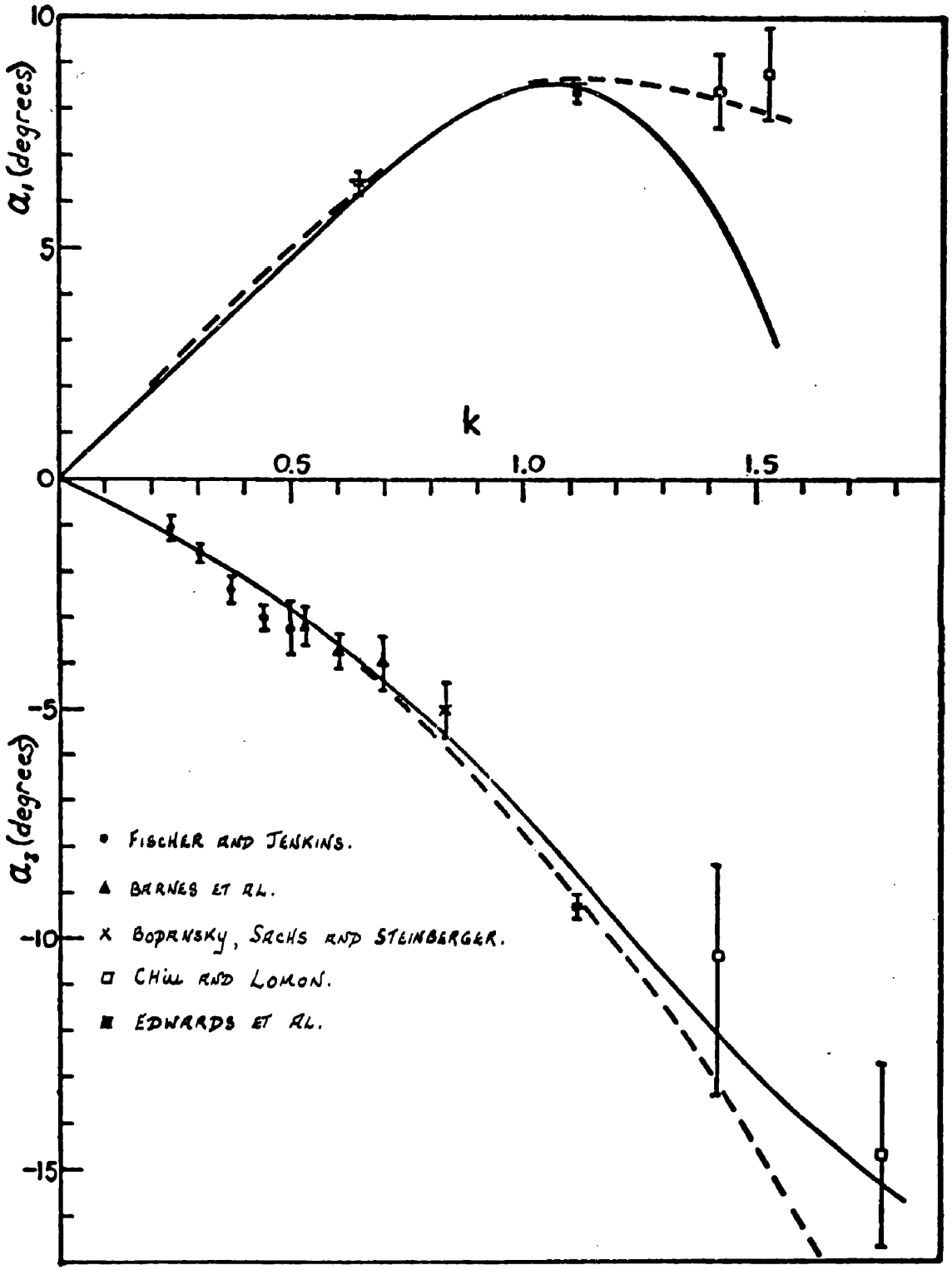

Fig.30. A plot of the S -wave phase shifts α_1 and α_3 against centre-of-mass momentum.

TABLE 5.

Panofsky Ratio	Year	Group
0.94 ± 0.30	1951	Panofsky et al.
1.50 ± 0.15	1957	Cassels et al.
1.87 ± 0.10	1958	Fisher et al.
1.60 ± 0.17	1959	Kuehner et al.
1.46 ± 0.10	1959	Koller et al.
1.47 ± 0.10	1959	Derrick et al.
1.62 ± 0.06	1960	Samios et al.
1.56 ± 0.05	1961	Jones et al.

is now fairly conclusive, in agreement with the results of the Liverpool measurements, finally quoted in Chapter 1.

In the previous discussion (Chapter 1), it was stated that despite any precise experimental measurements of tho π^-/π^+ ratio in deuterium, the exact derivation of R, the free nucleon ratio was somewhat precarious. Fortunately, this part of fig.(4) has been by-passed very recently by a very neat experiment, undertaken by Gatti et al (1961) at C.E.R.N., indicated by the dotted line. They measured the differential cross-section for the reaction

$$\pi^- + p \rightarrow \gamma + n$$

by detection of the emerging neutron using time of flight. The incident pion energy was 92 MeV, which was equivalent to a γ-ray energy of 188 MeV in the centre-of-mass of the reaction. They derived a value

$$R = 1.34 \pm 0.15$$

using the π^+ experimental results of Beneventano et al (1956). The result of Gatti et al was in good agreement with the value of 1.30 predicted by Dispersion relations, and opened the way to more measurements closer to threshold by this method.

If the value of R is therefore taken as 1.30,

then

$$P \times R(\downarrow) = 2.08 \pm 0.08$$

which is in good agreement with

$$P \times R(\uparrow) = 2.0 \pm 0.15$$

Although the threshold discrepancy was theoretically solved by the introduction of the retardation term into the interaction Hamiltonian, this step has been borne out by the experimental results of the energy dependence of a_0^+, presented in this thesis. To extend the experimental values of a_0^+ closer to threshold (151.4 MeV) requires the measurements to be carried out at very forward angles ($\sim 30^\circ$). It is doubtful if any new information would be gained, because of the difficulties in making accurate measurements by the present method. For example, there is a very rapid increase in the background radiation in moving to forward angles as can be seen from fig.(10).

An isotropic distribution based on the results of Adamovich et al. was assumed for the determination of a_0^+ from the differential cross-sections. Any deviation from isotropy had a verysmall effect ($\sim 2\%$) on the values of a_0^+ near threshold, but changed the value at the higher γ-ray energies by as much as 15%. An

accurate angular distribution is therefore of importance in the Y-ray interval up to 200 MeV, to give an accurate assessment of the energy dependence of a_o^+ , and in addition to provide a precise determination of the pion-nucleon coupling constant. It is difficult to foresee how any new information on the π^-/π^+ ratio from deuterium will accurately determine R. The most likely measurements to assess R are those similar to that carried out by Gatti et al, taken in conjunction with the π^+ cross-section from hydrogen.

The role of the π meson in understanding nuclear phenomena is already demanding a higher degree of experimental accuracy with the introduction of the pion-pion interaction. In view of the recent experimental evidence of the pion-hyperon and kaon resonance states, it may be that a complete understanding of the role of the pion will not become available until the K-mesons and hyperons are also included in the overall picture.

Publications

1. On The Separation of π^+ Mesons By a Time of Flight Method. G.M. Lewis, E. Gabathuler and R.E. Azuma. Nuclear Instruments 8, 230 (1960).

2. The Photoproduction of Positive Pions from Hydrogen near Threshold. G.M. Lewis, R.E. Azuma, E. Gabathuler, D.W.G.S. Leith and W.R. Hogg. Submitted to Physical Review for publication (1961).

3. The L/K-Capture Ratio in ^{126}I. J. Scobie and E. Gabathuler Proc. Physical Society 72, 437 (1958).
(additional work performed in the University of Glasgow.)

REFERENCES.

Adamovich, M.J. (1960) Proceedings of the Rochester Conference.

Adamovich, M.I., Gorzhevskaya, E.G., Larionova, V.G., Popova, V.M., Kharlamov, S.P., and Yagudina, F.R.,(1960), J.E.T.P. 11, 4, p.779.

Adamovich, M.I., Kuzmicheva, G.V., Larionova, V.G., and Kharlamov, S.P. (1958), J. Exptl. Theoret. Phys. (U.S.S.R.) 35, 27.

Aitken, T., and Gabathuler, E., (1961) Internal Report.

Akimov (1959) Proceedings of the Kiev Conference.

Anderson, J.A., Bang, V.X., Burke, P.G., Carmony, D.D. and Schmitz, N. (1961), Phys. Rev. Letters, Vol.6, No.7.

Ashkin, J., Fazzini, T., Fidecaro, G., Goldschmidt-Clermont, Y., Lipman, W.H., Merrison, A.W., and Paul, H., (1960) Nuovo Cim. 16, 490.

Azuma, R.E., Lewis, G.M., (1957), Phil. Mag. 2, 1325.

Baldin, A., (1958) Nuovo Cim. 8, 569.

Ball, J.S., (Thesis) UCRL-9172 (1960); Phys. Rev. Letters 5, 73, (1960).

Barbaro, G. and Goldwasser, E.L., (1959) Proceedings of the Kiev Conference.

Barnes, S.W., Rose, B., Giacomelli, G., Ring, J., Miyake, K., and Kinsey, K., (1960) Phys. Rev. 117, 226.

Barnes, S.W., Winet, W.H., Miyahe, K., and Kinsey, K., (1960) Phys. Rev. 117, 238.

Bellamy, E.H., Hogg, W.R., and Millar, D. (1960), Nuclear Instruments 7, 293.

Beneventano, M., Barnardini, G., Carlson-Lee, D., Stoppini, G., and Tau, L., (1956), Nuovo Cim. 4, 323 (1956S) N.C.S. 2, 926.

Bernardini, G., (1959) Rochester Conference Report.

Bernardini, G., Goldwasser, E.L. (1954) Phys. Rev. 95, 857; Phys. Rev. 94, 729.

Bethe, H.A., and de Hoffmann, F., (1955) "Mesons and Fields" Vol.2 (Row, Peterson & Co.)

Birks, J.B., (1951), Proc. Phys. Soc. A, 64, 874 (1953) Scintillation Counters (London: Pergamon Press).

Bodansky, D., Sachs, A.M., and Steinberger, J., (1954) Phys. Rev. 93, 1367.

Brueckner, K.A., and Case K.M., (1951) Phys. Rev. 83, 1141.

Brueckner, K.A., and Watson, K.M., (1952) Phys. Rev. 86, 923.

Cassels, J.M., Fidecaro, G.M., Wetherell, A.M., and Wormald, J.R., (1957) Proc. Phys. Soc. A. 70, 405.

Cassels, J.M., Jones, D.P., Murphy, P.G., and O'Neill, P.L. (1959) Proc. Phys. Soc. 74, 92.

Chew, G.F., (1954) Phys. Rev. 95, 1669.

Chew, G.F., (1955) Theory of Pion Scattering & Photo-production U.C.R.L. 1857.

Chew, G.F., Goldberger, M.L., Low, F.E., and Nambu, Y., (1957) Phys. Rev. 106, 1345.

Chew, G.F., and Low, F.E., (1956) Phys. Rev. 101, 1579.

Chiu, H Y., and Lomon, E., (1959) Ann. Phys. (N.York) 6, 50 and 1958 CERN Conference p.49.

Cini, M., Gatto, R., Goldwasser, E.L., and Ruderman, M., (1958) Preprint, Nuovo Cim. 10, 242.

Crowe, K.M., (1957) Nuovo Cim. 5, 541.

Derrick, M., Fetkovich, J., Fields, T., and Deahl J., (1959) Bull. Amer. Phys. Soc., 4, 401.

De Tollis, B., E. Ferrari and Munczek, H., (1960) Nuovo Cim. 18, 200.

De Wire, J.W. (1959) Cornell University Report.

Donoho, P.L. and Walker R.L., (1957) Phys. Rev. 107, 1198.

Evans, H.C., and Bellamy E.H., (1959) Proc. Phys. Soc. Vol 74 p. 483.

Feld, B.T., (1953) Phys. Rev. 89, 330.

Feld, B.T., Frisch, D.H., Lebow, I.L., Osborne, L.S. and Clark J.S. (1952) Phys. Rev. 85, 680.

Fermi, E. (1952), and Anderson, H.L., (1952), Phys. Rev. 86, 794.

Fischer, G.E., and Jenkins, E.W., (1959) Phys. Rev. 116, 749.

Fisher, J., March, R., and Marshall, L., (1958) Phys. Rev. 109, 533.

Gartenhaus, S., and Blankenbecler, R., (1959) Phys. Rev. 116, 1305.

Gatti, G., Millman, P., Middelkoop, W.C., Yamagata, T., and Zavattini, E., (1961) Phys. Rev. Letters Vol 6, No. 12, p.706.

Gell-Mann M., and Watson, K.M., (1954) Annual Review of Nuclear Science, 4, 219.

Goldberger, M.L., (1955) Phys. Rev. 99, 979.

Goldwasser (1960) Proceedings of the Rochester Conference.

Gooding, T.J. and Pugh, S.F. (1960) Private Communication.

Gourdin, M., Lurie, D., and Martin, A., (1960) Nuovo Cim. 5, 20.

Hamilton, J., and Woolcock, W.S., (1960), Phys. Rev. 118, 291.

Janes, G.S., and Kraushaar, W.L., (1954) Phys. Rev. 93, 900.

Jenkins, T.L., Luckey, D., Palfrey, T.R., and Wilson, R.R., Phys. Rev. 95, 179.

Jones, D.P., Murphy, P.G., O'Neill P.L., and Wormald, J., (1961) Proc. Phys. Soc. 77, 77.

Keck, J., (1952), Phys. Rev. 85, 410.

Kirk, J., Journal of Scientific Instruments 1961 - to be published.

Koller, E.L., and Sachs, A.M., (1959) Phys. Rev. 116, 760.

Kroll, N.M., and Ruderman, M.A., (1954) Phys. Rev. 93, 233.

Kuehner, J.A., Merrison, A.W., and Tornabene, S., (1959) Proc. Phys. Soc. 73, 545.

Lazarus, A.J., Panofsky, W.K.H., and Tangherlini, F.R., (1959) Phys. Rev. Vol 113, No. 5, 1330.

Lederman, L., (1956) Proc. VI Annual Rochester Conference.

Leiss, J.E., Robinson C.S., and Penner, S., (1955) Phys. Rev. 98, 201.

Leiss, J.E., and Penner, S., (1959) Bull Ann. Phys. Soc. II, 4, p.273.

Leith, D.W.G.S., (1959) Private Communication.

Lewis, G.M., Azuma, R.E. (1959) Proc. Phys. Soc. (London) Vol.73, p.873.

Lewis, G.M., and Azuma, R.E., (1961) Private Communication.

Lewis, G.M., Gabathuler, E., and Azuma, R.E., (1960) Nuclear Instruments, 8, 230.

Low, F.E. (1954) Phys. Rev. 96, No.5, 1428.

Low, F.E., (1955) Phys. Rev. 97, 1392.

McDaniel, B.D., Silverman, A., Wilson, R.R., and Cortellessa, G., (1958) Phys. Rev. Letters Vol.1, No.3, p.109.

McMillan, E.M., Peterson, J.M., and White, R.S., (1949) Science 110, 579.

Malmberg, J.H., and Robinson, C.S., (1958), Phys. Rev. 109, 158.

Mandelstam, S., (1958) Phys. Rev. 112, 1344.

Marshak, R., (1952) "Meson Physics" McGraw-Hill Book Company Inc. New York.

Martin, R.L., (1952), Phys. Rev. 87, 1052.

Moravcsik, M.J., (1956) Phys. Rev. 104, 1451.

Oehme, R. and Taylor, J.G. (1959) Phys. Rev. 113, 371.

Orear, J., (1956) Nuovo Cim. 4, 856.

Panofsky, W.K.H., Aamodt, R.L., Hadley, J., (1951) Phys. Rev. 81, 565.

Penfold, A.S., and Leiss, J.E., (1958) "Analysis of Photo Cross Sections", University of Illinois.

Powell, W., Hartsough, W., and Hill, M., (1951) Phys. Rev. 81, 213.

Rich, M., and Madey, R., (1954), "Range-Energy Tables", UCRL-2301.

Robinson C.S., (1959) Illinois Univ. Techn. Rep. 8, ONR 1834.

Rutherglen, J.G., Walker J., Miller, D., and Patterson J., (1960) Proceedings of the Rochester Conference.

Samios, N.P., (1960) Phys. Rev. Letters, 4, 470.

Schiff, L.I., (1961), Phys. Rev. 83, 252.

Steinberger, J., and Bishop, A.S., (1950) Phys. Rev. 78, 494.

Sternheimer, R.N., (1954) Rev. Sci. Inst. 25, 1071.

Stork, D.H. (1954), Phys. Rev. 93, 868.

Taylor, C.J., Jentschke, W.K., Romley, M.E., Ely, F.S., and Kruger, P.G., (1951) Phys. Rev. 84, 1034.

Uretsky, J.L., Kenney, R.W., Knapp, K.A., Perez-Mendez, V., (1958) Phys. Rev. Letters, Vol,1. No.1.

Walker, R.L., Teasdale, J.G., Peterson, V.Z. and Vette, J.I. (1955) Phys. Rev. 99, 210.

Watson, K.M., (1952) Phys. Rev. 85, 852.

Watson, K.M., (1954) Phys. Rev. 95, 228.

Whalin, E.A., and Reitz, R.A. (1955) Rev. Sci. Inst. 26, 59.

White, G.K., (1959) "Experimental Techniques in Low Temp. Physics", (Oxford: Clarendon Press).

White, R.S., Jacobson, M.J., and Shulz, A.G., (1952) Phys. Rev. 88, 836.

Wilson R.R., (1957) Nuclear Instruments 1, 101.

Wolfe, B., Silverman, A. and De Wire, J.W. (1955), R.S.I. 26, 504.